Schweizerische Eidgenossenschaft
Confédération suisse
Confederazione Svizzera
Confederaziun svizra

Federal Department of the Environment, Transport, Energy and Communications DETEC

Swiss Federal Office of Energy SFOE
Energy Research and Cleantech

Final report 30 August 2021

BigIce

Assessment of solar-ice systems for multi-family and tertiary buildings

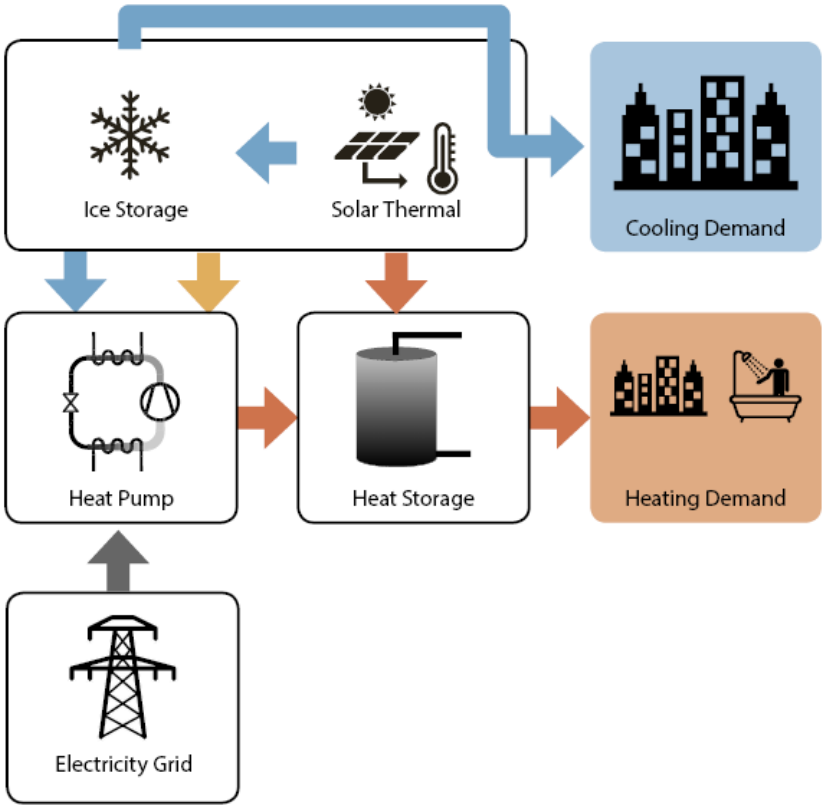

INSTITUT FÜR SOLARTECHNIK

OST Ostschweizer Fachhochschule

Date: August 30, 2021

Location: Rapperswil

Subsidiser:

Swiss Federal Office of Energy SFOE
Energy Research and Cleantech Section
CH-3003 Bern
www.bfe.admin.ch

Subsidy recipients:

Institut for Solar Technology SPF, Eastern Switzerland University of Applied Sciences (OST)
Oberseestr. 10
CH-8640 Rapperswil
www.spf.ch

Authors:

Dr. Daniel Carbonell, Dani.Carbonell@ost.ch
Maike Schubert, Maike.Schubert@ost.ch
Dr. Martin Neugebauer, Martin.Neugebauer@ost.ch

Collaborators:

Mattia Battaglia, Jeremias Schmidli, Cherrie Chong

SFOE project coordinators:
Andreas Eckmanns, Andreas.Eckmanns@bfe.admin.ch
Elimar Frank, Elimar.Frank@frank-energy.com

SFOE Contract number: SI/501726-01

Abstract

Heat pump is a very efficient technology to cover heating and cooling demands on the building sector with high share of renewables. It is foreseen that the deployment of heat pumps will increase significantly in the future Swiss energy system. However, heat pumps need a heat source and the use of traditional sources such as air or ground are not possible everywhere due to regulations, noise, space or social barriers to cite some. Thus, alternative renewable heat sources such as solar are very attractive. Solar-ice systems use solar energy as a source for the heat pump with an ice storage to cover the mismatch between solar availability and heat pump needs. A solar-ice system is kind of *a ground source heat pump fully regenerated (for free)* where the borehole field is substituted by solar collectors and a high energy density storage exploiting the latent heat of water.

The main potential for solar-ice systems is on the multi-family building market where those systems are becoming very popular in Switzerland. However, no standard design exists for those cases and dynamic system simulations are often used to consider the effects of many aspects such as collector area, ice storage volume, weather data, building demands and other possible heat sources that are coupled to each other. Understanding the main factors influencing the efficiency of such systems and developing a simple feasibility tool for planners would foster the distribution of solar-ice systems. Such a tool should enable planners to assess solar-ice systems on early stages of the planning phase with just little available data such as, e.g., yearly heat demands and solar irradiation.

Within the project we aimed to explore the potential of solar-ice systems for multifamily buildings. By means of dynamic system simulations with a large parameter variation analysis, the effects of different weather data, hydraulics on the primary (solar, ice and heat pump) loop, building demand profiles and sizes of key components such as collector field and ice storage, were analyzed in detail. Additionally, the cooling potential was addressed as well. In a last step, a fast algorithm that can predict the energetic performance of a solar ice system with little input data was developed based on a machine learning approach. The aim was to develop a tool between a rule-of-thumb approach, which does not exist at the moment, and a planning tool. Such a simplified tool would not substitute a planning tool that will always be used during a real planning phase, but be employed until a decision about the realization of a solar-ice system is made and thus avoid the need for simulations at early stages.

A simulation study using the dynamic system simulation software TRNSYS with 3600 runs has been performed to analyze different factors influencing the efficiency of solar-ice systems and to provide a data basis for the development of the fast algorithm tool. The simulation framework is based on very extensively validated models both at component as well as at system level giving confidence to the results obtained. Different machine learning algorithms were employed to develop a fast prediction tool.

An analysis of the influence of the possible hydraulic schemes for solar-ice systems include the cases with and without the use of direct solar heat in the heat pump evaporator as well as in the warm storage. These combinations lead to four cases that were compared numerically. The possibility to use solar heat in the heat pump by-passing the ice storage and directly in the warm storage has significant advantages from an energetic point of view.

Solar-ice systems do have the potential for free cooling by simply stopping the melting of the ice storage in spring in order to have a cold reservoir for space cooling in summer. This passive *free* cooling option is possible without any increase of electrical demand in a well designed solar-ice system for locations with low cooling demand like Geneva. For locations with higher cooling demand like Locarno additional cooling capacity can be provided by using the heat pump for domestic hot water with no significant decrease in the system efficiency if both, heating and cooling, are considered.

For increasing the market share of solar-ice systems an easy to use feasibility tool is necessary in order to assess solar-ice systems as possible solutions during early stages of the decision making process. From the results presented in this study, developing such a tool for a fast dimensioning of solar-ice systems is conceivable. It was shown that only using yearly data for climatic conditions and the heating demand of the building a prediction accuracy of $\pm 10\,\%$ (for $90\,\%$ of the data) can be reached. Adding the winter share of the heating demand and irradiation as additional (optional) parameters this error can be further reduced to $\pm 5\,\%$.

The most important results of this report are summarized in the following section Main findings.

Zusammenfassung

Mit Wärmepumpen lässt sich der Heiz- und Kühlbedarf von Gebäuden sehr effizient mit einem hohen Anteil an erneuerbaren Energien decken. Es wird erwartet, dass die Verbreitung von Wärmepumpen im zukünftigen Schweizer Energiesystem stark ansteigen wird. Allerdings sind gängige erneuerbare Quellen, wie Erdwärme oder Luft z. B. auf Grund von Bewilligungseinschränkungen, Lärmbelästigung oder Platzbedarf nicht überall möglich. Das macht alternative erneuerbare Energiequellen, wie Solarenergie, sehr attraktiv. Solar-Eis-Systeme nutzen Solarwärme als Quelle für die Wärmepumpe, wobei ein Eisspeicher den Versatz zwischen Verfügbarkeit der Solarwärme und Wärmebedarf puffert. Ein Solar-Eis-System ist eine Art *Erdwärme-Wärmepumpensystem mit voller Regeneration des Erdreichs (gratis)*, in dem das Sondenfeld durch Solarkollektoren und einen Speicher ersetzt wird. Der Eisspeicher hat eine hohe Energiedichte, da er die latente Wärme des Wassers nutzt.

Der Mehrfamilienhaussektor hat das grösste Potential für Solar-Eis-Systeme in der Schweiz, dort werden Solar-Eis-Systeme immer beliebter. Jedoch gibt es bisher kein standardisiertes Design für solche Systeme und die Auslegung wird häufig über dynamische Systemsimulationen gemacht, um die Effekte der Wechselwirkung zwischen Kollektorfeldgrösse, Eisspeichervolumen, Wetterdaten, Heizwärmebedarf und möglichen weiteren Wärmequellen zu berücksichtigen. Die Haupteinflussfaktoren auf die Systemeffizienz zu verstehen und die Entwicklung eines einfachen Machbarkeits-Tools würde die Verbreitung von Solar-Eis-Systemen fördern. Ein solches Tool sollte es Planern ermöglichen Solar-Eis-Systeme mit wenigen Eingabedaten (z.B. jährlicher Wärmebedarf und solare Einstrahlung) in einer frühen Planungsphase schnell und einfach bewerten zu können.

Im Rahmen dieses Projektes wurde das Potential von Solar-Eis Systemen für Mehrfamilienhäuser untersucht. Über eine grosse Parameterstudie mit dynamischen Systemsimulationen wurden die Effekte von unterschiedlichen Wetterdaten, hydraulischen Einbindungen auf der Primärseite (Solar, Eisspeicher und Wärmepumpe), Heizwärmebedarfsprofil und Dimensionen der Schlüsselkomponenten detailliert untersucht. Zusätzlich wurde das Kühlpotential berücksichtigt. In einem letzten Schritt wurde ein schneller Algorithmus entwickelt, der auf maschinellem Lernen basiert und die Systemeffizienz von Solar-Eis Systemen mit wenigen Eingabedaten vorhersagen kann. Ziel war es ein Tool zu entwickeln, dessen Anwendbarkeit zwischen einer Faustformel (die es bisher nicht gibt) und einem Planungstool liegt. Ein solches vereinfachtes Tool wird kein Planungsinstrument ersetzen das für die Realisierung nach wie vor verwendet werden muss, aber es wird ermöglichen in der Entscheidungsphase Solar-Eis Systeme einfach, schnell und ohne Systemsimulationen zu berücksichtigen.

Eine Simulationsstudie mit der Simulationssoftware TRNSYS mit 3600 Simulationen wurde durchgeführt, um die verschiedenen Einflussfaktoren auf die Effizienz von Solar-Eis-Systemen zu analysieren und um eine solide Datenbasis für die Entwicklung des schnellen Algorithmus zu erhalten. Die Simulationsumgebung basiert auf gut validierten Modellen, sowohl auf Komponenten- als auch auf Systemebene. Verschiedene Ansätze des maschinellen Lernens wurden berücksichtigt, um das Machbarkeitstool zu entwickeln.

Eine Analyse des Einflusses verschiedener hydraulischer Einbindungen für Solar-Eis-Systeme umfasst Fälle mit und ohne direkte Nutzung von Solarwärme im Verdampfer der Wärmepumpe und in den warmen Speichern. Diese Kombinationen führen zu vier Fällen, die über Simulationen verglichen wurden. Die Möglichkeit Solarwärme direkt in der Wärmepumpe zu nutzen, ohne über den Eisspeicher zu gehen und direkt die warmen Speicher zu erwärmen bringt signifikante energetische Vorteile.

Solar-Eis-Systeme haben Potential für Freecooling, wobei lediglich das gezielte Abschmelzen des Eisspeichers im Frühjahr gestoppt wird, um Kälte für die Raumkühlung mit in den Sommer zu nehmen. Diese passive Freecooling-Option verursacht in gut dimensionierten Solar-Eis-Systemen in Gebieten mit geringem Kühlbedarf, wie z.B. Genf, keinen Anstieg des Strombedarfs. In Gebieten mit höherem Kühlbedarf, wie Locarno, kann zusätzliche Kühlkapazität geschaffen werden, indem Warmwasser über die Wärmepumpe bereitgestellt wird. Dabei sinkt die Systemeffizienz nicht, wenn Heizen und Kühlen berücksichtigt werden.

Um den Marktanteil von Solar-Eis-Systemen zu steigern ist ein einfaches Tool für Machbarkeitsstudien wichtig, um Solar-Eis Systeme in der Entscheidungsphase ohne grossen Aufwand berücksichtigen zu können. Ausgehend von den hier vorgestellten Ergebnissen ist die Entwicklung eines solchen Tools für eine schnelle Dimensionierung von Solar-Eis-Systemen denkbar. Es konnte gezeigt werden, dass unter Verwendung von jährlichen Daten über das Wetter und den Heizwärmebedarf des Gebäudes eine Vorhersage der Effizienz mit einer Genauigkeit von $\pm 10\,\%$ (für 90 % der Daten) erreicht werden kann. Wird zusätzlich der Heizwärmebedarf und die solare Einstrahlung in den Wintermonaten als Eingabeparameter berücksichtigt, kann die Genauigkeit auf $\pm 5\,\%$ gesteigert werden.

Die wichtigsten Resultate sind im Abschnitt Main findings zusammengefasst.

Résumé

Les pompes à chaleur présentent une technologie très efficace en vue de couvrir les besoins en chaleur et en rafraîchissement du secteur des bâtiments tout en faisant la part belle aux renouvelables. Au sein du futur système énergétique Suisse, une augmentation significative du déploiement des pompes à chaleur est prévue. Cependant, en raison des contraintes législatives, de bruit, d'espace ou sociales pour n'en citer que quelques-unes, l'utilisation de sources de chaleur traditionnelles telles que l'air ou le sol ne sont pas possible partout. Les pompes à chaleur requérant une telle source de chaleur, les sources de chaleur alternatives telles que le solaire sont par conséquent très attractives. Afin de couvrir le déphasage entre la disponibilité en énergie solaire et les besoins de la pompe à chaleur, les systèmes solaire-glace utilisent l'énergie solaire comme source pour la pompe à chaleur. Un système solaire-glace est similaire à une pompe à chaleur géothermique complètement régénérée (sans dépenses supplémentaires) pour lequel le champ de forage est remplacé par des capteurs solaires ainsi qu'un stockage à haute densité énergétique utilisant la chaleur latente de l'eau.

Le marché des bâtiments plurifamiliaux constitue le principal potentiel pour les systèmes solaire-eau où ils deviennent très populaires en Suisse. Cependant, aucun dimensionnement standard n'existe pour ce type d'application et des simulations dynamiques du système sont souvent utilisées pour tenir compte des effets de différents aspects tels que la surface des capteurs, le volume du stockage de glace, les données météorologiques, les besoins en chaleur du bâtiment ainsi que les autres sources de chaleur couplées au système. La compréhension des principaux facteurs influençant l'efficacité de tels systèmes ainsi que le développement d'un outil de faisabilité simple pour les concepteurs pourraient favoriser la distribution de systèmes solaire-glace. Un tel outil permettrait aux concepteurs d'évaluer un système solaire-glace au début de la conception, lorsque peu de données sont disponibles (besoin annuels en chaleur et ensoleillement par exemple).

Au cours du projet, le potentiel des systèmes solaire-glace pour les bâtiments plurifamiliaux a été exploré. Les effets de différentes données météorologiques, éléments hydrauliques sur le circuit primaire (solaire, glace et pompe à chaleur), profils de besoins du bâtiment et taille des éléments clefs tels que le champ de capteur et le stockage de glace ont été analysés grâce à des simulations dynamiques du système en faisant varier les paramètres dans une large plage. De plus, le potentiel de rafraîchissement a également été considéré. Pour finir, basé sur une approche de machine learning, un algorithme rapide permettant de prédire les performances énergétiques d'un système solaire-glace a été développé, le but étant de développer un outil entre la règle empirique (qui n'existe pas pour le moment) et un outil de planification. Un tel outil simplifié ne doit pas être substitué à un outil de planification qui sera toujours utilisé durant la phase effective de planification. Il doit permettre de faciliter la décision en ce qui concerne l'implémentation de systèmes solaire-glace et éviter d'avoir à effectuer des simulations durant les premières phases du projet.

Afin d'analyser les différents facteurs influençant l'efficacité de systèmes solaire-glace et de fournir une base de donnée nécessaire au développement de l'outil basé sur un algorithme rapide, une étude numérique de 3600 essais a été effectuée avec le logiciel de simulation dynamique TRNSYS. Le cadre des simulations est basé sur des modèles largement validés aussi bien à un niveau composant qu'à un niveau système, d'où une bonne fiabilité des résultats obtenus. Pour l'outil de prédiction rapide, plusieurs algorithmes de machine learning ont été utilisé.

Pour l'analyse de l'influence des possibles schémas hydrauliques des systèmes glace-solaire, les cas où la chaleur solaire est directement utilisée par l'évaporateur de la pompe à chaleur ainsi que par le stockage à haute température ont été considérés. Ces combinaisons ont mené à quatre cas qui ont été comparés numériquement. D'un point de vue énergétique, la possibilité de by-pass du stockage de glace afin d'utiliser directement la chaleur solaire dans la pompe à chaleur ou dans le stockage à haute température présente des avantages significatifs.

En ce qui concerne le refroidissement naturel, les systèmes solaire-glace permettent d'avoir un stockage à basse température destiné au rafraîchissement des locaux en été si l'on arrête simplement le processus de fonte du stockage de glace au printemps. Cette option de refroidissement naturel passif est possible sans augmentation de la consommation électrique pour un système solaire-glace bien conçu et une localisation à faible besoin de rafraîchissement telle que Genève. Pour les localisations où le besoin de rafraîchissement est plus élevé tels que Locarno, une capacité de rafraîchissement additionnelle peut être obtenue en utilisant la pompe à chaleur pour la production d'eau chaude sanitaire. Ceci sans diminution significative de l'efficacité du système à partir du moment où le chauffage et le rafraîchissement sont considérés simultanément.

Afin d'augmenter la part de marché des systèmes solaire-glace, un outil facile d'utilisation est nécessaire afin

d'évaluer le potentiel des systèmes solaire-glace durant les phases précoces du processus de prise de décision. Considérant les résultats présentés dans cette étude, le développement d'un tel outil pour le dimensionnement rapide de systèmes solaire-glace est imaginable. En effet, en ne considérant que les données annuelles pour les conditions climatiques et les besoins en chaleur du bâtiment, une justesse des prédiction de $\pm 10\,\%$ (pour $90\,\%$ des données) peut être atteinte. Cette erreur peut être réduite à $\pm 5\,\%$ si l'on ajoute en tant que paramètres additionnels (optionnels) la proportion de chaleur requise en hiver ainsi que l'ensoleillement.

Les principaux résultats de ce rapport sont résumés dans la section Main findings.

Main findings

The two new (MFB30) and refurbished (MFB90) multi-family buildings including the ideal and real user behaviour considered in the simulation study result in different heat demand distributions. They differ considerably in their total sum, their distribution over the months and the ratio between space heating and domestic hot water demand, which leads to significant differences in energetic efficiency. The ideal user behaviour and/or the new building lead to a higher winter share than the real user behaviour and/or the old building. The lower the total heating demand, the higher is the domestic hot water share of it. A higher winter share causes a lower system efficiency because of the lower winter irradiation and the higher domestic hot water share leads to a decrease of system efficiency due to higher sink temperatures.

Scaling factors of ice storage and collector area in m^3/MWh and m^2/MWh respectively, are based on the total heating demand. Compared to buildings with low insulation standard, the winter share is 20 % to 40 % higher for buildings with high insulation standard considering ideal user behaviour, and about 7 % to 15 % higher winter shares are obtained for real user behaviour. Considering ideal user behaviour, buildings with high insulation standard show 5 % to 25 % lower SPF_{SHP} than those with low insulation standard for the same scaling factors in ice storage volume and collector field area, because the scaling refers to the yearly total heat demand. As an alternative, one might contemplate using winter demands for the scaling factors, which will not consider the share between the DHW and SH, but will reduce the differences due to winter SH demands. On the other hand, solar-ice systems in the refurbished building are limited by the absolute system size as collector field area and ice storage volume are large.

A comparison of different hydraulic integration of the solar heat into the primary side of the heating system shows that the system efficiency profits from more options for the release of solar heat. Solar-ice systems in regions with cold and foggy winter seasons profit more from the option of taking solar heat as a source for the heat pump while systems in regions with sunny winters and buildings with low heat demand profit more from the direct use of solar heat for heating the warm storages. For all cities studied the hydraulic that allows solar heat to be released in the ice storage, as a source for the heat pump and directly for heating or preheating the warm storages, shows the highest SPF_{SHP}. For MFB30 the hydraulics that are less flexible reach a 30 % to 60 % lower SPF_{SHP}, for MFB90 those show a SPF_{SHP} that is 20 % to 50 % lower.

Simulations have been analyzed in detail for eight different cities with four different heat demand profiles. For all cases and all locations it was possible to reach SPF_{SHP} of 3.5 to 4.5 with careful sizing of the systems assuming normal or warm weather conditions. Common size to reach energetic efficiencies close to 4 with lowest possible costs are in the range of $0.32\,m^3_{lat}/MWh$ to $0.48\,m^3_{lat}/MWh$ for the ice storage and in the range of $1.5\,m^2/MWh$ to $2.5\,m^2/MWh$ for the collector area. As the efficiency of solar-ice systems is strongly dependent on the weather data, for all systems three different sets of weather data – warm, normal, and cold – have been simulated. The resulting differences of up to 25 % for the same city using cold weather data instead of the normal version, lead to the conclusion that the common way of scaling solar-ice systems for the worst-case scenario of cold years with low irradiation will lead to oversized and consequently expensive systems. Instead, scaling to a typical year representative of a long period, e.g. a decade, would be more appropriate.

For the case of MFB90 and real user behaviour, the levelized cost of heat range from 17 Rp./kWh to 20 Rp./kWh for cities such as Bern, Locarno, Geneva and Basel. Assuming an ideal behaviour for MFB90 the heat cost increases to a range between 19 Rp./kWh and 24 Rp./kWh. For a new building MFB30 and a real user behaviour the cost range from 19 Rp./kWh to 27 Rp./kWh. The MFB30 with ideal user behaviour leads to a cost range of 28 Rp./kWh to 34 Rp./kWh. As a reference, the heat cost of ground source heat pump (GSHP) systems without regeneration for the location of Bern is in the range of 19±2.4 Rp./kWh to 15±1.9 Rp./kWh for MFB30 and MFB90 respectively. For these conditions, solar-ice systems are in the range of 22±0.8 Rp./kWh and 18±0.8 Rp./kWh. Thus, despite the fact that depending on a case-to-case basis, solar-ice systems can currently compete cost wise with GSHPs, ground source heat pump systems without regeneration are expected to be cheaper in most of the cases. On the other hand, if regeneration needs to be added in the GSHP system, then the cost of solar-ice is expected to be the cheaper solution. Future work on ice slurry technology being carried out at our institute is expected to bring the installation cost down by 10 % on the solar-ice systems reducing the cost gap between both technologies. Cost targets to achieve same installation cost as GSHP are expected to be in the range of $500\,CHF/m^3$ to $1000\,CHF/m^3$ and $600\,CHF/m^3$ to $700\,CHF/m^3$ for ice storage and collector field (unglazed and selective) respectively.

The cooling potential of solar-ice systems for multifamily buildings was studied for three cases: i) passive cooling with the same collector field area and ice storage volume as the reference case, ii) passive *free* cooling with an insulated ice storage (in order to have lower heat gains in spring and conserve more ice to cover the cooling needs in summer) and iii) active cooling with the help of the heat pump for DHW provision. The cooling demand of locations with low cooling needs (e.g. Geneva with normal weather conditions) could be covered by passive cooling with an ice storage sized for reaching an SPF_{SHP} of four, while locations with higher cooling demand (e.g. Locarno) needed the active use of the heat pump in DHW operation, causing an about 7 % lower overall system efficiency (including the cooling). The system efficiency considering both heating and cooling ($SPF_{SHP,c}$) increases by about 3 % to 5 % for passive cooling compared to the SPF_{SHP} of a reference system without cooling. Thus, both passive and active cooling with a solar-ice system seem to be an energy efficient solution for different cooling demands. However, solar-ice systems are not likely to be a good alternative for buildings with cooling dominated demands such as office buildings since only about 80 kWh/m_{lat}^3 to 100 kWh/m_{lat}^3 (m_{lat}^3 is the volume of the ice storage that can be iced) can be provided as free cooling.

Among various machine learning schemes the tree boosting method XGBoost showed the best performance when predicting SPF_{SHP}. Already with the limited input set of yearly total heating demand, yearly total irradiation on the collector field and volume of the ice storage, half of the more than 1000 predicted values were within ± 3 % and 90 % within ± 10 %. Furthermore, the method was also tested for its robustness towards a variation in location, when up to eight out of twelve locations simulated were used for training and the other four for testing. There it showed an almost identical performance to a random splitting already with only five training locations, which are very encouraging results towards the development of a feasibility tool for solar-ice systems valid for all of Switzerland.

The Viessmann VitoFriocal system using plastic absorbers without the possibility to use solar heat directly into the warm storages have not been analysed in the present work. We have quantified the penalization of not using solar heat directly into the warm storages with a decrease of the SPF_{SHP} in the range of 10 % to 50 % depending on weather conditions. Nevertheless, the plastic absorbers are way cheaper than uncovered selective collectors and cost comparisons would be of interest. The detailed analysis of this system has not been provided due to missing data for system validation. However, we have recently started a collaboration with an institute in Germany to validate this system with real monitoring data. In particularly, we aim to include this system in the fast algorithm tools in near future.

Recommendations for sizing/designing solar-ice systems

From all the results shown in this report it is possible to give some general recommendations:

- The scaling criteria used in this report is based on relating the collector field and ice storage volume with the total heat demand in MWh. Optimal sizing from an economic and energetic point of view are within a range of ice storage volumes of 0.32 m^3_{lat}/MWh to 0.48 m^3_{lat}/MWh and collector areas of 1.5 m^2/MWh to 2.5 m^2/MWh for most cases. This rule is valid for solar-ice systems with uncovered selective collectors allowing direct use of solar heat to cover DHW and SH demands.

- It has been shown that winter demands play a crucial role on the system efficiency. Thus, we would recommend to scale ice storage volume and collector area respect to the winter heat demand. For example, optimal ranges of collector areas of 1.5 m^2/MWh to 2.5 m^2/MWh and ice storage volumes of 0.32 m^3_{lat}/MWh to 0.48 m^3_{lat}/MWh lead to 62 m^2 to 103 m^2 and 13 m^3_{lat} to 20 m^3_{lat} respectively, for Zurich using normal weather conditions, MFB30 and ideal user behaviour. Scaling with winter demands with the same absolute sizes would lead to 2.3 m^2/MWh_{winter} to 3.9 m^2/MWh_{winter} and 0.50 m^3_{lat}/MWh_{winter} to 0.75 m^3_{lat}/MWh_{winter}.

- The common approach of planers to size heating systems for the worst case climate scenario will lead to significantly oversized solar-ice systems including additional investment costs. Instead, systems should be sized using weather data from a representative period, e.g. a decade.

- The use of solar heat in series with the heat pump (*direct* use in the evaporator by-passing the ice storage) is recommended unless different heat transfer fluids are present on the collector and evaporator loop.

- The use of solar heat directly in the warm storages is recommended if collectors allow to achieve high temperatures like for the case of uncovered selective collectors.

- Passive *"free"* cooling achieved by simply stopping the active melting of the ice during spring is a nice-to-have feature that can increase the overall energetic efficiency of the system including heating and cooling demands by about 2 % to 5 %. A non-insulated ice storage can cover most of cooling demands on cities with low cooling needs and improve the comfort of some more demanding climates such as Locarno. The cooling degree hours were reduced by 15 % to 30 % for warm weather and by 45 % to 85 % for normal weather.

- As a rule-of-thumb, around 80 kWh/m^3_{lat} to 100 kWh/m^3_{lat} can be provided as free cooling. This means roughly about all the latent capacity of the ice storage, since the latent capacity *lost* is compensated or even supersede by the sensible cooling. However, this depends very much on the heating demand during spring which is key to maintain the ice in the storage compensating the heat gains though the walls of the ice storage.

- For achieving higher cooling demands, the heat pump can be forced to operate on DHW summer mode to double the cooling provision with little energetic penalization (from 5 % to 10 %) on the overall efficiency including cooling ($SPF_{SHP,c}$) with respect to the purely heating one (SPF_{SHP}). This active DHW mode can provide, in addition to the free cooling provided by the ice storage alone, up to around 30 % of the DHW needs in summer or about a monthly DHW demand (including circulation losses). Thus, in total one can roughly assume the latent capacity of the storage plus the DHW demand of one month can be provided as cooling demands.

- A first evaluation of the potential of solar-ice systems, with little information available, can be done with simple linear formulas of the form:

$$\mathrm{SPF_{SHP}} = b + w_1 \cdot \mathrm{Q_d} + w_2 \cdot \mathrm{H_{T,\ field}/Q_d} + w_3 \cdot \mathrm{V_{ice,lat}} + w_4 \cdot \mathrm{Q_{sh}/\ Q_{dhw}} + w_5 \cdot \mathrm{H^{winter}_{T,\ field}/Q_d} + w_6 \cdot \mathrm{T^{winter}_{amb}} + w_7 \cdot \mathrm{Q^{winter}_{sh}/Q_{sh}}$$

where all inputs needed from the user such as Q_d [MWh], $H_{T,\ field}/Q_d$, $V_{ice,lat}$ [m^3/MWh], $Q_{sh}/\ Q_{dhw}$, $H^{winter}_{T,\ field}/Q_d$, T^{winter}_{amb} [°C] and Q^{winter}_{sh}/Q_{sh} represent one yearly value each. The values of the constant b and the coefficients w_i for yearly values can be found in the table below. Those are given for two different input sets, one with four input values (Y_2) and one with seven (Y_5).

	b	w_1	w_2	w_3	w_4	w_5	w_6	w_7
Y_2	0.929	-0.014	0.893	1.015	0.294	-	-	-
Y_5	3.131	0.041	0.419	1.004	-0.812	2.223	0.202	-4.085

The description of this model and the resulting error distribution is provided in section 5.5. The models proposed are only valid for solar-ice systems with uncovered selective collectors able to provide direct solar heat to the warm storage. More accurate predictions using advanced machine learning methods are expected to be implemented in a free online tool where cost and many other features could also be included.

Contents

List of abbreviations

$\mathbf{Q_d}$	total heat demand including SH and DHW
$\mathbf{Q_{sh}}$	space heating demand
$\mathbf{Q_{aux}}$	auxiliary heat allocation
$\mathbf{Q}_{sh}^{winter}$	sum of November, December, January and February space heating demand
$\mathbf{Q_{dhw}}$	DHW heat demand
$\mathbf{H}_{T,\ field}$	total irradiation on collector field surface
$\mathbf{H}_{T,\ field}^{winter}$	sum of November, December, January and February irradiation on collector field surface
$\mathbf{T}_{amb}^{winter}$	averaged ambient temperature in November, December, January and February
$\mathbf{T}_{supply,\ sh}$	supply temperature for the space heating
$\mathbf{A_{col,a}}$	absolute collector area
$\mathbf{V_{ice,a}}$	absolute ice storage volume
$\mathbf{A}_{col}$	scaling factor for collector field area
$\mathbf{V}_{ice}$	scaling factor for ice storage volume
$\mathbf{V_{ice,a,lat}}$	absolute latent ice storage volume
$\mathbf{V_{ice,lat}}$	scaling factor for latent ice storage volume
DHW	Domestic Hot Water
SH	Space Heating
MFB	Multi Family Building
GSHP	Ground Source Heat Pump
MFB30	Multi Family Building in Minergie-Standard with a heating demand of about 30 kWh/m^2 a
MFB90	refurbished Multi Family Building with a heating demand of about 90 kWh/m^2 a

1 Introduction

Switzerland has ambitious energy goals for 2050 (Swiss Federal Council, 2013) that require a drastic change of the energy supply system. Recent studies and perspectives on the future Swiss energy system (BFE, 2020, Marcucci et al., 2021) foresee a widespread deployment of heat pumps to achieve full decarbonization with net zero or even negative emissions. It is clear that heat pumps will be a key enabler technology. The main question that remains, however, is which heat sources these future heat pumps will use. Heat pumps can utilize several heat sources such as air, ground, lake, river and waste water or solar energy. None of these sources is available or can be used everywhere. Thus, most of them will play a certain role in the future Swiss energy system.

In this project combinations of solar thermal and heat pump systems with ice storages, so-called solar-ice systems, are investigated for new and refurbished multi-family buildings under different climatic conditions in Switzerland. Solar-ice systems are an alternative to air and ground-source heat pump systems and have the potential to be more efficient with respect to the use of electricity. As opposed to ground-source systems, solar-ice systems do not need space for boreholes drilled around or below the building. This is an advantage when fossil fuel-based heating systems are replaced in existing buildings in urban areas and might be important for the reduction of CO_2-emissions, especially for large refurbished buildings. Solar-ice systems, unlike air and ground source systems, are not affected by noise or ground water regulations. These arguments have been decisive for the growing deployment of these systems in Switzerland despite of their higher installation cost of the commissioned systems compared to air and ground source heat pump systems.

In comparison to ground source, solar-ice systems offer a solution with similar or higher energetic efficiency without the need of regeneration. Hence, one can think of a solar-ice systems as *full freely-regenerated* ground source heat pump system where the borehole field is substituted by solar thermal collectors and an ice storage. This feature might become even more important if future regulations start to impose ground regeneration. Currently, solar-ice systems might be a bit more expensive than ground source systems without regeneration, but they are certainly cheaper if regeneration is necessary. Moreover, near future developments are expected to decrease the solar-ice installation cost by eliminating the need of heat exchangers in the ice storage (Carbonell et al., 2017b).

Solar-ice systems are becoming popular in the Swiss and German markets and experts are needed to design, plan and further develop this type of systems. The Institute for Solar Technology (SPF) has more than a decade of experience in solar-ice systems. A de-icing concept was developed in the High-Ice project (Philippen et al., 2015) funded by the Swiss Federal Office of Energy (SFOE). The de-icing concept was presented in Philippen et al. (2012) and simulation models were developed (Carbonell et al., 2016a,b, 2015) and validated with monitoring data (Philippen et al., 2014). The concept of de-icing is currently marketed by the electricity company EWJR in Rapperswil-Jona with Energie Solaire as main planners. A follow-up project called Ice-Ex (Carbonell et al., 2017a) also funded by SFOE was conducted to analyze experimentally and numerically ice on heat exchangers including ice-on-coils, ice-on-plates and ice-on-capillary mats. An ice storage model with all these heat exchanger types was developed and validated for ice-on-capillary mats (Carbonell et al., 2018b) and ice-on-plates (Carbonell et al., 2017a). Results from the Ice-Ex project were used as a base to develop, within an Innosuisse project, an ice-on-plate ice storage that Energie Solaire is currently marketing.

In summary, a lot has been done in the last decade, with developments that successfully entered the market. However, designing a solar-ice system for a specific building is challenging due to the interactions between the main components of the system like collector field, ice storage (heat exchangers), heat pump, and building demands. The main components are strongly influencing each other in terms of energy flows. Hence, only very experienced planners are able to design and install solar-ice systems that work efficiently and do not need an extensive optimization phase after commissioning. The current project is a step towards covering some of the current open questions and to provide tools for easily conducted feasibility studies to implement solar-ice systems in real buildings knowing little data on the building heat demand.

1.1 Motivation

Different ways of how solar heat is provided to the different components on a solar-ice system are offered on the market. However, possible advantages or disadvantages of different hydraulic connections have not yet

been analyzed in a systematic way. As a consequence it is difficult for the market participants to make proper decisions when assessing the different solar-ice system concepts.

Solar-ice systems are competing with other heat pump based systems such as air or ground source heat pump systems. Therefore, finding reference conditions to compare these solutions is of importance. Usually dynamic simulations tools such as TRNSYS or Polysun use Meteonorm as a source for weather data. However, the selection of the weather data is crucial in order to estimate the performance of solar-ice systems, since these systems rely on the energy extracted from the collector field (from solar and air) as the only heat source. Results presented in Carbonell et al. (2016b) showed an increase of 25 % on the average system efficiency (SPF_{SHP}) using real data for 11 years compared to the climatic data obtained from Meteonorm in Zurich for one year. As an order of magnitude this means that 0.5 m^2 collector area per MWh of total heat demand could be reduced to achieve the same SPF_{SHP}. In a single family home in Zurich this represents a saving of 5 m^2 of collector area corresponding to an 8 % reduction of the total system investment cost. A more recent study presented in Schmidli et al. (2019) compared the Meteonorm and SIA weather data with 10 years of real weather data and differences in self-sufficiency were in the range of 5 % to 15 %. The efficiency of ground source heat pumps on the other hand is not significantly affected by the weather differences between different years in the same location. Thus, for a fair comparison between the systems, appropriate weather data should be used. Within this project, the influence of the selected weather data has been analyzed using SIA weather data (Zweifel, 2010) in Switzerland based on cold, normal, and warm years.

All projects carried out previously at SPF, such as High-Ice Philippen et al. (2015) and Ice-Ex Carbonell et al. (2017a), were based on single family houses. In multi-family buildings cooling needs are becoming of particular interest. In future climate scenarios, increased cooling demand during summer will add stress to energy supply systems (Jakubcionis and Carlsson, 2017). Therefore, new approaches for energy efficient cooling are needed. Solar-ice systems have the potential to partially cover cooling demands using free-cooling and current systems installed in the field are aiming at offering this possibility. However, there is no systematic study that analyses the potentials of cooling demands and the energetic benefits. One part of this project is the analysis of whether the ice produced in the ice storage of a solar-ice system during the heating season can be stored during spring and used for cooling during summer with minimal additional energy consumption.

Due to the complexity of solar-ice systems planners need to use dynamic simulations to assess and dimension the systems even at very early planning stages. Thus, there is a need to provide a tool for a quick feasibility assessment without the need to simulate the solar-ice system. Such a tool for simplified system sizing would help to foster the distribution of solar-ice systems and thus to exploit the potential of solar energy for providing heat in buildings. With the project Big-Ice the data bases and the algorithms for this tool have been created, which will be applicable for Swiss climates.

To cover all previous aspects, systematic studies for multi-family buildings were necessary, analysing the influence of building demands (insulation standards and user behaviour), hydraulic connections, weather data and sizes of ice storage and collector field of solar-ice systems. Within the current project the respective data was generated using numerical models and tools well validated along a decade of simulation work. In order to carry out the large amount of simulations in an automatic way, the open-source python framework *pytrnsys* [1] developed at our institute has been used.

[1] `https://pytrnsys.readthedocs.io/en/latest/`

1.2 Objectives and structure of the report

The goal of this project was to quantify various influencing factors from an energetic and economic perspective using different building types, demand profiles as well as weather data using detailed dynamic system simulations with TRNSYS. Another goal was to develop a fast-algorithm based on the large amount of results from a systematic parametric study. This algorithm aims at predicting the cost-energetic efficiency of the system based on only a few inputs without the need of dynamic system simulation.

The specific objectives of the projects were:

- Objective 1: analyze and quantify the effects of different hydraulics in the primary loop (connections of solar collectors, ice storage and heat pump).
- Objective 2: quantify the potentials of solar-ice systems in terms of energy efficiency and costs in multi-family buildings with different weather conditions.
- Objective 3: analyze and quantify the potentials to cover cooling demands in multi-family buildings.
- Objective 4: develop a fast-algorithm that can be used to assess the energetic performance during a first evaluation phase for multi-family buildings.

This report is presented along 8 chapters. The fast algorithms developed here are based on machine learning, which is a new topic for this kind of application. Thus, the description of the necessary theory to follow the discussions is provided in chapter 2. The theory of solar-ice systems, heat exchangers in ice storages and modelling approaches was described in other reports (Carbonell et al., 2017a, Philippen et al., 2015) and peer-reviewed publications (Carbonell et al., 2018b, 2016a,b, 2015) and will therefore not be repeated here. The methodology of the approach followed during the project is provided in chapter 3. The specific objectives described above have been targeted in chapters 4, 5 and 6. The energetic analysis part of Objectives 1,2 and 3 are covered in chapter 4. Specifically, the analysis of the hydraulic integration of Objective 1 is presented in section 4.3. The energetic efficiency dependency on different demand profiles using two insulation standards (representing new and refurbished buildings) and two kinds of user behaviour is addressed in section 4.2. An analysis of different locations and the dependency to different weather conditions is shown in section 4.4. Objective 3 targeting the cooling potential has been covered in section 4.5. The cost analysis is addressed in chapter 6. The development and results of the fast-algorithms is presented in chapter 5. Finally, the conclusions, outlook and next steps are discussed in chapter 7 and chapter 8 respectively.

2 Supervised Learning

The algorithms proposed within this project to provide fast calculations for assessing the energetic and cost economic performance of solar-ice systems are based on machine learning. The relevant theory of supervised learning is described within the current chapter.

2.1 Introduction

In machine learning, *supervised learning* denotes the task of learning a function F to map an input $\mathbf{x} \in \mathcal{I}$ to an output $y \in \mathcal{O}$ based on known data points $Z_1, \ldots, Z_m$ (Russell and Norvig, 2016). Here, $\mathcal{I}$ is the input and $\mathcal{O}$ the output space. The entirety $\mathbf{Z}$ of these m data points will be referred to as data set in the following. In general, for an input of n dimensions the j^{th} point takes the form:

$$Z_j = (\mathbf{x}_j, y_j) = (x_{j,1}, \ldots, x_{j,n}, y_j) \tag{1}$$

When $\mathcal{O}$ is a discrete space this task is referred to as a *classification problem*, while it is called a *regression problem* for a continuous $\mathcal{O}$. In the current project the variable of interest is the energetic system efficiency, which takes continuous values, making it a regression problem.

When building a model from a data set, the set is commonly divided into a *training* and a *test set*. The model is fit onto the training set in an iterative fashion. Afterwards, the test set is used to evaluate the prediction capabilities of the model. Since the test set only contains data separate from those used for training, it provides an unbiased assessment of the performance of the trained model (Russell and Norvig, 2016).

Essentially, supervised learning is an optimisation problem which aims to minimise a *loss function* $L(\mathbf{Z})$. Typical loss functions are the root mean squared error (RMSE):

$$L(\mathbf{Z}) = \sqrt{\frac{1}{m}\sum_{j=1}^{m}\left(y_j - F(\mathbf{x}_j)\right)^2} \tag{2}$$

and mean absolute error (MAE):

$$L(\mathbf{Z}) = \frac{1}{m}\sum_{j=1}^{m}\left|y_j - F(\mathbf{x}_j)\right|. \tag{3}$$

In general, increasing the complexity of $F(\mathbf{x})$ facilitates a reduction of the loss function (or the prediction error) on the training set. When this is overdone, however, the model may become too dependent on the training set, hence performing poorly when predicting unseen data. This is called *overfitting*. In contrast, when the complexity of the model is kept too low, it can lead to an insufficient prediction capability for both the training and testing set. This is then referred to as *underfitting*. These polar phenomena are illustrated in Fig. 1. In the ideal case, the minimum of the prediction error on the test set is achieved (Yu et al., 2006).

Within the project several machine learning methods have been tested to an exploratory level to find the ones best suited for the desired application. The theory behind these methods is described in the following. The two methods that were investigated more thoroughly, based on the results of the exploratory study, are simple linear regression and XGBoost.

2.2 Linear regression

For a given input $\mathbf{x} = (x_1, \ldots, x_n)$ the *linear regression* model function F takes the form

$$F(\mathbf{x}) = b + \sum_{i=1}^{n} w_i x_i, \tag{4}$$

where b is a constant and $w_i \in \mathbb{R}$ for $i \in \{1, \ldots, n\}$. This means that a linear relation between the output y and each of the respective inputs x_i is assumed. This method is implemented in the current project through a least square fitting method (scipy community, 2021a) and referred to as simple linear regression.

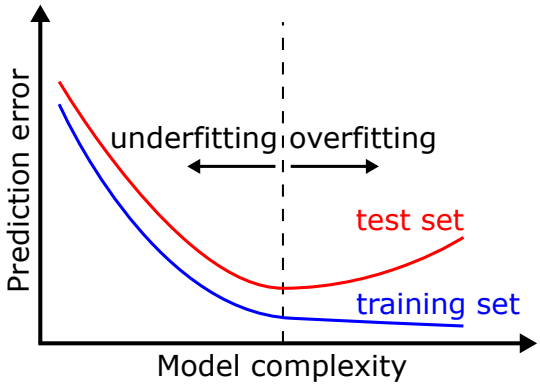

Figure 1: Illustration of the dependence of the prediction error on the model complexity for the training and test set. The domains of under- and overfitting, described in the text, are indicated.

To address the problem of overfitting *regularisation* can be applied. This means that a *penalty term* P including the so-called hyperparameter λ is added to the cost function $L(\mathbf{Z})$. There are several types of regularisation, each with a different penalty term (Zou and Hastie, 2005):

- Penalty term for the *Lasso* model

$$P = \lambda \sum_{i=1}^{n} |w_i| \,. \tag{5}$$

  This is also known as L1 regularisation. This can lead to some of the coefficients being zero. Hence, the Lasso model is also able to perform feature selection.

- Penalty term for the *Ridge* model

$$P = \lambda \sum_{i=1}^{n} w_i^2. \tag{6}$$

  This is also known as L2 regularisation.

- Penalty term for the *Elastic Net* model

$$P = \lambda \left(\alpha \sum_{i=1}^{n} |w_i| + \frac{1-\alpha}{2} \sum_{i=1}^{n} w_i^2 \right). \tag{7}$$

  The Elastic Net model combines L1 and L2 regularization, aiming to combine the advantages of both methods. This is done by tuning the mixing parameter α.

2.3 Multi-dimensional linear interpolation and nearest neighbour

Linear interpolation denotes a straightforward method of constructing unknown data points from known ones. It can be easily understood in one dimension. For two known data points $Z_1 = (x_1, y_1)$ and $Z_2 = (x_2, y_2)$ with $x_1 < x_2$ a value y at the coordinate x can be constructed like

$$y = y_1 + \frac{x - x_1}{x_2 - x_1} (y_2 - y_1) \,. \tag{8}$$

This is, however, only valid if $x \in [x_1, x_2]$. The approach can be extend to n dimensions, where the interpolation can be done with Delaunay triangulation (Klyachin and Shirokii, 2012, scipy community, 2021b). The condition for $\mathbf{x} \in \mathbb{R}^n$ is then to be in the convex hull of the training set $\{\mathbf{x}_1, \ldots, \mathbf{x}_m\}$. This restriction is illustrated in Fig. 2 for $n = 2$. While fulfilling the condition of being within the convex hull of the training set

is still fairly easy in two dimensions, it becomes increasingly difficult for higher n. Consequently, the portion of the input space $\mathcal{I}$ for which an output value can be constructed is drastically reduced by this condition. As shown in chapter 5 this restricts the use of the multi-dimensional linear interpolation for the current project significantly. Hence, this method was not examined beyond the exploration stage.

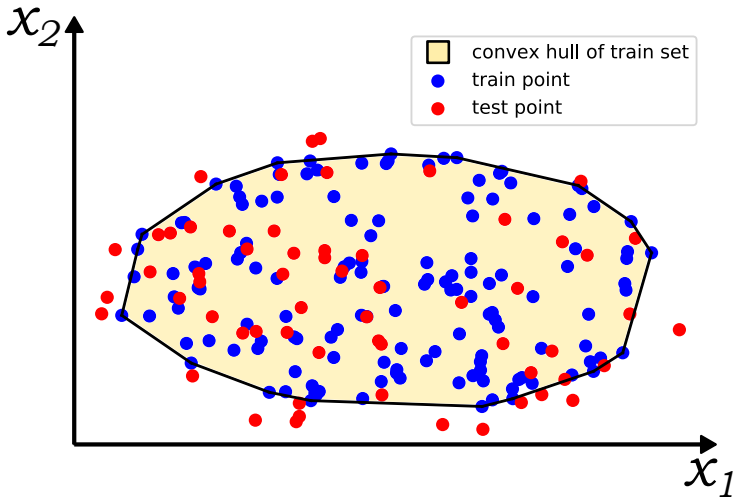

Figure 2: Illustration of the restriction for linear interpolation in multidimensional space: Predictions can only be made for test points that are within the convex hull of the training set. For the two-dimensional case sketched only a few test points are outside, but the problem increases substantially when going to higher dimensions.

Another approach to arrive at an output value y for an unknown data point with input $\mathbf{x}$ is to simply take the output value of the known data point closest in $\mathbf{x}$. There are no restrictions for $\mathbf{x}$ with this approach. Deviations, however, can be large for data points far from the known set. This method is also known as the *nearest neighbour method*. It is used as a reference in the current project for more sophisticated algorithms, since it is readily available and easy to use.

2.4 Neural networks

Artificial neural networks (ANNs) mimic the behavior of a brain by implementing a network of model neurons. These model neurons or nodes are typically linked to a weighted set of inputs. If the sum of the weighted inputs is above a certain threshold the node is activated. The node is in turn connected to other nodes via links. These links act as the inputs for the next layer of nodes, and are again weighted (Russell and Norvig, 2016). Optimizing the weights for each link allows for a training of such a network to map a multidimensional input space to an output space without prior knowledge of the input-output relationship. These networks are effective in tasks involving incomplete data sets or somewhat fuzzy information, and are able to solve highly complex problems such as in image classification, pattern recognition, speech and text systems. They are less effective in handling tasks that require high accuracy and precision, such as in logic and arithmetic (Kalogirou, 2001). The neural network employed in the current project is a multilayer feed-forward neural network.

2.5 XGBoost

The machine learning methods described so far are all based on one function or hypothesis. The essence of *ensemble learning* on the other hand is to employ a combination of multiple hypotheses. In a *boosting system* this is realized through weighting different subsets of the training set. When a function is found that fits well on one subset, the weights of the complementary subset are increased to find another function to fit another subset well. This process is continued to set up an ensemble of functions. The functions in this ensemble are called *weak learners*. Finally, those functions are linearly combined with weights corresponding to the inverse of their respective loss functions to arrive at the so-called *strong learner* (Russell and Norvig, 2016).

One boosting system that is widely employed and is used in this project is *XGBoost* (xgboost developers, 2021). It is based on *decision trees*, which means that the data is arranged into a tree-like structure through differentiating data at nodes. At a node each data point can fall into two categories, and after a few layers of nodes the data is split into several subgroups. With XGBoost N decision trees are set up as weak learners and are finally combined through a weighting algorithm into a strong learner, as illustrated by Fig. 3. The setting up of the decision trees and weighting is done in a computationally resourceful and scalable manner (Chen and Guestrin, 2016).

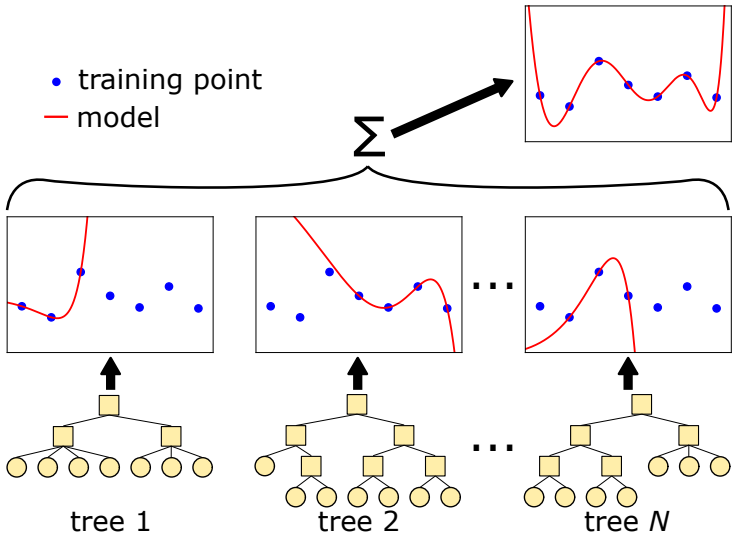

Figure 3: Illustration of the mechanism behind XGBoost. The data are arranged through N different decision trees in a boosting manner resulting in models that represent subsets of the full data well. Eventually, the trees are combined through a weighted sum (indicated by Σ) to form a complete model.

3 Methodology

Dynamic simulations using the simulation environment TRNSYS-17 (Klein et al. (2010)) were used to assess the potentials of solar-ice systems. A reference multi-family building was defined for two different insulation standards and two different user behaviours. In total twelve different locations in Switzerland were used for the analyses. The basic components to model a solar-ice system are: collectors, heat pump, ice storage, sensible thermal storages, building, and system control. The ice storage model was based on ice-on-capillary heat exchangers, which was presented and validated in Carbonell et al. (2018b). The remaining component models were provided in Carbonell et al. (2016a), where a complete solar-ice system based on a de-icing concept was validated with the data acquired by monitoring a pilot plant located in Jona, Switzerland, for a year Philippen et al. (2014). The description of the control for non de-icing solar-ice concepts, as the ones used in this report, can be found in Carbonell et al. (2017c).

The time step of the yearly simulations was set to 120 seconds. As a verification process for the numerical accuracy several systematic checks were done for all simulations. Heat balances are calculated for all individual components, hydraulic loops, and also from the system perspective. The convergence criterion for TRNSYS is set to 5×10^{-4}, which allows to consistently achieve heat imbalances below 1 % with respect to the total heat demand. For the analysis presented in chapter 4 simulations have been performed for eight cities, three different kinds of weather data, and four different demand profiles. Collector field area and ice storage volume are scaled according to the total heat demand of the system, with five variations each, resulting in a combination of 25 cases for each building profile and weather data set. In total, the data set has a total number of 2400 simulations. Different groups of this data sets are used to investigate different dependencies of the system efficiency. For testing the machine learning algorithms in chapter 5 four additional cities have been simulated and hence a set of 3600 simulations was used. For section 4.3 three additional ways of hydraulic integration were simulated for four cities and two demand profiles which add additional 300 simulations. For section 4.5 the cooling potential is analyzed in an independent study with examples for three different cities with different cooling demands for free and heat pump supported cooling.

3.1 Simulation framework and presentation of results

To perform the simulations in an efficient way automatized parameter variations were set up using the pytrnsys [2] framework. The simulations were tracked during their execution including their success status in order to be able to repeat failed simulations without repeating successful ones. In an automatized post-processing, plots were created for checking heat balances and errors, which have been analyzed by spot checks for all cities and all demand profiles simulated, but due to the large number of simulations not for each simulation. Some simulations failed due to very large system dimensions leading to mass conservation problems. As simulations with collector field areas above 350 m^2 were not considered in the analysis because they are not realistic for a building with a maximum roof area of 400 m^2 those runs are not considered anyway.

For showing results of large data sets in Chapters 4 and 5 violin plots are used (Waskom, 2021). These type of plots are similar to box plots, but provide more information about the distribution of the results by showing a smoothed kernel density estimate represented by a contour (often resembling a violin, hence the name). For the plots shown in the current report (example see Fig. 4) the median of the respective distribution is indicated by a long-dashed line, while the 25 % and 75 % quartiles are indicated by short-dashed ones. Consequently 50 % of the points of each distribution fall between the short-dashed lines. The contour allows to represent non-trivial distributions: for the example in Fig. 4 the maximum density of the distribution for the first two (blue and orange) correlates with the median value, while for the green and red violin the maximum of the distribution is shifted to the upper part of the violin and the data points below the median are distributed over a wider range. It should be noted that since the contour is obtained through a smoothing process, its extrema are not representing the real maximum and minimum values of the data set, but are in general slightly overestimating those.

[2] `https://pytrnsys.readthedocs.io/en/latest/`

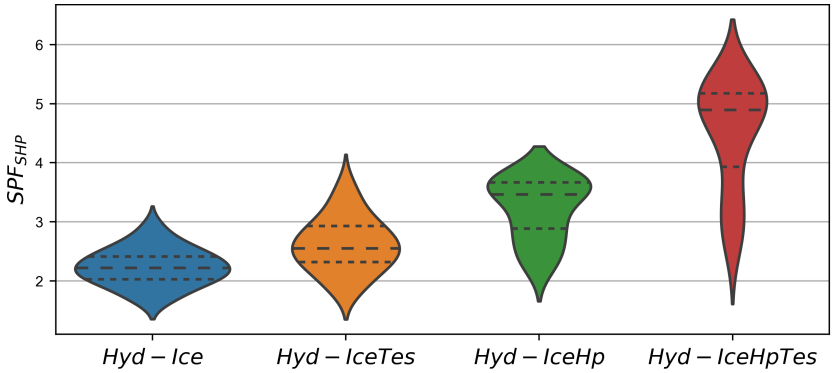

Figure 4: Example for violin plots with data sets of 25 simulations for each violin.

3.2 Possible hydraulic integration

The solar-ice systems that are sold on the market or analyzed in the literature can be classified by the way the solar heat is used. Besides the common use of regenerating the ice storage, solar heat can be used directly to load the warm storage (direct heat mode) or to work in series with the heat pump providing heat to the evaporator (series mode). These combinations lead to four principle system concepts shown in Fig. 5. Viessman (Isocal) sells a system with non-selective unglazed collectors with designs according to Hyd-IceHp. Consolar has a system for single family houses with hybrid collectors and a hydraulic according to Hyd-IceTes. Energie Solaire SA offers systems with Hyd-IceTes and Hyd-IceHpTes hydraulics together with their selective uncovered collectors. Comparisons between these hydraulics are necessary to quantify the benefits of adding hydraulic possibilities.

The main energy source of the system is solar radiation. Some additional energy is extracted from the air, especially when uncovered collectors are used. The authors are only aware of one system installed in the field using covered collectors (Philippen et al., 2014) and therefore all simulations provided in this work are obtained using uncovered collectors. One of the objectives of this paper is to quantify the benefits of the use of solar direct heat and therefore the use of thermal collectors with selective coatings are of importance. In this project, uncovered selective collectors made of stainless steel have been used for all simulations. A part of the total solar radiation is transformed by the collectors to useful heat for the system. This energy is transferred, either to the heat pump if series operation is active (Hyd-IceHp and Hyd-IceHpTes), to the ice storage (possible in all hydraulics), or to the combi-storage (Tes) if the use of solar direct heat is possible (Hyd-IceTes and Hyd-IceHpTes). When the heat pump is running, two operation modes are possible: i) the heat pump uses the solar energy directly as a heat source in a series operation mode (Hyd-IceHp and Hyd-IceHpTes) or ii) the heat pump uses only the ice storage as its direct source (all systems). If none of these heat sources is available, which means that the ice storage is full of ice and solar radiation and ambient temperature are very low, the temperature of the heat pump evaporator drops below the minimum value allowed [3] and the heat pump stops. In this case a direct electric back-up, implemented as two electric rods located in the storages for DHW and SH, can be used.

In all simulations an ice storage with only one heat exchanger was used. This leads to a disadvantage for the two hydraulics Hyd-Ice and Hyd-IceTes, where collector heat does not go directly to the heat pump. With only one heat exchanger in the ice storage the heat pump cannot be running while the ice storage is loaded with solar heat. Hence, on cold and sunny days this might lead to an extended use of the electric rods in the sensible thermal storages for DHW and SH. Nevertheless, in all systems in multi-family buildings we are aware of consider the option of using solar heat directly in the heat pump evaporator.

[3] assumed to be −8 °C

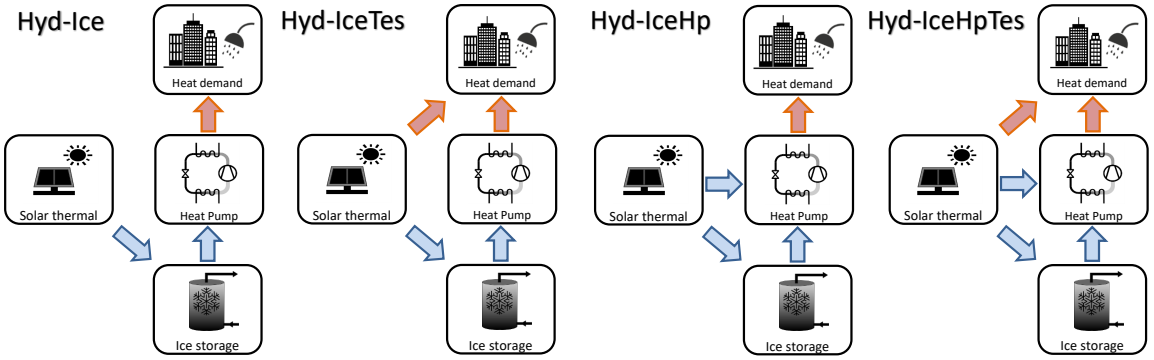

Figure 5: Principle concept of solar-ice systems. The arrows show the heat fluxes that are on different temperature levels, i.e. red and blue for high (>30 °C) and cold (<10 °C) respectively.

3.3 Adapted control strategies for cooling

To provide solar-ice systems with a cooling functionality the ice produced in the heating season is stored for later use in the cooling season. Thus, the ice storage cannot serve as a heat sink for the evaporator during this period. Therefore, the system layout needs to provide a connection of the solar collector to the heat pump. For the simulations estimating the cooling potential of solar-ice systems the hydraulic integration Hyd-IceHpTes was used and the control of the system was adapted to different possibilities (active and passive) for cooling. In order to use the solar-ice system for cooling during summer, two different control strategies have been analyzed. They both extend a base solar-ice control that was described in Carbonell et al. (2017a). Since cooling implies high peak power during summer, large heat exchanger areas are necessary in the system. Therefore, a system without deicing is considered for this double purpose, in which the heat exchangers cover the whole storage volume. During normal heating operation the control has the following priorities

1. Use the solar heat for direct charging of the domestic hot water storage.
2. Use the solar heat for direct charging of the space heating storage (only during heating season).
3. Switch on the heat pump when needed to provide the heat demand with the solar collectors as the main heat source.
4. Operate the heat pump with the ice storage as the main heat source in case of too low source temperatures on the solar collectors.
5. Use the low-grade solar heat to load/regenerate the ice storage.

The cooling was added to the control by avoiding active regeneration of the ice storage below an ice fraction of 50 % from March to September to preserve the ice in the latent storage. Some ice melting from the maximum ice fraction of 80 % to 50 % was included to still enable heat extraction in case of high heating demand during March and April.

The first cooling strategy is the passive (free) cooling mode. In this approach, no additional changes besides the stopping of the ice storage charging in spring are present. The goal of this strategy is to cover as much demand as possible by simply storing ice in the respective storage during the heating period to be used during the cooling period. This approach will have only little influence on the SPF of the heating system but the total amount of cooling capacity will be strictly limited to the ice storage volume, the heat gains from the ground and the heating demand during spring.

The second approach is the passive cooling using an insulated ice storage. This decreases the gains from the ground in spring and more ice can be shifted to summer for cooling. On the other hand gains are also

missing in winter such that the ice storage is cooled down faster and the full freezing capacity is reached more early. This leads to a decrease in the system efficiency due to extended use of the electric backup heaters.

Since for many applications the passive cooling approach will not be able to cover the cooling demand, cooling with the heat pump in DHW mode was added as a second control strategy. In this mode the direct charging of the domestic hot water storage tank by solar collectors is completely suppressed during the summer months on top of the changes described for the first mode. In fact, solar collectors are not used at all during summer months, not even as a source for the heat pump to provide the DHW demands. This forces the heat pump to extract heat from the ice storage during the preparation of domestic hot water which will add more cooling capacity to the system. This will, however, result in a decreased overall heating system efficiency SPF_{SHP}, since the heat pump will run in time periods where solar collectors could cover the DHW demand more efficiently. On the other hand it will provide cooling demands at a very low cost compensating the higher electricity needs for extra DHW needs in summer.

3.4 Weather data

In order to systematically assess the influence of both changing location and also the different weather data profiles at one location, the SIA weather data was used. The SIA weather data uses the standard SN EN ISO 15927-4, to generate a collection of so called *Design Reference Years*. This collection is based on measurement data from the years 1984 to 2003. It contains weather data of 40 different locations in Switzerland, each with an extreme warm, an extreme cold and a normal design reference year as described in Zweifel (2010). From all of these, eight locations have been chosen in order to cover most of the weather types in the inhabited regions of Switzerland: Basel (BAS), Bern (BER), Davos (DAV), Geneva (GVE), Zurich (SMA), Lucern (LUZ), Locarno (OTL) and St. Gallen (STG). For testing the machine learning algorithms four more cities have been simulated: Buchs Aarau (BUS), Lugano (LUG), La Chaux-de-Fonds (CDF), and Sion (SIO).

Zurich, Bern and Basel represent the climatic conditions of the densely populated Swiss Plateau with medium heating demand and low cooling demand. Luzern ans St. Gallen are chosen to include cities from densely populated regions within the alps. The city of Geneva is included as an example of slightly warmer climatic conditions with medium heating demand and medium cooling demand. The location of Locarno in the Swiss south has reduced heating demand and increased cooling demand compared to other Swiss cities while still being in a heating dominant region. Davos represents a typical alpine location with high winter demands, but also high irradiation. Two different types of user behaviour have been used: i) ideal user behaviour with a heating set point temperature at 21 °C and ii) real user behaviour with a heating set point temperature at 23 °C. In the real user behaviour windows are shaded already at a room temperature of 20 °C and in the ideal user behaviour at a room temperature of 22 °C. The new building, MFB30, has an automatic ventilation unit while the renovated building, MFB90, does not. For simulations including cooling, the cooling set point temperature was at 26 °C. The summary of the resulting demands for SMA, GVE and OTL can be found in Table 1. The heating demand for domestic hot water is given for Zurich (SMA), it changes only slightly depending on the water supply temperatures that vary depending on the location.

3.5 Ice Storage Model

The ice storage model used is described in detail in Carbonell et al. (2018a) and the TRNSYS source code is available at Git-Hub[4]. For the simulations a capillary mat model was used. The distance between the capillary mats was set to 10 cm. The distances between the capillary pipes in the mat was assumed to be 3 cm according to products available on the market. The total ice storage volume was set relative to the yearly heating and domestic hot water demand expressed in MWh. Values in the range of 0.2 m^3/MWh to 1 m^3/MWh were considered to cover a large range. Previous studies showed that cost competitive systems compared to ground source heat pump systems for single family houses were in the range of 0.4 m^3/MWh (Carbonell et al., 2017c).

For all simulations an assumption of 80 % maximum ice fraction is assumed. Therefore the ice storage volumes simulated can be either represented as a function of the total volume 0.2 m^3/MWh, 0.4 m^3/MWh, 0.6 m^3/MWh, 0.8 m^3/MWh and 1 m^3/MWh or as a function of the latent volume 0.16 m^3_{lat}/MWh, 0.32 m^3_{lat}/MWh,

[4] https://github.com/SPF-OST/TrnsysType861_IceStorage.git

Table 1: Heating, cooling and DHW demands in SMA, GVE and OTL for MFB30, ideal for normal weather data.

Month	Zurich (SMA)		Geneva (GVE)		Locarno (OTL)		DHW (SMA)
	Heat (kWh)	Cold (kWh)	Heat (kWh)	Cold (kWh)	Heat (kWh)	Cold (kWh)	(kWh)
Jan	6738	0	5788	0	3182	0	1581
Feb	4023	0	2809	0	300	0	1347
Mar	2300	0	303	0	17	0	1406
Apr	358	0	300	0	350	0	1460
May	261	0	0	0	0	60	1535
Jun	0	0	0	270	0	1055	1460
Jul	0	216	0	940	0	1350	1351
Aug	0	0	0	420	0	1640	1577
Sept	0	0	0	0	0	0	1363
Oct	171	0	0	0	0	0	1558
Nov	3465	0	2931	0	942	0	1398
Dec	6188	0	4679	0	3156	0	1525
Total	23505	216	16809	1630	7947	4045	17564

$0.48\,m^3_{lat}/MWh$, $0.64\,m^3_{lat}/MWh$ and $0.8\,m^3_{lat}/MWh$. Results obtained in this report can be used for any ice storage concept that allows a different maximum ice fraction by using as reference the ice storage volumes using the m^3_{lat}/MWh.

Furthermore, it was assumed that the ice storage is buried in the ground next to the building and it has quadratic layout and a height of 2.5 m. The ice storage is not insulated and therefore the heat conductivity of concrete $1.73\,W/(mK)$ and a wall thickness 15 cm is used, resulting in a U-value of $11.5\,W/(m^2K)$. The ground model and the ground data used is described in detail in Carbonell et al. (2016b). The ice storage can be also installed on the cellar. However, assuming a *"typical"* cellar temperature without modelling the coupling of the cellar heat exchange with the building is difficult.

3.6 Performance indicators

The main performance indicator for the systems is the System Performance Factor calculated as described in Malenkovic et al. (2012):

$$SPF_{SHP} = \frac{Q_{dhw} + Q_{sh}}{P_{el,T}} = \frac{Q_d}{P_{el,T}} \tag{9}$$

Q is the yearly heat demand and $P_{el,T}$ the yearly electricity consumption of the heating system. The subscripts SHP, dhw, sh and d stand for solar and heat pump, domestic hot water, space heating, and total heat demand respectively.

The yearly electricity consumption is calculated as:

$$P_{el,T} = P_{el,pu} + P_{el,hp} + P_{el,back-up} \tag{10}$$

where the subscripts pu, hp, aux refer to the circulation pumps (for evaporator, condenser, and solar loop), heat pump, and back-up heating.

$P_{el,back-up}$ is the energy used from the direct electric back-up system. This back-up is implemented with two electrical rods for DHW and SH in the storage. The back-up is switched on when the temperature of the brine at the inlet of the evaporator drops below $-8\,°C$. This is the case when the ice storage is at its maximum allowed ice fraction and the energy gained in the collector field is not sufficient (night or foggy times with low ambient temperatures).

In order to compare results from one simulation with a particular set up to a reference (ref) case, the relative increase of SPF_{SHP} is used:

$$\Delta SPF = 100 \cdot \frac{SPF_{SHP} - SPF_{ref}}{SPF_{ref}}\ [\%] \tag{11}$$

For the analysis of the cooling potential the energy for space cooling was also included into the SPF value as follows:

$$SPF_{SHP,c} = \frac{Q_{dhw} + Q_{sh} + Q_{cool}}{P_{el,T}} \quad (12)$$

3.7 Description of space heating and domestic hot water demands

3.7.1 Reference building

A Multi-Family Building (MFB), as described in Mojic et al. (2018) and updated in Iturralde et al. (2019), was used as reference building for the simulations. It has an energy reference area (A_E) of 1205 m^2 for the new and 1169 m^2 for the refurbished building. The energy reference area consists of common areas and three residential floors with a total of six apartments. Further key figures of the reference building are the ratio of the thermal building envelope to the energy reference area of 1.3 and the window share in relation to A_E of 25 %. A depiction of the building can be seen in Fig. 6. The zones and internal loads correspond to the specifications of the data sheet SIA 2024 (Schneider, 2015). The potential of a solar-ice system was studied for new and refurbished buildings designed with different building envelopes to cover typical heating demands for both. The building was modelled as a solid structure and the building envelope for the new building (MFB30) was designed in such a way that the heating requirement meets the Swiss *Minergie* standard for sustainable buildings, with mechanical ventilation that has a heat recovery efficiency of 80 %. For the weather station in Zurich (SMA) it has a standard space heating demand of 24 kWh/m^2 a for the ideal user behaviour. The building envelope of the refurbished building (MFB90) is designed in a way that it has a common heating demand of an older building after renovation, its standard space heating demand results in 92 kWh/m^2a for Zurich (SMA) with ideal user behaviour.

The results obtained with a detailed building model from IDA-ICE were used to fit a simplified building model using the SIA standard ISO 13790:2008 (D) (2008). The TRNSYS building model used is a modified version of Leconte et al. (2014) as described in Carbonell et al. (2016b).

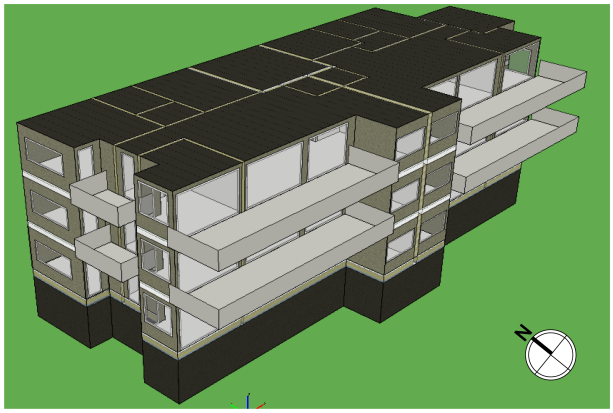

Figure 6: IDA ICE model view of the reference building.

3.7.2 DHW profile

A DHW profile was created using the Load Profile Generator software (Plugradt, 2010). A single profile for each of the six apartments was considered:

- Couple under 30 years old, both at work.
- Family with two children (14-16), one at work, one at home.
- Family both at work, two children (9-12).

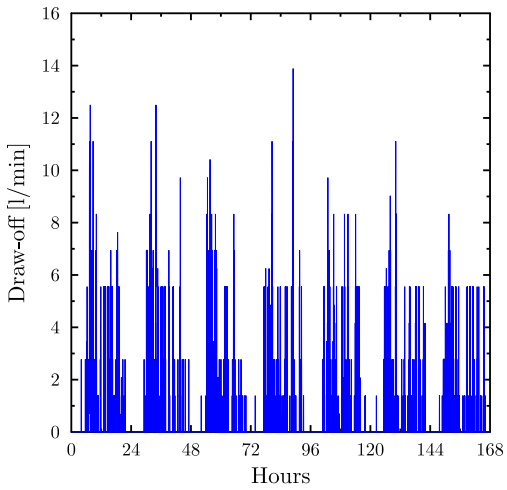

Figure 7: Example of one week of the DHW draw-off profile of the multi-family house.

- Retired couple, both at home.
- Shift worker couple.
- Family, two children (6-12), both parents at home.

The six single profiles of the apartments were merged to one DHW profile including an annual tapped consumption of 17.6 MWh at a delivery temperature of 35 °C. Fig. 7 shows the DHW draw-off profile for the first week of the year. The DHW demand is in the order of 16 kWh per m^2 of heated surface area. A scaling factor of the consumption in l/h was applied to use 45 °C as delivery temperature. Circulation losses were included such that the minimum return temperature of the circulation loop was 53 °C. During the heating period a part of the circulation losses into the building were counted as internal gains. These temperatures were chosen to fulfill the standards that will be used in Switzerland in a near future. The pipe length from the circulation loop has been defined such that the circulation losses were around 30 % of the DHW demand. In total, the DHW demand including circulation losses accounted for 22 kWh/m^2.

3.7.3 Different demand profiles

For this study four different demand profiles have been used assuming new (MFB30) and retrofitted (MFB90) building and two kinds of user behaviour, ideal and real. Adding a heat recovery ventilation unit into an existing building is difficult and expensive and thus, most refurbished buildings do not have one. Consequently, for the MFB90 a heat recovery ventilation unit is not considered. Due to the lower insulation standard MFB90 needs higher supply temperatures for space heating ($T_{supply,sh}$=45 °C instead of 35 °C for MFB30).

The user behaviour has been studied in the SFOE project VenTSol (not published yet) at SPF. Assumptions for real and ideal user behaviour are shortly described in Table 2. T_{room} means the set temperature for rooms in winter and T_{shade} is the temperature below which windows are not shaded in winter.

Table 2: Assumptions for different user behaviour

	ideal	real
T_{room} [°C]	21	23
T_{shade} [°C]	23	21

The four different resulting demand profiles lead to different monthly distributions of the heating demand, which are decisive for the efficiency of the solar-ice system. Fig. 8 shows the monthly distribution of the total heat demand for MFB30 with ideal user behaviour (green) and the relative increase of the other three demand profiles compared with this case. For MFB30 with ideal user behaviour the demand for space heating concentrates to the winter months (November, December, January, and February) while from April to October nearly no space heating is needed. For real user behaviour and buildings with lower insulation standard (MFB90) heating demand is distributed to spring and fall months as well. For both user behaviours with MFB90 and real user behaviour for MFB30 the increase of heating demand is highest in October, followed by April. In January and February the increase of heating demand is lower than on yearly average for comparing MFB30 ideal with both of the real cases. These two months are the months in which the ice storage has the highest ice fraction, therefore the heat pump will have the lowest efficiency during this period. If the ice storage reaches the maximum ice fraction the auxiliary heater has to provide part of the heat and lowers further the system's efficiency. In spring and fall the ice storage is free of ice and solar irradiation is higher and therefore the source temperature of the heat pump and consequently the system efficiency are higher. Comparing MFB30 ideal with MFB90 ideal shows also a lower increase of heat demand in January and December than the yearly average, but the effect is smaller than for the buildings with real user behaviour.

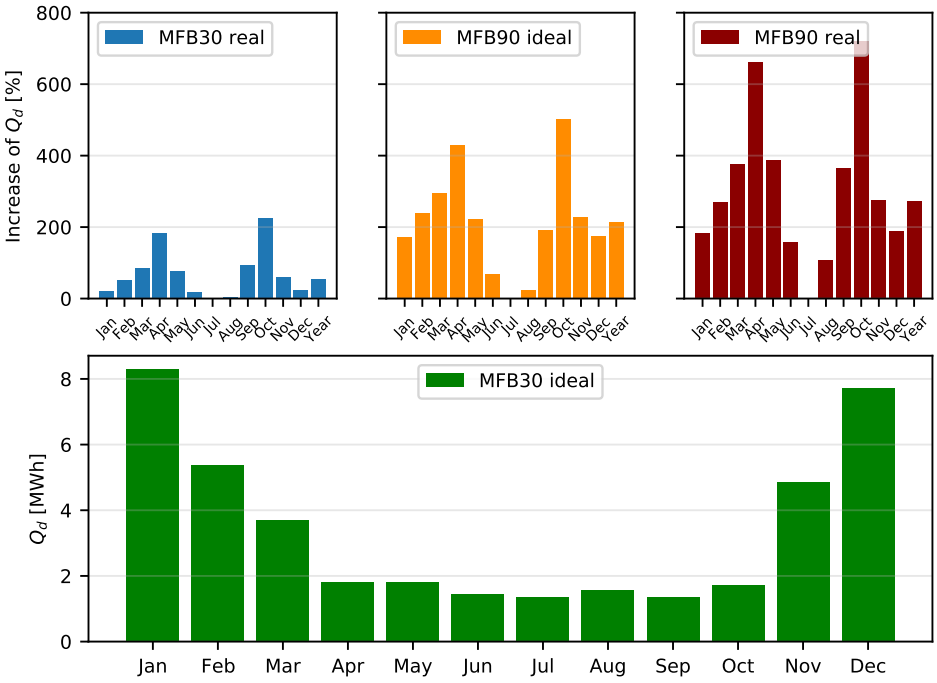

Figure 8: Monthly heat demand (DHW and SH) for MFB30 with ideal user behaviour (green) used as reference. Relative increase of the monthly heat demand for MFB30 with real and MFB90 with real and ideal user behaviour in Zurich (SMA) respect to the reference.

3.8 Collector area and ice storage volume sizes

The range for parameter variation for all analyses was chosen widely in order to cover all relevant cases and to get an extensive data base for the machine-learning analysis. Dynamic system simulations were carried out for a set of ice storage volumes of 0.2 m^3/MWh, 0.4 m^3/MWh, 0.6 m^3/MWh, 0.8 m^3/MWh and 1.0 m^3/MWh and a set of collector areas of 1 m^2/MWh, 1.5 m^2/MWh, 2 m^2/MWh, 2.5 m^2/MWh and 3 m^2/MWh, where the MWh unit refers to the total yearly heat demand Q_d. We have assumed a maximum ice fraction

of 80 %, which related to the latent volume leads to 0.16 m^3_{lat}/MWh, 0.32 m^3_{lat}/MWh, 0.48 m^3_{lat}/MWh, 0.64 m^3_{lat}/MWh and 0.8 m^3_{lat}/MWh. As will be shown in chapter 6 this size range includes with a safe margin cost competitive solutions while achieving system performances in the range of ground source heat pump systems. However, companies such as Viessman (Isocal), tend to size the ice storage as 1 m^3/MWh for single family homes and well above 2 m^3/MWh for multi-family buildings using as source non-selective plastic collectors that are used more as air heat exchangers than as solar collectors. However, the maximum ice fraction they plan with is well below 80 %. Others, such as Energie Solaire SA, tend to size the ice storage with values around 0.2 m^3/MWh making use of a high collector field in the range of 2.5 m^2/MWh. Results from this report show that there is no need to go above 0.8 $m3_{lat}$/MWh for a cost-competitive solution if uncovered selective collectors are used.

The absolute values of collector area in m^2 and ice storage volume in m^3 depend on the total heat demand in MWh, which in turn depends on the location, weather data selected (warm, normal, and cold), building type and user behaviour. For obtaining the absolute sizes of the collector area and ice storage volume, the relative sizes are multiplied to the yearly heat demand using the specific weather data. Therefore, the absolute sizes of collector area in m^2 and ice storage volume in m^3 are different for the cold, warm and normal data sets for each location.

All parameter variations have been simulated for four heating demand profiles (two building types and ideal and real user behaviour) for the cities Zurich (SMA), Bern (BER), Davos (DAV), Locarno (OTL), Geneva (GVE), Lucerne (LUZ), St. Gallen (STG) and Basel (BAS). The letters in brackets refer to the SIA weather data set that was used for the city. The heat demand of the MFB90 with ideal user behaviour is three times higher than those of MFB30 with ideal user behaviour.

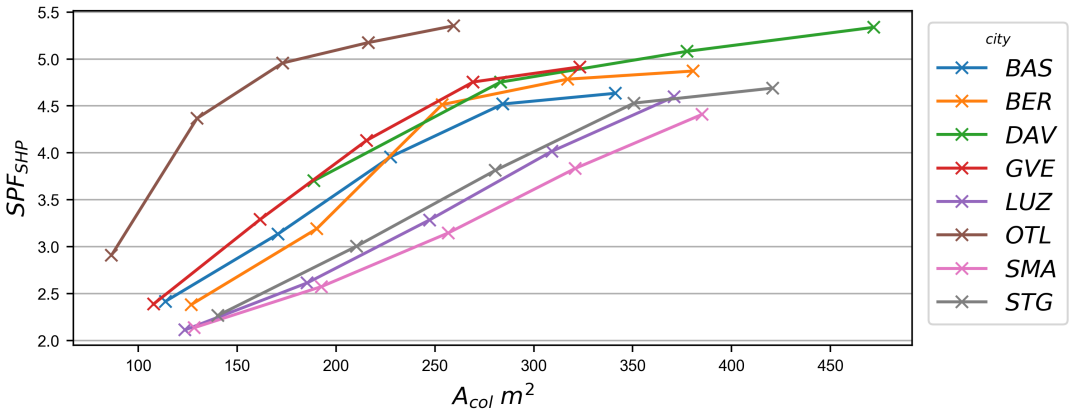

Figure 9: Collector field area and SPF_{SHP} for all eight cities and the building MFB90 with ideal user behaviour. As the size of the collector field scale with the heat demand of the building for some cities the collector field area becomes unrealistically large. Cases with collector field area above 350 m^2 are excluded from further analyses.

Applying the same scaling factors on both buildings lead to unrealistically high surface areas for some systems using the MFB90 (see Fig. 9). As the roof area of the building is only about 400 m^2 the absolute collector field area was limited to 350 m^2. Simulations with larger collector fields are excluded from all further analyses in chapter 4 and 6. For the development of the machine learning algorithm in chapter 5 all simulations are used. This affects only the building MFB90, for MFB30 all cases have a collector field area below 350 m^2.

3.9 Ground source simulations used as base line

Solar-ice systems are an alternative to ground source heat pump GSHP systems. Thus, it is of interest to compare both systems in terms of efficiency and cost. The simulation of the vertical ground heat exchanger is based on the EWS model from Huber and Pahud (1999). This model has been modified at our institute to include g-functions allowing to model the interaction of multiple boreholes. An analytical model presented

in Lamarche and Beauchamp (2007) has been used for the development of the g-functions which we have integrated into the TRNSYS EWS model (Wetter and Huber, 1997).

The borehole field has been sized using the SIA 384/6 standard initially. TRNSYS simulations with borehole lengths in the range of the preestimated length according to the standard have been carried out to find the correct length of the boreholes. Only cases with outlet ground source temperature after 20 years in TRNSYS above 0.5 °C are used for the cost calculation. The total heating demand divided by the total electricity consumed over the 20 years is used to report the overall SPF_{SHP} of the GSHP system.

3.10 Cost analysis

For each system the heat costs are calculated using the annuity method. The electricity prices are taken from the price list of a regional Swiss utility and represent typical prices for medium customers. To simplify the calculation and avoid the difficult assumption of life time of each component and its residual value, it has been assumed that all components last the analysis period and the replacement of components are included in the maintenance cost. However, one should keep in mind that ice storage casing is expected to last longer than any other components and thus the total cost would be reduced by accounting that.

To calculate the present value of the total system PV_{sys} the present values of costs for electricity used by the heating system (PV_{elec}) and maintenance (PV_{maint}) are added to the total investment costs (I):

$$PV_{sys} = I + PV_{elec} + PV_{maint} \tag{13}$$

The costs of electricity is calculated assuming a fixed yearly increase c of the energy price. The present value of electricity costs is:

for $r \neq c$:

$$PV_{elec} = E_0 \cdot \frac{1}{r-c} \cdot \left(1 - \left(\frac{1+c}{1+r}\right)^T\right) \tag{14}$$

for $r = c$:

$$PV_{elec} = E_0 \cdot \frac{T}{1+r} \tag{15}$$

where r is the rate of interest per annum; c the yearly price change rate of electricity; E_0 the electricity costs in year 1 and T the analysis period in years.

The yearly maintenance costs are derived from the investment costs I by a cost factor m. As simplification is assumed that part of the maintenance costs is allocated to replacement procurement's for pumps, brine, etc. A relatively high maintenance factor m of 1 % is therefore chosen. The present value of maintenance costs is:

$$PV_{maint} = I \cdot m \cdot b \tag{16}$$

with:

$$b = \frac{(1+r)^T - 1}{(1+r)^T \cdot r} \tag{17}$$

where m is the yearly maintenance costs factor related to the total investment I.

The annuity of the heating system, i.e. the yearly payment of equal amount over the observation period T, is calculated by multiplying the present value with the annuity factor a:

$$\text{Annuity} = a \cdot PV_{sys} \tag{18}$$

with:

$$a = \frac{1}{b} \tag{19}$$

The heat generation costs are obtained by dividing annuity by the yearly amount of heat delivered by the heating system:

$$\text{Heat cost} = \frac{\text{Annuity}}{Q_d} \text{ in CHF/kWh} \tag{20}$$

4 Energetic potential of solar-ice systems for multi-family buildings

4.1 Heat balance analysis for an example case

The efficiency of solar-ice system depends strongly on source and sink temperatures. For different insulation standards the sink temperature varies. The source temperature depends on weather data and sizes of collector field and ice storage. In order to give an overview of the basic operation modes in a solar-ice system the heat balances on monthly and on hourly basis for selected winter days are discussed in the following. Fig. 10 shows the monthly heat balance of a simulation for Zurich (SMA) with MFB30 and ideal user behaviour with an ice storage scaling factor of 0.6 m^3/MWh and a collector field scaling factor of 2 m^2/MWh. Some heat flows regarding the ice storage occur on positive and negative side:

- $Q_{latent}^{ice\text{-}storage}$: latent heat released/injected depending on whether ice is formed/melted
- $Q_{sens}^{ice\text{-}storage}$: sensible heat accumulated/released depending on whether the water in the ice storage is heated/cooled
- $Q_{env}^{ice\text{-}storage}$: heat losses/gains of the ice storage to/from surrounding ground

On the source side (positive values), besides the terms described above, the heat delivered from the collector Q_{col} in blue, the heat delivered by the electricity consumption of the heat pump compressor $El_{Hp,comp}$ in orange, and the heat delivered from the electric rods in the SH and DHW storages El_{Aux} (violet) are shown. On the demand side (negative values), the demands for space heating Q_{sh} in green, domestic hot water Q_{dhw} in red, pipe and storage losses $Q_{losses}^{summary}$ in bright blue as well as heat from the DHW circulation loop that is going to the building Q_{sh}^{circ} (brown) are plotted.

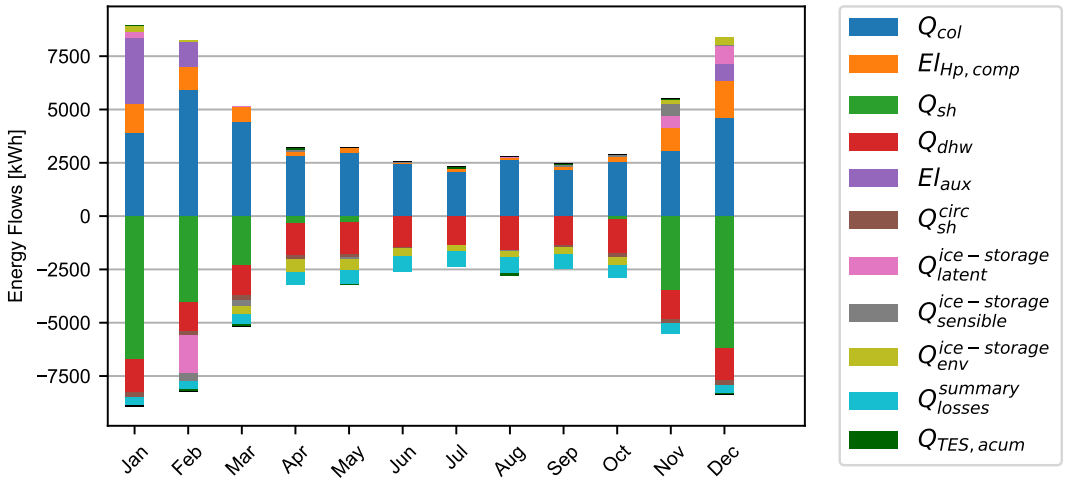

Figure 10: Monthly heat balance for MFB30 with ideal user behaviour for Zurich (SMA) with 25 m^3 (0.6 m^3/MWh) ice storage volume and 100 m^2 (2 m^2/MWh) collector field area resulting in an SPF_{SHP} of 3.1.

In summer, the collector field delivers most of the energy for the system (blue), only little electricity for the heat pump is necessary on top (orange). In November the space heating is needed (green) and therefore sensible (gray) and latent (pink) heat are delivered from the ice storage to cover the heating demand. From December on, the ice storage freezes completely, the heat sources are not sufficient and the electric rods in the buffer storages have to deliver part of the heat (violet). In February the ice storage is melted again (pink on the negative side).

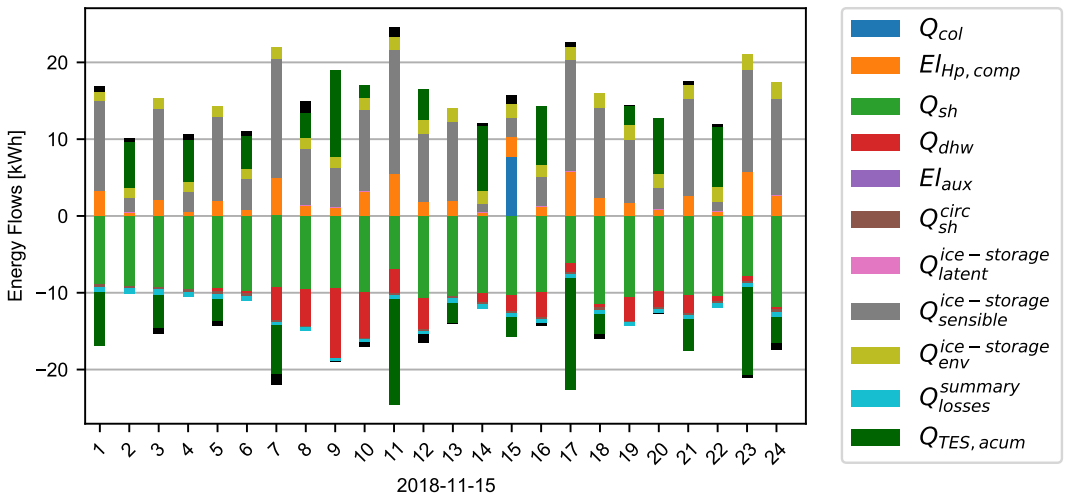

(a)

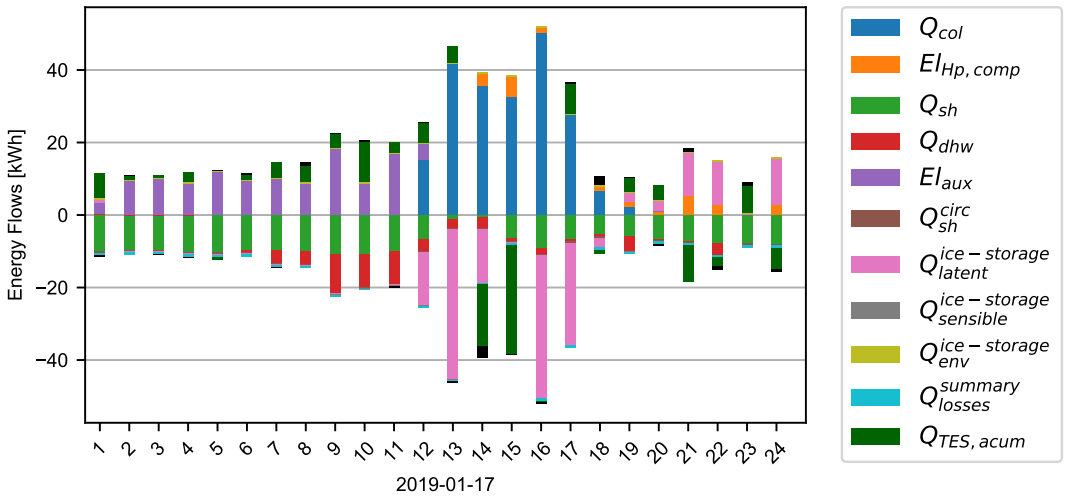

(b)

Figure 11: Hourly heat balance for two days in January and November for MFB30 with ideal user behaviour.

The monthly heat balance gives an impression of how the system works in each season, e.g. when the heating season starts for the building and weather conditions simulated. Fig. 11 shows the heat balances of two days in winter. Fig. 11a shows the 15th of November, which is the day with the first significant demand for space heating (green). The demand is covered mainly by the heat pump using sensible heat from the ice storage as a source. The ice storage is relatively cold already, therefore gaining some heat from the surrounding ground (ocher). This is a day without any direct solar irradiation and little diffusive irradiation (foggy or cloudy). The average dayly temperature is 2.6 °C, the solar collectors can only deliver heat at 15 h. Notice that the heat pump is working continuously during the 24 h with a need of the ice storage during all hours. This kind of behaviour, specially working continuously at night without the possibility to have solar input, and thus demanding more ice storage capacity, could be improved by increasing warm storage capacity as well as using the building mass by means of smart energy management concepts. However, these concepts are beyond the scope of the current project.

The second winter day that was chosen is the 17th of January which starts with a fully iced storage due to a long and very cold winter period. This is first day with high irradiation that leads to melting of ice. Until hour 11 the heat pump has no heat source and such is blocked. The electric rods are delivering the heat needed for space heating. From hour 12 heat from the collector field (blue) starts to melt the ice storage (pink). Afterwards the space heating demand is covered again by the heat pump (orange) using latent heat from the ice storage (pink) as source.

4.2 Impact of different insulation standards

Besides energy concepts for new buildings those for renovated ones play an important role on the market. Due to a higher heating demand and the difficulties in implementing heat recovery ventilation units, concepts for renewable energy systems have to be proven for renovated buildings as well. The simulations in this chapter have been carried out for two different buildings, MFB30 and MFB90, using two different set points for both room and window shading temperatures to show the influence of the user behaviour on the performance of an energy system. Different set points generate different shares for the monthly energy demand, higher room temperature leads to a higher heating demand of the building, where the highest increase of space heating demand can be found in spring and fall. The efficiency of a solar-ice system is strongly dependent on the distribution of the heat demand over the year. High share in winter causes a shift of the main working hours of the heat pump to winter, when the ice storage is cold or even already frozen to the maximum ice fraction and the solar collectors do not gain much heat to support the heat pump with higher temperatures at the evaporator. In cold winter days or with a system with scarce dimensions the direct electric back up heating in the SH and DHW storage will have to take over a certain part of the heat generation. The overall efficiency decreases directly with more heat delivered from the back up (see also Fig. 15).

Table 3: Heat demands for the two different buildings and two different assumptions about the user behaviour for Zurich (SMA) under normal weather conditions. DHW demand is constant about 17.6 MWh/a. Specific sizes of collector field and ice storage volume are 2.0 m^2/MWh and 0.6 m^3/MWh respectively.

	MFB30		MFB90	
user behaviour	ideal	real	ideal	real
total heat demand (MWh/a)	41	64	128	153
SH demand (MWh/a)	23.5	46	111	136
Q_{dhw}/Q_{sh}	75 %	38 %	16 %	13 %
Q_{sh}^{winter}/Q_{sh}	87 %	64 %	65 %	58 %
SPF_{SHP}	2.6	3.7	3.2	3.7

Tab. 3 shows SH and DHW demands for the new building (MFB30) and the refurbished building (MFB90) for the ideal and the real user behaviour. The different user behaviour almost doubles the space-heating demand in case of the new building from 23.5 MWh to 46 MWh. The share of space heating demand in the winter months is much higher in the ideal case due to the lower total space heating demand. Here, the months from November to February are considered as winter months, as temperatures and solar irradiation in November are

critical for the state of the ice storage. For the refurbished building (MFB90) the relative differences are lower due to a general higher heating demand. The yearly heat demand for DHW is about 17.6 MWh for Zurich (SMA). The new building (MFB30) with ideal user behaviour needs about 75 % of its yearly space heating demand for domestic hot water while the refurbished building with ideal user behaviour needs 13 %. Higher ratio of DHW demand to space heating demand and higher winter shares lower the SPF_{SHP} of the system.

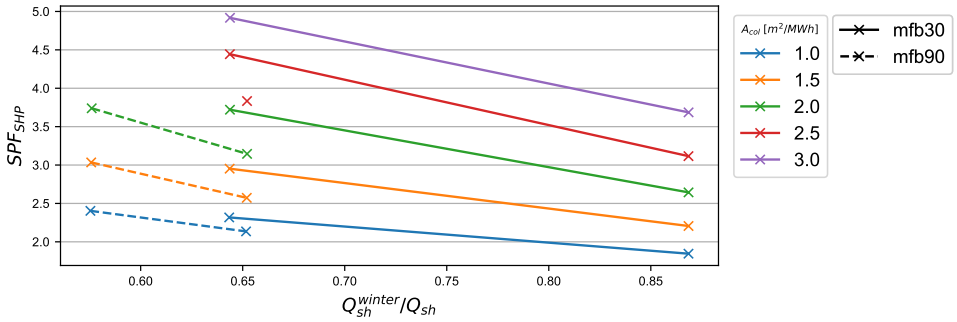

Figure 12: Dependency of the SPF_{SHP} on the winter share of the total heat demand for Zurich SMA (for different buildings and user behaviour). The following parameter are fixed: normal weather data and scaling factor for the ice storage of 0.6 m^3/MWh, what leads to a volume of about 38 m^3 in Zurich SMA or a volume usable for latent heat of 30 $m_{lat}{}^3$.

The dependency of the SPF_{SHP} on the winter share of the total heat demand is shown in Fig. 12 for the example case Zurich (SMA) with an $V_{ice} = 0.6\,m^3$/MWh for different A_{col}. For each building the higher winter share is the one with ideal user behaviour, the lower one for real user behaviour. The SPF_{SHP} increases with decreasing the heat demand winter share of the building (Q_{sh}^{winter}/Q_{sh}) due to low solar irradiation and ambient temperatures in winter period. Focussing on the region with Q_{sh}^{winter}/Q_{sh} of 0.65, one can see that MFB90 with ideal user behaviour has a similar winter share as MFB30 with real user behaviour, but MFB90 shows a lower SPF_{SHP}. The difference between MFB30 and MFB90 for same winter share increases with higher ice storage volumes. The yearly increase in heating demand of 102 % between MFB30 real and MFB90 ideal is smaller than the increase for each winter month with the highest upturn in January (124 %) and December (125 %). However, this is not the only parameter that affect difference between building demands, the ratio of DHW and SH is also very important.

Different buildings and user behaviours have different ratios between domestic hot water heat demand and its space heating counterpart. Well insulated buildings reach more than 75 % in the DHW/SH ratio (Q_{dhw}/Q_{sh}) while MFB90 with real user behaviour has a ratio of 13 % (numbers from SMA as example). As domestic hot water has to be provided at a higher temperature a large share of domestic hot water demand lowers the SPF_{SHP}. Fig. 13 shows the dependency of the SPF_{SHP}, the lower domestic hot water share is always the real building for each configuration and building type. For buildings with same insulation standard, the lower the domestic hot water share, the higher the SPF_{SHP}, therefore the same building with real user behaviour shows higher SPF_{SHP} than with ideal user behaviour. Comparing MFB30 with real user behaviour (Q_{dhw}/Q_{sh} 38 %) to MFB90 with ideal user behaviour (Q_{dhw}/Q_{sh} 16 %) MFB30-real shows a higher SPF_{SHP} with higher Q_{dhw}/Q_{sh} for two reasons: i) The building MFB90 with ideal user behaviour has a higher winter share of the total heat demand than MFB30 with real user behaviour. ii) In the refurbished building (MFB90) heat is delivered at a higher temperature for space heating since a radiant floor is not typically installed (40/45 °C instead of 30/35 °C for MFB30). Therefore, the temperature difference between heat delivered for SH and DHW is smaller and so is the SPF_{SHP}.

To make the source and sink temperatures for the different demand profiles visible Fig. 14 shows the cumulative heat at the evaporator (dashed lines) and the condenser (solid lines) of the heat pump normalized to the total heat demand (Q_d) vs the temperature at which the heat was delivered for all buildings and user behaviours for Zurich (SMA) with normal weather data. The increase of Q_{cond} between 55 °C to 60 °C shows the share of DHW demand. The increase of Q_{cond} at about 30 °C to 40 °C shows the share of space heating demand. For MFB90 the delivery temperature for space heating is higher than for MFB30. MFB30 with ideal

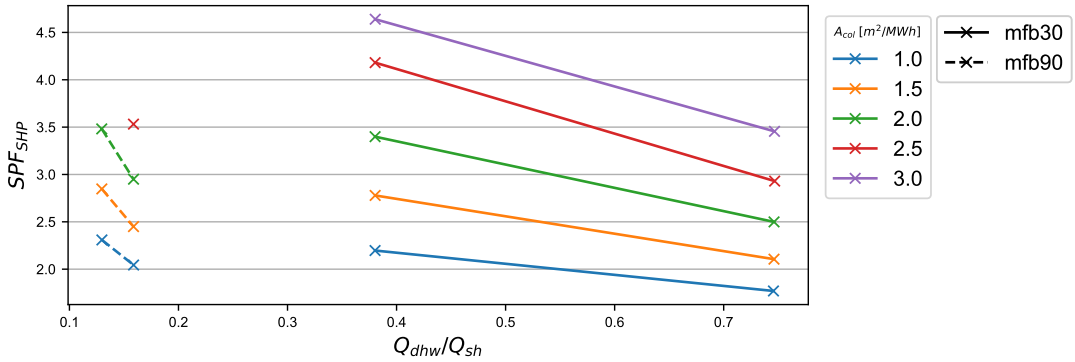

Figure 13: Dependency of the SPF_{SHP} on the domestic hot water share of the total heat demand for Zurich SMA for the buildings MFB30 and MFB90 and different user behaviour. The following parameter are fixed: normal weather data and scaling factor for the ice storage of 0.6 m^3/MWh.

user behaviour has clearly the highest DHW share. Together with the much higher Q_{dhw}/Q_{sh} and the higher winter share of space heating demand this explains the lower SPF_{SHP} for MFB30 with ideal user behaviour.

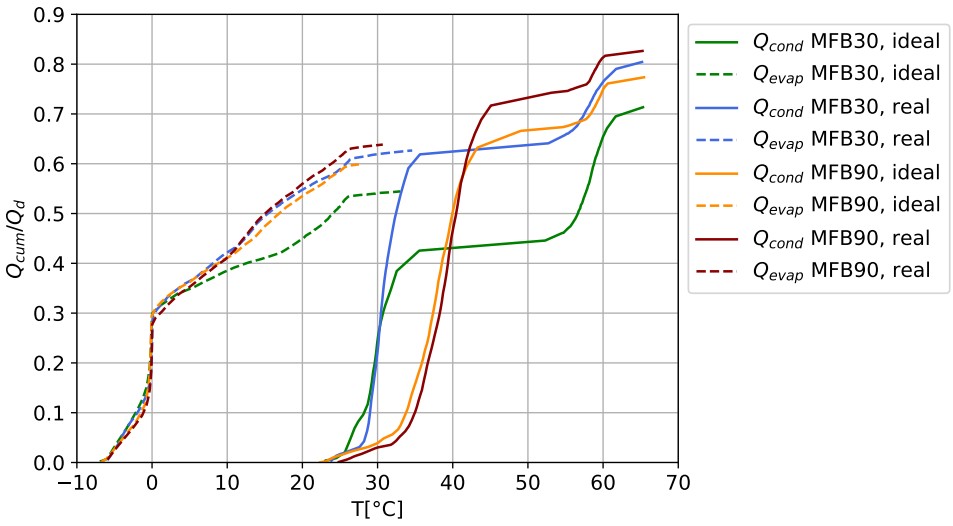

Figure 14: Normalized cumulative amount of heat delivered at the evaporator (dashed lines) and the condenser (solid lines) of the heat pump vs temperatures at which this heat is delivered. The different colors indicate different demand profiles (MFB30 and MFB90 and ideal and real user behaviour).

System efficiency of the solar-ice system is strongly dependent on the distribution of the heating demand over the different months. The effects of the different influencing factors are interacting and are hence difficult to predict. Ice storage and collector field area are scaled to the total yearly demand in all simulations. This scaling method penalizes systems with high insulation standard resulting in a high winter share of heat demand. Scaling to the total winter demand instead of the yearly demand leads to lower differences in the system efficiencies between the different buildings and systems. Table 4 shows the results for scaling to total demand in comparison to those for scaling with winter demand. The scaling for winter demand is chosen such that the absolute ice storage volume and collector field area are similar for MFB30 and MFB90 with real user behaviour. The differences in SPF_{SHP} between MFB30 and MFB90 are 33 % smaller using a scaling to winter demand.

Table 4: Comparison of results and absolute ice storage volume and collector field area for scaling with yearly total heat demand and winter total heat demand.

scaled to Q_d: A_{col}=2.0 m^2/MWh, V_{ice}=0.6 m^3/MWh				
	MFB30		MFB90	
	ideal	real	ideal	real
SPF_{SHP}	2.6	3.7	3.2	3.7
$V_{ice,a}$ [m^3]	25	38	77	92
$A_{col,a}$ [m^2]	82	128	256	306
scaled to Q_d^{winter}: A_{col}=3.5 m^3/MWh, V_{ice}=1.1 m^3/MWh				
	MFB30		MFB90	
	ideal	real	ideal	real
SPF_{SHP}	3.0	3.6	3.4	3.6
$V_{ice,a}$ [m^3]	29	39	86	92
$A_{col,a}$ [m^2]	92	124	273	294

Besides winter share and Q_{dhw}/Q_{sh} the amount of heat provided by the auxiliary heater is a main influencing factor on the SPF_{SHP}. Fig. 15 (left) shows the dependency of SPF_{SHP} on A_{col} (m^2/MWh) for different V_{ice} (m^3/MWh). The SPF_{SHP} is increasing with higher collector field and ice storage scaling factors but is saturating at an SPF_{SHP} of about 4.5. Fig. 15 (right) shows the ratio between heat provided by the auxiliary heater and the total demand vs the collector field scaling factor A_{col} for different ice storage scaling factors V_{ice}. For systems with A_{col} of 2.5 m^2/MWh or bigger and V_{ice} of 0.6 m^3/MWh or larger the auxiliary heater for domestic hot water or space heating is not used anymore. These system dimensions correlate with the saturation effect in the SPF_{SHP} when extending the scaling factors. As long as the amount of auxiliary heating is lowered by increasing the system size the benefit to the system efficiency is large, beyond that only little is gained by further up-scaling the collector field area and ice storage volume. To allow better performance with larger components the control of the system could be changed. In the simulations of this study heat from solar to ice storage has always priority in order to avoid reaching the maximum ice fraction in the storage. In largely sized systems, where the maximum ice fraction is not reached in winter, a change of this priority would lead to more solar heat directly used for preheating or heating directly, therefore the SPF_{SHP} would benefit more. The ice storage volume is stated as scaling factor to the total volume here. The maximum ice fraction was 80 % in all simulations, therefore, the maximum volume for providing latent heat is only 80 % of m^3/MWh (V_{ice})

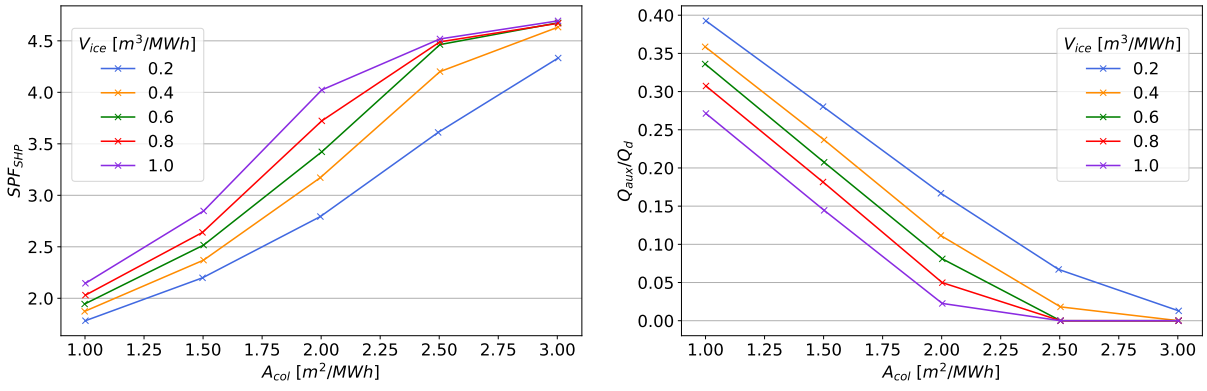

Figure 15: Comparison of SPF_{SHP} (left) and Q_{aux}/Qd (right) vs the collector field scaling factor for different ice storage scaling factors. Multiply by 0.8 to convert storage volume to m^3_{lat}/MWh.

Fig. 16 shows the distributions in SPF_{SHP} of all four cases (combinations of MFB30 and MFB90 with ideal and real user behaviour) for all cities, including all combinations of scaling factors for ice storage volume and

collector field, except those that lead to a collector field area above 350 m^2. The new building (MFB30) with ideal user behaviour shows the lowest SPF_{SHP} values. The statistical distributions of all simulations sorted by the different heat demand profiles show the same trends as the examples for Zurich (SMA) discussed above. The system efficiency is lowest for MFB30 with ideal user behaviour. But as the total heat demand is much lower than for the other buildings it still has the lowest absolute electricity demand for the heating system. Furthermore, due to the smaller absolute ice storage volume and collector field area it is the system with lower installation cost.

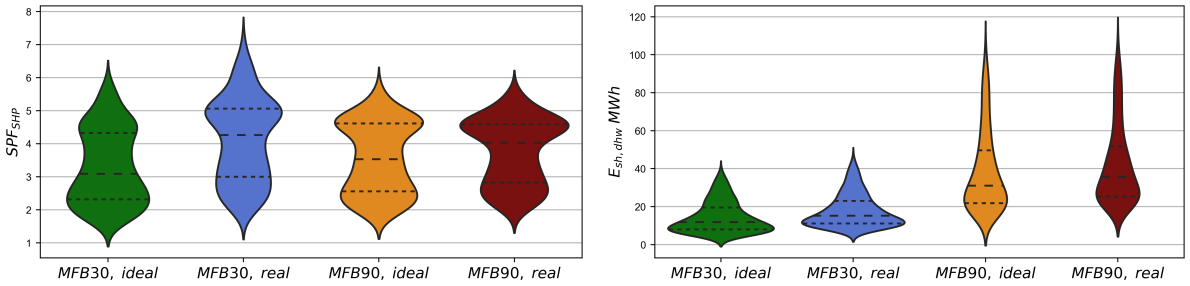

(a) (b)

Figure 16: Comparison of the SPF_{SHP} (a) and $E_{sh,dhw}$ (b) for different buildings and different user behaviour for all eight cities for all weather conditions.

The system efficiency of solar ice systems are strongly dependent on the yearly profile of the heat demand. For different building-types the same scaling factors do not lead to similar SPF_{SHP} values, hence the type of building has to be considered for reaching the goal of an energy efficient and economic solar-ice heating system.

4.3 Analyses of hydraulic configurations

All simulations from this section have been carried out using the multi-family buildings MFB30 and MFB90 described in section 3.7.1 with ideal user behaviour at four different cities. The normal weather data from the SIA data base Zweifel (2010) for the Zurich weather station SMA was used to represent Zurich, BER for Bern, OTL for Locarno, and DAV for Davos.

The different hydraulic integrations have been explained in section 3.2 and shown in Fig. 5. Fig. 17 shows the results of the hydraulic comparison for Zurich (a and c) and Locarno (b and d). For the hydraulic scheme Hyd-Ice solar heat is only going to the ice storage, for Hyd-IceTes solar heat goes to ice storage with first priority and also to direct heating of the SH and DHW storage. Hyd-IceHp allows solar heat to go to the ice storage and to the heat pump as source and Hyd-IceHpTes allows solar heat to go to the ice storage, the heat pump and the warm storages.

The comparison shows that the more possibilities are allowed by the hydraulic integration, the higher is the SPF_{SHP}. In the simulations for Locarno with MFB30 Hyd-IceTes shows better results than Hyd-IceHp. For MFB90 with much higher heating demand Hyd-IceHp shows better efficiency than Hyd-IceTes like for Zurich as well. With the very low heating demand and high irradiation in winter months in Locarno the MFB30 case can profit more from directly used heat than from the option of solar heat going to the heat pump. Zurich has low irradiation in winter, therefore the system for MFB30 with low heating demand profits already more from the option of solar heat going to the heat pump than from the option of using solar heat for direct heating or preheating of the warm storages.

The sensitivity of the SPF_{SHP} on the collector area for each hydraulic setup is shown in Fig. 18 for Bern and Locarno. The more options a hydraulic configuration has for the release of solar heat, the stronger is the influence of the collector field area on the SPF_{SHP}. For the hydraulic Hyd-IceHpTes in Bern, MFB30 an increase of the scaling factor for the collector field of 0.6 m^2/MWh, or about 19 m^2 in this case, leads to an increase of SPF_{SHP} of about 1. The slope of the dependency between the scaling factor of the collector field

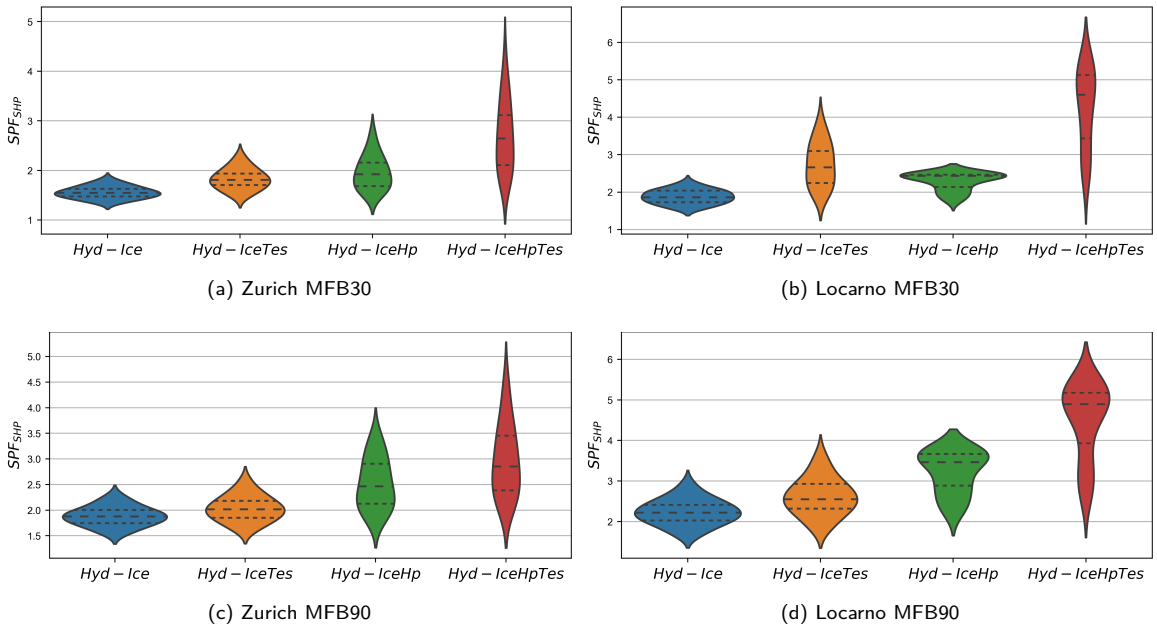

(a) Zurich MFB30

(b) Locarno MFB30

(c) Zurich MFB90

(d) Locarno MFB90

Figure 17: System performances for ice storage volumes of 0.2 m^3/MWh to 1.0 m^3/MWh and collector areas of 1.0 m^2/MWh to 3.0 m^2/MWh for the different hydraulic configurations for ideal user behaviour in the cities of Zurich and Locarno with the normal year defined in SIA and MFB30 with ideal user behaviour.

area and the SPF_{SHP} differs for different cities. For the hydraulic Hyd-IceHpTes the average of all eight cities is that an increase of 0.75 m^2/MWh leads to an increase of SPF_{SHP} of 1.

One should keep in mind that the system performance of the hydraulics Hyd-Ice and Hyd-IceTes are limited as the ice storage in the simulations contains one heat exchanger only. Therefore, the solar heat can't be used to regenerate the ice storage while the heat pump is in operation. Considering this option with two independent heat exchangers in the ice storage would certainly bring additional efficiency to those hydraulic configurations. However, since allowing a direct solar use in the evaporator doe not add additional cost, not allowing this option is not recommended unless one uses a different heat transfer fluid on any of the loops. For example an ice-slurry concept with the supercooling method (Carbonell et al., 2017b, 2020a) would use water in the heat pump evaporator and thus has a separate circuit from the antifreeze solution of the collector filed. om In this case, the solar heat is injected to the ice storage via an external heat exchanger and the heat pump circuit goes without any heat exchanger into the slurry tank. since, this concept is out of the scope of the current project, this configuration has not been analysed.

Based on the results presented in this section regarding different hydraulics, it is clear that an appropriate implementation of the hydraulic is of high importance. The hydraulic Hyd-IceHPTes, allowing solar heat to be transferred to the ice storage, to the warm storage for direct solar heating and to the heat pump, shows the best efficiency for all four cities. Allowing this more complex hydraulic can save costs due to smaller dimensions of ice storage volume and collector field area for reaching SPF_{SHP} values in the range of 3.5 to 4.0. One can see that going directly from the collectors to the heat pump evaporator is a recommended option with almost no extra cost. The main question that remain is under which conditions solar heat can be provided directly to the warm storages. Results from this report have been obtained using uncovered selective collectors that allow solar heat at higher temperatures. In future works it would be of interest to include simulations using non-selective uncovered collectors and compare cost and efficiency. For all other analysis in chapter 4.2, 4.5, 4.4 and chapter only the hydraulic allowing all possibilities Hyd-IceHPTes is used.

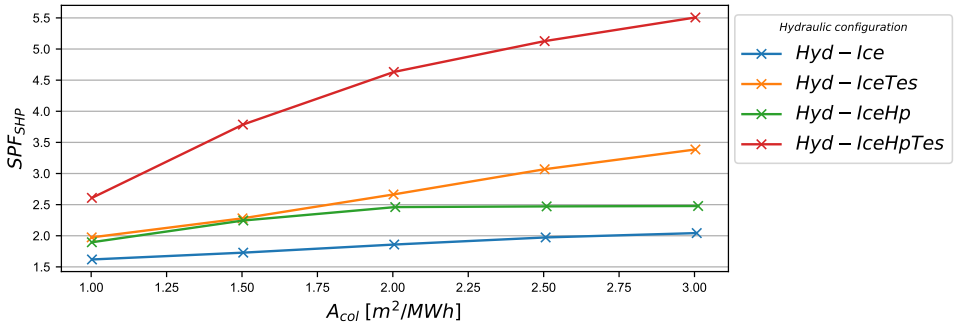

(a) Locarno, 0.6 m^3/MWh

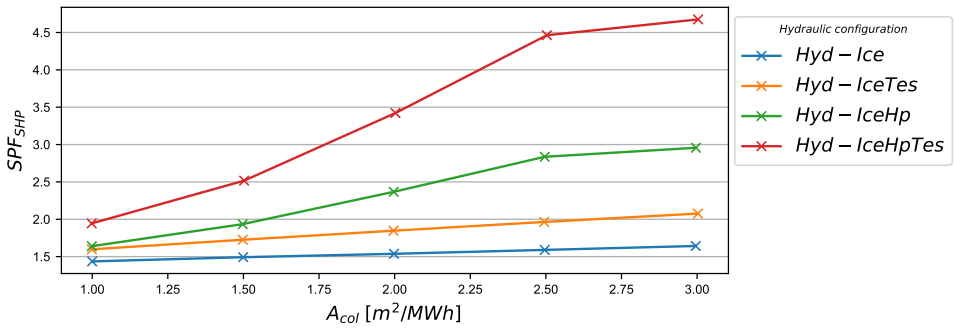

(b) Bern, 0.6 m^3/MWh

Figure 18: System performance as function of collector area and different hydraulic configurations for ice storage sizes of (a) 0.6 m^3/MWh and for OTL (b) 0.6 m^3/MWh for Bern (BER).

4.4 Influence of different locations and weather data

In this section only data for the building MFB30 with ideal user behaviour are used for discussing the influence of different locations and weather data. All eight cities are considered and the full range of scaling factors, 1.0 m^2/MWh to 3.0 m^2/MWh for collector field and 0.2 m^3/MWh to 1.0 m^3/MWh for ice storage, is used.

4.4.1 Analysis of different locations

As described in section 3.4, the SIA standard Zweifel (2010) features three weather data sets – cold, warm, and normal – for each of the 40 weather stations in Switzerland that are part of it. Results including all simulations for MFB30 with ideal user behaviour using cold, warm, and normal weather data sets are shown in Fig. 19. The scaling of collector field and ice storage volume is applied to the heating demand for different weather data. The largest resulting collector field area with the used scaling is 180 m^2 for Davos (DAV) under cold weather conditions.

Davos (DAV), which is located in the Swiss Alps and characterized by having very cold and sunny winters, shows the best performance of all simulated locations with a median SPF_{SHP} of 4.4, closely followed by Locarno (OTL) with a median SPF_{SHP} of 4.2. Davos has a cold climate, resulting in a high heating demand, but very high irradiation in winter months (November to February). Snow covering the solar-thermal collectors is not considered in the simulations. Therefore, these results are only valid if snow is removed periodically. The second best results are obtained for Locarno, which is south of the Alps. It has high solar radiation in winter and warmer temperatures compared to the other cities with SPF_{SHP} ranging from 2.2 for cold years, up to 6.0 for warm years with a median SPF_{SHP} of 4.2. The SPF_{SHP} for the remaining cities are on the same order of magnitude and significantly lower than those obtained for Davos and Locarno, with a median SPF_{SHP} in the range of 2.5 to 3.2. Cities that are affected a lot from fog in the winter-months have low winter irradiation (Zurich and Lucerne followed by Bern and St Gallen) and such have lower SPF_{SHP} median values.

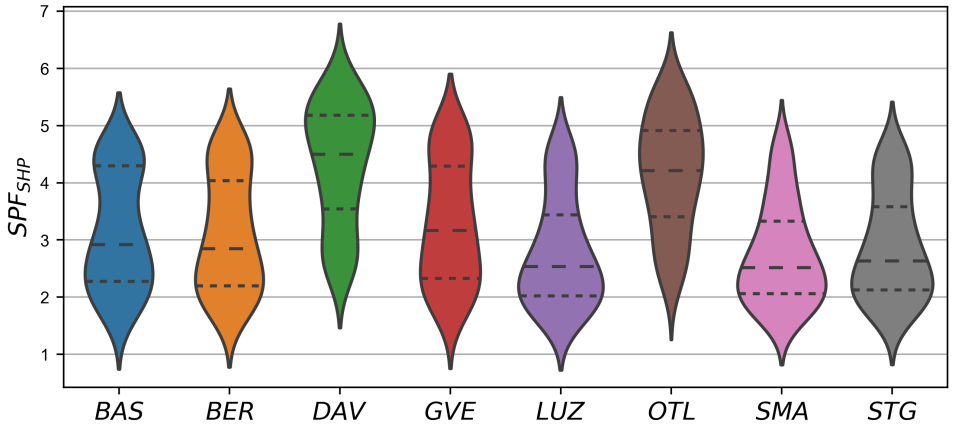

Figure 19: System performance as a function of location for all the simulated ranges of 1.0 m^2/MWh to 3.0 m^2/MWh and 0.2 m^3/MWh to 1.0 m^3/MWh for MFB30 and ideal user behaviour using cold, warm and normal weather data sets. 3.1

The irradiation data for four cities are compared in Table 6.

For all buildings and cities with normal weather data some system configurations can be found with a resulting SPF_{SHP} between 3.5 to 4.5 for four cities. Examples for scaling factors representing the system configuration that is closest to SPF_{SHP} of 4 are shown in Table 5.

Table 5: Example dimensions for reaching a SPF_{SHP} value of about 4 for different cities with normal weather data sets. The ice storage volume refers to the whole ice storage, to convert to latent heat (m^3_{lat}) one needs to multiply the ice volume by 0.8.

City	MFB30, ideal			MFB30, real			MFB90, ideal			MFB90, real		
	Q_D MWh	$A_{col,a}$ m^2	$V_{ice,a}$ m^3	Q_D MWh	$A_{col,a}$ m^2	$V_{ice,a}$ m^3	Q_D MWh	$A_{col,a}$ m^2	$V_{ice,a}$ m^3	Q_D MWh	$A_{col,a}$ m^2	$V_{ice,a}$ m^3
SMA	41	123	33	64	128	51	128	321	51	153	383	122
BER	37	56	22	64	96	51	127	254	51	155	234	93
OTL	24	24	19	49	73	10	86	130	34	116	116	93
DAV	47	71	28	89	90	53	189	283	38	227	227	91

4.4.2 Influence of warm, normal and cold data sets

All simulations shown in Fig. 19 have been presented in Fig. 20 using the total winter (November, December, January, and February) irradiation reaching the collector area ($H_{T,field}^{winter}$) on the x-axis. Results correlate well using winter irradiation on the collector plane as an independent variable for each weather data set, i.e. cold, normal, and warm and for each ice storage volume. Notice that each irradiation value has five points on the vertical representing the 0.2 m^3/MWh, 0.4 m^3/MWh, 0.6 m^3/MWh, 0.8 m^3/MWh and 1.0 m^3/MWh ice storage volume scaling factors used. Cases with similar winter irradiation show higher SPF_{SHP} values for warmer weather data.

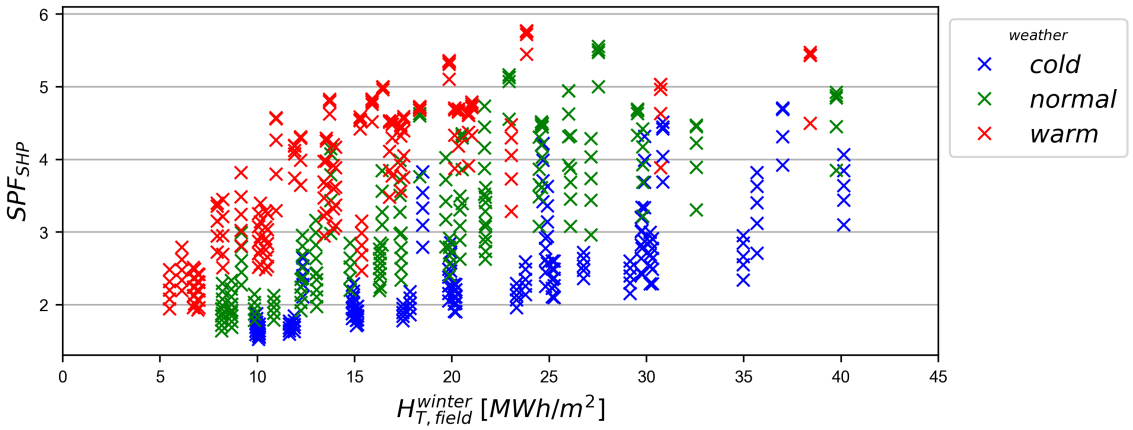

Figure 20: System performance as a function of the winter irradiation (November to February) on the collector surface for the 8 different cities, collector areas of 1.0 m^2/MWh to 3.0 m^2/MWh and ice storage volumes of 0.2 m^3/MWh to 1.0 m^3/MWh.

Simulation results for all cities, ice storage volumes of 0.6 m^3/MWh, and a collector field area of 2.0 m^2/MWh are shown in Fig. 21 for cold (blue), normal (green), and warm (red) years. The SPF_{SHP} is shown in Fig. 21(a) and the relative change of the system performance ΔSPF is shown in Fig. 21(b).

Blue bars show the ΔSPF between using the cold and the normal weather data, and red bars show the ΔSPF between using the warm and the normal weather data. Using the cold instead of the normal year leads to an average decrease of the ΔSPF for all cities of 20 %. For all cities except Davos, the decrease on SPF_{SHP} is in the range of 10 % to 30 %. Using the warm compared to the normal year, leads to an average increase of the ΔSPF of 25 %. Changes in SPF_{SHP} between normal and cold/warm weather data below 5 % can be observed for Davos and Locarno and correspond to very small changes in the winter irradiation between the different weather data (0.3 % to 5.5 %).

The classification as warm or cold years is based on temperature levels, while solar-ice systems are mainly influenced by the winter solar irradiation. Table 6 summarizes the the specific irradiation into collector plane ($H_{T,field}/m^2$), the specific winter irradiation into the collector plane ($H_{T,field}{}^{winter}/m^2$) and the total heat demand for four cities including all sets of weather data. Davos has a very high solar radiation in winter which is even higher in the cold as compared to the normal year. Geneva has a higher irradiation in winter in the normal than in the warm year. Davos shows low differences in SPF_{SHP} and also low differences in the winter irradiation between the different weather data sets. Geneva shows its highest winter irradiation for the normal weather data set, but the SPF_{SHP} is nevertheless higher for the warm and lower for the cold weather data because the building has a similar winter share for warm weather data like for normal. The differences in system efficiency appear to be bigger for cities with low winter irradiation than for those with a generally high winter irradiation. In many cases this is due to the higher use of direct electric heat in winter, since it is more dominant for low winter irradiation.

The large differences between the SPF_{SHP} obtained using normal and cold years suggest that the tendency of planners to use cold year data to size the system according to a worst case scenario leads to an oversize of the complete system entailing the corresponding additional cost. Instead, it would be better to size the

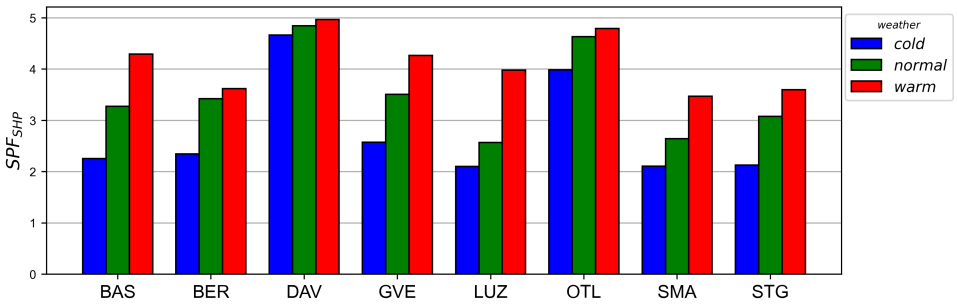

(a) SPF_{SHP} for cold, normal and warm weather data

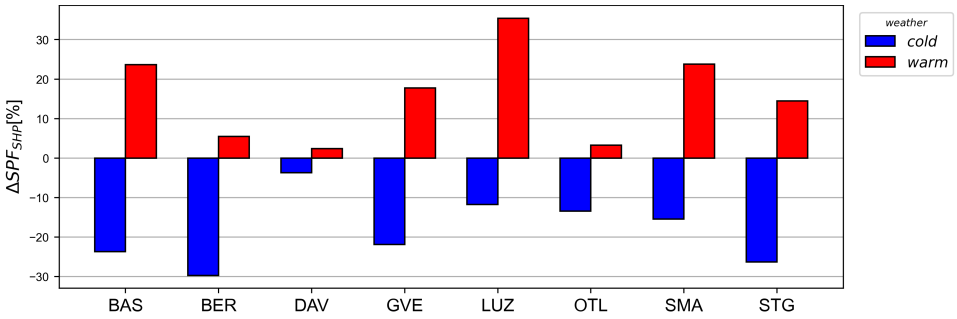

(b) differences of SPF_{SHP} between cold/warm and normal

Figure 21: Influence of cold, normal and warm weather data sets on system performance for all cities for 0.6 m^3/MWh and 2 m^2/MWh with building MFB30 and ideal user behaviour.

Table 6: Global yearly irradiation into collector plane ($I_{T,Col,W}$) and global winter irradiation into collector plane ($I_{T,Col,W}$) for some cities and weather data files, as well as total heat demand and the winter share of space heating demand.

City	Type	$H_{T,field}/m^2$ [kWh/m^2]	$H^{winter}_{T,field}$ [kWh/m^2]	Q_D [MWh]	Q^{winter}_{sh}/Q_{sh} [%]
Davos (DAV)	warm	1723	420	37	85
	normal	1674	419	47	78
	cold	1621	442	61	72
Zurich (SMA)	warm	1395	226	30	96
	normal	1235	212	41	87
	cold	1047	179	57	80
Geneva (GVE)	warm	1460	192	28	99
	normal	1475	257	34	96
	cold	1203	203	49	82
Bern (BER)	warm	1404	225	31	96
	normal	1371	265	37	95
	cold	1116	215	55	80

system and assess its performance using an average-synthetic year that represents a long period of time, e.g., a decade. Schmidli et al. (2020) compared a solar-ice system considering PV and showed that using a real weather data for 10 years the SPF_{SHP} can vary up to 20 % compared to using the SIA weather data for a normal year. Taking representative weather data that are typical for the location calculated would lead to more reliable results.

4.5 Cooling potential of solar-ice systems

As a base case, a system dimensioned to reach an SPF_{SHP} of 4 has been simulated. Three cases were simulated for the cities Zurich (SMA), Geneva (GVE) and Locarno (OTL):

- Passive Cooling: cooling by using cold from the ice storage in summer months for cooling the building.
- HP Cooling: domestic hot water is generated by heat pump in summer for cooling the ice storage.
- Passive Cooling+: like passive cooling, but with an insulated ice storage to minimize thermal gains in spring to shift more ice to the summer months.

The overall heat balance of the Passive Cooling+ system for Locarno with an insulated ice storage is shown in Figure 22. The heat sources of the system are the collector gains Q_{col}, the electricity consumption of the heat pump $El_{Hp,comp}$ as well as the auxiliary heaters in the space heating and domestic hot water tank El^{Aux}. The heat sinks of the system are the domestic hot water demand Q_{dhw}, the space heating demand Q_{sh}, and the losses of circulation loop, pipes and sensible storages $Q_{loss}^{summary}$. Depending on the average state of the ice storage in a month the accumulated heat $Q_{lat,sens}^{ice-storage,\,acum}$ and the heat transfer through the ice storage wall $Q_{env}^{ice-storage}$ can have positive or negative monthly values. The results show that with the chosen system size the ice storage starts to be fully iced in January and the electric backup has to provide some of the heat in January, only. This is a result of the sizing concept that aims reaching an SPF_{SHP} in the range of 4. These results are obtained using warm weather conditions. For the simulations with normal weather conditions the same scaling factors were used. Tab. 7 shows the maximum latent volume available in absolute terms.

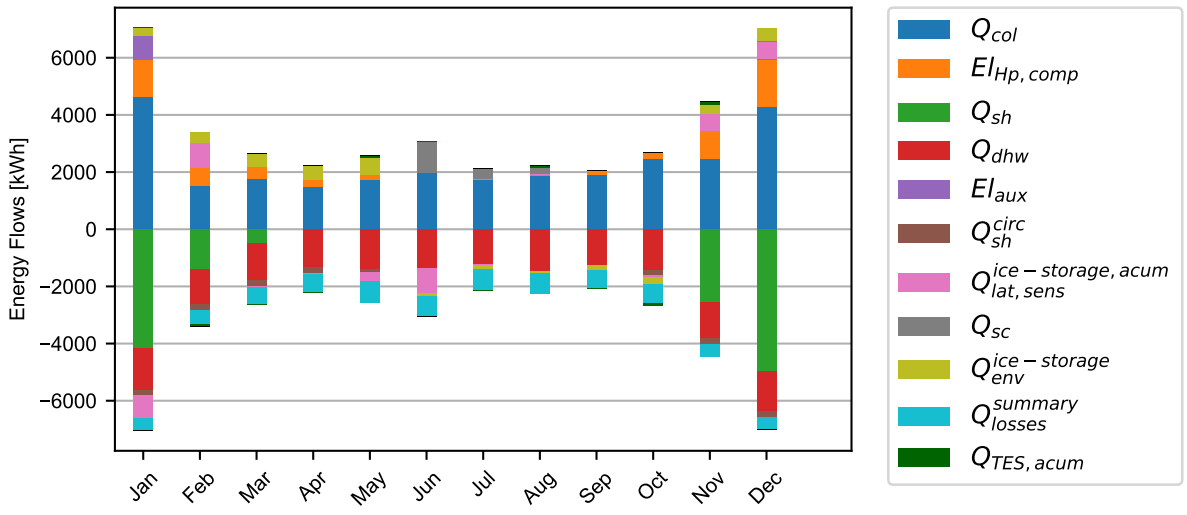

Figure 22: Heat balance on the solar-ice system for passive cooling in Zurich with warm weather data (MFB30, ideal user behaviour).

In order to analyze the cooling potential of the passive control approach in detail, the corresponding energy balance of the ice storage is shown in Fig. 23. The balance involves the cold Q_{sc} delivered by the ice storage to the space cooling system, the heat gains and losses through the ice storage wall $Q_{env}^{ice-storage}$, the heat and cold delivered to the ice storage by the solar collector, and the heat pump delivered $Q_{col}^{delivered}$ and extracted $Q_{HP}^{extracted}$ as well as the cooling energy accumulated in the ice storage $Q_{sens+lat}^{ice-storage,\,acum}$. Fig. 23 shows the monthly cumulative values starting from September. The total amount of heat extracted from the ice storage between September and February accumulated as latent heat ($Q_{sens+lat}^{ice-storage,\,acum}$) adds up to 1300 kWh. Not all energy is kept during spring. In the months between March and August 750 kWh of cooling energy in the ice storage are lost due to natural melting by heat gains from the ground. In turn the heat pump extracts

Table 7: Absolute values of ice storage latent capacity and collector field area for the cities considered in the cooling analysis (building: MFB30, ideal).

	warm		normal	
City	$V_{ice,a,lat}$ m^3_{lat}	$A_{col,a}$ m^2	$V_{ice,a,lat}$ m^3_{lat}	$A_{col,a}$ m^2
Zurich	14	75	20	103
Geneva	14	57	16	68
Locarno	13	30	15	36

about 930 kWh in this time span, such additional 180 kWh of heat are extracted from the ice storage. The cooling delivered from the ice storage sums up to about 1400 kWh over the months June, July and August. The highest cooling is delivered in June when the ice storage has biggest capacity, in July and August only little of the cooling demand of the building can be delivered (see also Fig. 22). In January the gains from the collector field into the ice storage sum up to 2600 kWh. Since the used cooling control stops normal operation to prevent melting not before the beginning of March, this leads to some active regeneration of the ice storage. The heat extracted from the ice storage for space heating and domestic hot water demand covers some of the gains of the ice storage. Thus, the cold accumulated in latent form ($Q_{sens+lat}^{ice-storage,acum}$) remains relatively constant from February to April. From June to August, free cooling from the ice storage is used as cooling demands. In June, July and August the ice storage shows small losses due to high ice storage temperatures.

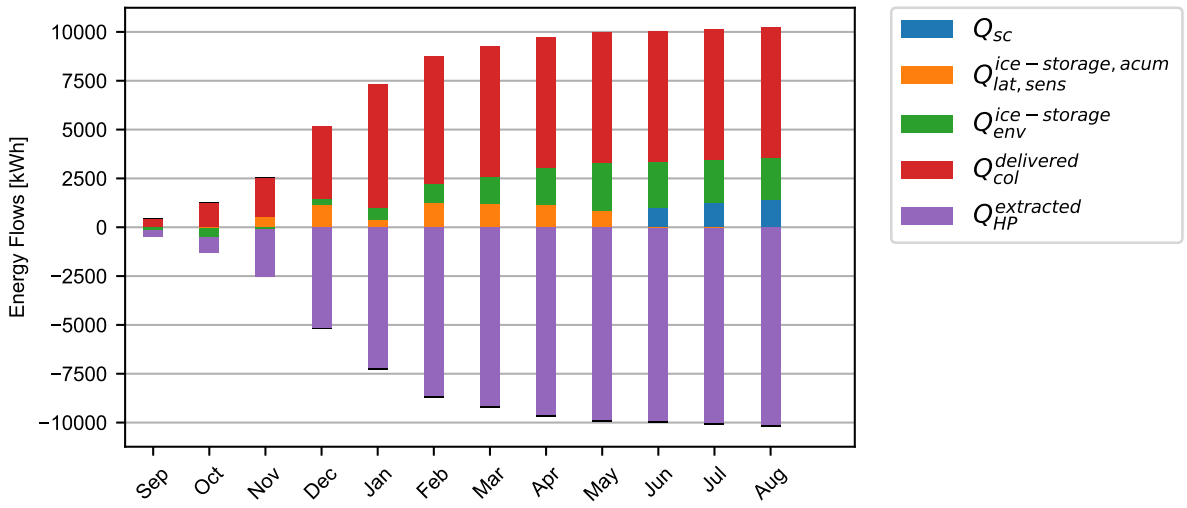

Figure 23: Accumulated sums of the heat balance on the ice-storage of the passive cooling system in Zurich with warm weather data (MFB30, ideal user behaviour).

Passive (free) cooling, with non-insulated and insulated ice storage, and heat pump supported cooling are compared in the following by analyzing the yearly heat balance of the ice storage and histograms showing how many hours the room temperature (T_{room}) is above the cooling set temperature ($T_{set,cooling}$) of 26 °C. This difference is expressed as ΔT.

Fig. 24 (a) shows the accumulated energy balance for the ice storage for the whole year for all three types of cooling that are studied here. The amount of cooling delivered from the ice storage is with 1450 kWh slightly larger for the Passive Cooling+ (with insulated ice storage) than for the normal passive cooling due to lower gains in spring. In turn the losses in summer when cooling is provided and the ice storage warms up are lower as well. The amount of heat extracted by the heat pump is lower for the passive cooling with insulated ice storage because the gains in winter are lower. This has an influence in the system performance since the

electric backup has to be used more frequently in January when the ice storage is insulated. The heat pump supported cooling shows with 3080 kWh significant higher cooling potential. The heat pump extracts more heat from the ice storage because it is used for providing domestic hot water in summer.

Fig. 24 (b) shows histograms for the number of hours for different ΔT above the set temperature for cooling (26 °C). For a comparison of the cooling potential the *equivalent cooling degree hours* **CDH** are used, which are calculated as the number of hours where T_{room} is above the set point for cooling of 26 °C ($T_{set,cool}$) multiplied with the ΔT between T_{room} and $T_{set,cool}$. Passive cooling reduces the CDH from the no cooling case from 3150 to 2120 and 2050 for non-insulated and insulated ice storage respectively. For heat pump supported cooling, the improvement of comfort is obvious in the histogram. The maximum overheating is about 2 K above the set temperature for only a few hours. The cooling degree hours are reduced to 320.

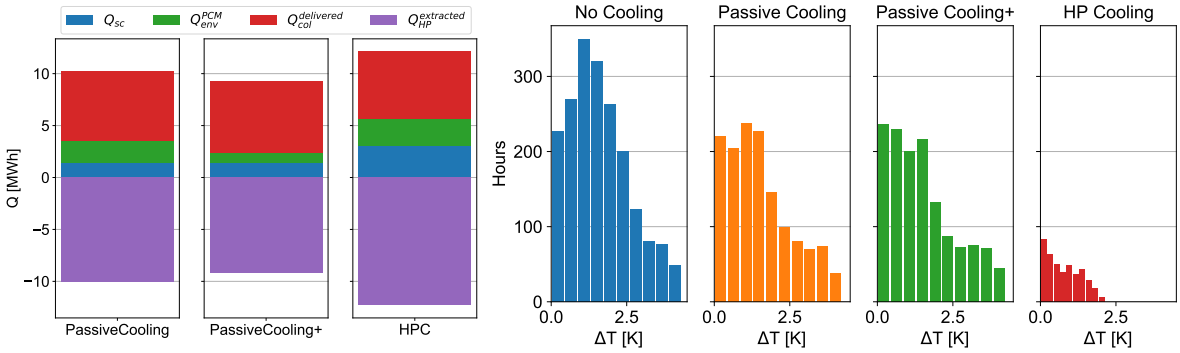

(a) Yearly heat balance of the ice storage

(b) Histogram of temperature difference between T_{room} and $T_{set,cooling}$

Figure 24: Cooling potential of the different ways of cooling for Zurich with warm weather conditions. (a) shows the accumulated heat balances over one year, (b) shows the number of hours with different DeltaT above the set temperature for cooling of 26 °C.

Fig. 25 shows the cooling potential for Locarno with normal weather conditions. The passive cooling without insulated ice storage reduces significantly the maximum of temperatures reached in summer as well as the number of hours with temperatures above 26 °C. The equivalent cooling degree hours are reduced from 2461 CDH to 1380 CDH between no cooling and passive cooling with non-insulated ice storage. The passive cooling using an insulated ice storage increases the comfort in summer (30 % lower cooling degree hours and 25 % higher cooling provided by the ice storage), but will still be not sufficient to cover the cooling demand. The heat pump supported cooling covers a large part of the cooling demand of the building. The equivalent cooling degree hours are summarized in Tab. 8 for comparison.

For Geneva, which has a lower cooling demand than Locarno the passive cooling is almost sufficient to cover the cooling demand (Fig. 26). The amount of cooling extracted from the ice storage increases from about 1100 kWh for passive cooling with a not insulated ice storage to about 1300 kWh for both, passive cooling with insulated ice storage and heat pump assisted cooling.

Even though passive cooling with insulated ice storage and heat pump supported cooling can improve the comfort in summer more than the passive cooling with a non-insulated ice storage, both have the disadvantage of reducing the system efficiency. The values for SPF_{SHP} and SPF_{SHPc}, which represents the system efficiency including the cooling provided by the solar-ice system, are summarized in Tab. 8. For the passive cooling without storage insulation there is no significant decrease of the SPF_{SHP} considering only the heating case. The SPF_{SHPc} including the cooling provided by the system is higher than the SPF_{SHP} of the reference without cooling for all cases. The passive cooling with insulated ice storage penalizes the SPF_{SHP} by up to 5 % to 10 %. Heat pump supported cooling causes a decrease of the SPF_{SHP} by the order of 10 % to 20 %, the SPF_{SHPc} is 5 % to 10 % lower than the SPF_{SHP} of the reference without cooling.

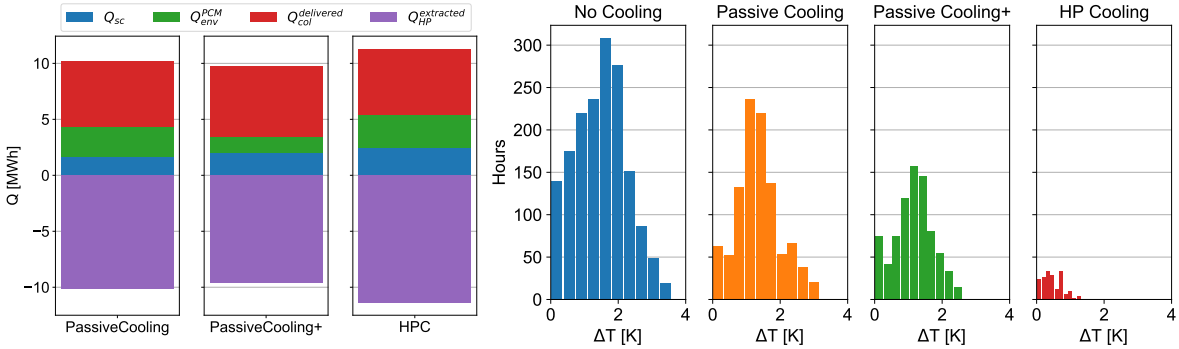

(a) Yearly heat balance of the ice storage

(b) Histogram of temperature difference between T_{room} and $T_{set,cooling}$

Figure 25: Cooling potential of the different ways of cooling for Locarno with normal weather conditions. (a) shows the accumulated heat balances over one year, (b) shows the number of hours with different DeltaT above the set temperature for cooling of 26 °C.

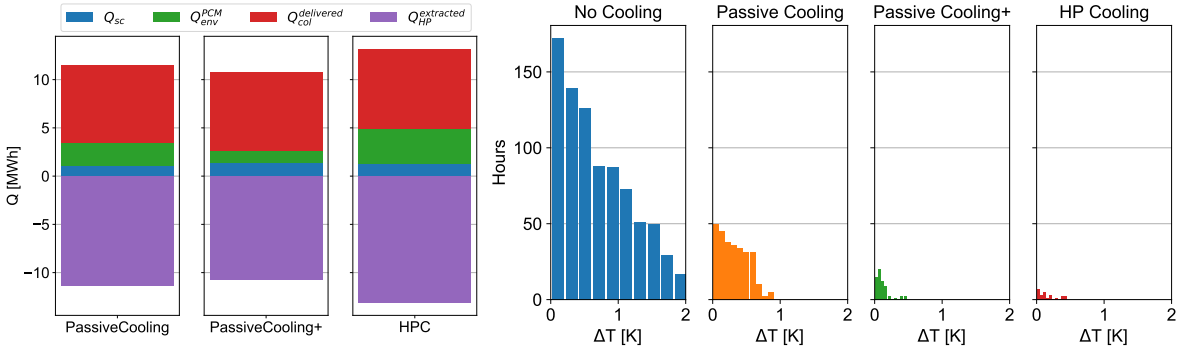

(a) Yearly heat balance of the ice storage

(b) Histogram of temperature difference between T_{room} and $T_{set,cooling}$

Figure 26: Cooling potential of the different ways of cooling for Geneva with normal weather conditions. (a) shows the accumulated heat balances over one year, (b) shows the number of hours with different DeltaT above the set temperature for cooling of 26 °C.

Table 8: Summary of SPF_{SHP}, SPF_{SHPc} and equivalent cooling degree hours (CDH) for the three cities with warm and normal weather conditions for MFB30 for all three types of cooling compared to the reference without cooling.

City	No Cooling		Passive Cooling			Passive Cooling+			HPC		
Warm	$SPF_{SHP,ref}$	CDH	SPF_{SHP}	SPF_{SHPc}	CDH	SPF_{SHP}	SPF_{SHPc}	CDH	SPF_{SHP}	SPF_{SHPc}	CDH
Zürich	4.1	3151	4.0	4.2	2125	3.8	4.0	2052	3.3	3.8	326
Geneva	4.3	5135	4.3	4.4	4398	3.7	3.9	4021	3.5	4.1	1243
Locarno	4.2	8345	4.0	4.3	7285	4.0	4.4	6905	3.1	3.9	3955
Normal	$SPF_{SHP,ref}$	CDH	SPF_{SHP}	SPF_{SHPc}	CDH	SPF_{SHP}	SPF_{SHPc}	CDH	SPF_{SHP}	SPF_{SHPc}	CDH
Zürich	3.1	20	3.1	3.1	0	2.4	2.4	0	2.9	2.9	0
Geneva	3.5	576	3.5	3.6	89	3.4	3.5	7	3.1	3.2	4
Locarno	4.1	2461	4.0	4.3	1380	3.7	4.0	929	3.5	3.8	87

As a rule of thumb a cooling energy of about 80 kWh/m_{lat}^3 to 100 kWh/m_{lat}^3 can be provided by passive cooling considering an ice storage without insulation. The cooling potential can be increased by insulating the ice storage or by heat pump assisted cooling where the heat pump is used for providing domestic hot water in summer. Insulating the ice storage usually brings not much in terms of comfort improvement with the additional cost expenses of the insulation. Using the heat pump for providing DHW is an option to provide larger cooling demands with an overall efficiency penalty of 5 % to 10 %. With the heat pump for summer DHW mode one can bring, on top of the 80 kWh/m_{lat}^3 to 100 kWh/m_{lat}^3 cooling from the ice storage, about 15 % to 30 % respect of the summer DHW demand including circulation losses (June, July and August).

5 Development of a fast algorithm for energetic performance assessment

5.1 Data set and inputs

To explore different machine learning methods for reproducing the system simulation results in a simpler scheme, the full data set of nominal size 3600 (see Chapter 3) was used. The actual number of data points in the set is $m = 3437$ with the difference coming from fringe cases where the simulations did not converge. The values of all these points in the $H_{T,\,field}/Q_d$ and SPF_{SHP} space are shown in Fig. 27. There the lower half of the distribution in $H_{T,\,field}/Q_d$ is shown as blue points, while the upper is shown in red. The range of $SPF_{SHP} \in (3.5, 4.5)$, which is the most relevant for application purposes, is indicated by lighter colors.

By default $m_{\text{train}} = 2400$ of these data points were randomly allocated to the training set $\mathbf{Z}_{\text{train}}$, while another $m_{\text{test}} = 1029$ were randomly selected to form the test set $\mathbf{Z}_{\text{test}}$. This follows the established ratio of 70:30 between training and test set sizes. The performance of different machine learning methods was examined based on different input sets $\mathbf{x}$ listed in Tab. 9. The sets labelled with Y represent yearly data, while those denoted with M represent monthly data where applicable. Inputs with a "winter" label are based on values for January, February, November and December (sums for $H_{T,\,field}^{winter}$ and Q_{sh}^{winter}, average for T_{amb}^{winter}). The sizes of the input sets vary between $n = 3$ for Y_1 and $n = 62$ for M_4. Up to Y_5 and M_3 one input parameter is added to the previous set for each increase of the index number.

For a point Z_j in the test set each method provides a prediction $F(\mathbf{x})$ based on the input $\mathbf{x}$ for the simulation result value of ${SPF_{SHP}}^j$. This means that the relative prediction error for Z_j is

$$E_r(Z_j) = \frac{F(\mathbf{x}) - {SPF_{SHP}}^j}{{SPF_{SHP}}^j} \tag{21}$$

The performance of a method or an input configuration was then assessed based on the distribution of the E_r for all $Z_j \in \mathbf{Z}_{\text{test}}$. These distributions are presented in the form of split violin plots in the following sections.

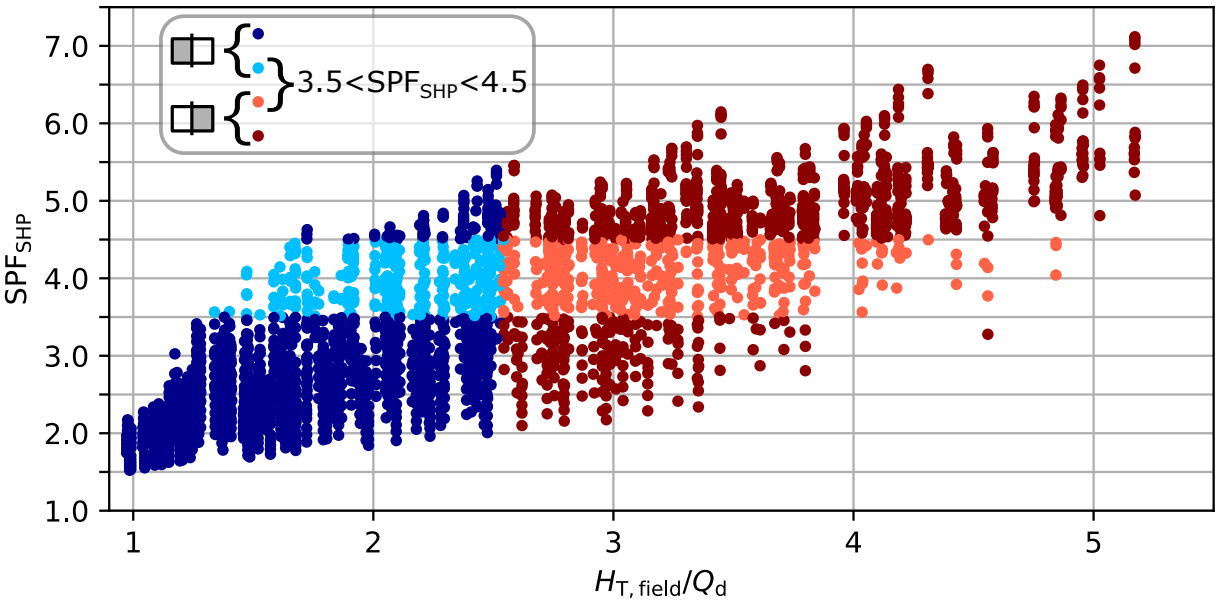

Figure 27: Full data set used for exploring machine learning methods: The SPF_{SHP} is plotted against the total radiation on the collector surface scaled by the overall heat demand $H_{T,\,field}/Q_d$. The data points with values from the lower half of the distribution in $H_{T,\,field}/Q_d$ are shown in blue, while those from the upper are shown in red. The most relevant range in SPF_{SHP} from 3.5 to 4.5 is indicated by lighter colors.

	x_1	x_2	x_3	x_4	x_5	x_6	x_7	x_8	x_9
Y_1	$\mathrm{Q_d}$	$\mathrm{H_{T,\,field}/Q_d}$	$\mathrm{V_{ice}}$	-	-	-	-	-	-
Y_2	$\mathrm{Q_d}$	$\mathrm{H_{T,\,field}/Q_d}$	$\mathrm{V_{ice}}$	$\mathrm{Q_{sh}/\ Q_{dhw}}$	-	-	-	-	-
Y_3	$\mathrm{Q_d}$	$\mathrm{H_{T,\,field}/Q_d}$	$\mathrm{V_{ice}}$	$\mathrm{Q_{sh}/\ Q_{dhw}}$	$\mathrm{H^{winter}_{T,\,field}/Q_d}$	-	-	-	-
Y_4	$\mathrm{Q_d}$	$\mathrm{H_{T,\,field}/Q_d}$	$\mathrm{V_{ice}}$	$\mathrm{Q_{sh}/\ Q_{dhw}}$	$\mathrm{H^{winter}_{T,\,field}/Q_d}$	$\mathrm{T^{winter}_{amb}}$	-	-	-
Y_5	$\mathrm{Q_d}$	$\mathrm{H_{T,\,field}/Q_d}$	$\mathrm{V_{ice}}$	$\mathrm{Q_{sh}/\ Q_{dhw}}$	$\mathrm{H^{winter}_{T,\,field}/Q_d}$	$\mathrm{T^{winter}_{amb}}$	$\mathrm{Q^{winter}_{sh}/Q_{sh}}$	-	-
Y_6	$\mathrm{Q_d}$	$\mathrm{H_{T,\,field}/Q_d}$	$\mathrm{V_{ice}}$	$\mathrm{Q_{sh}/\ Q_{dhw}}$	$\mathrm{H^{winter}_{T,\,field}/Q_d}$	$\mathrm{T^{winter}_{amb}}$	$\mathrm{Q^{winter}_{sh}/Q_{sh}}$	$\mathrm{(H_{T,\,field}/Q_d)^2}$	$\mathrm{(V_{ice})^2}$
	$x_1 \dots x_{12}$	$x_{13} \dots x_{24}$	x_{25}	$x_{26} \dots x_{37}$	$x_{38} \dots x_{49}/x_{38}$	$x_{50} \dots x_{61}/x_{39}$	x_{62}/x_{40}	-	-
M_1	$\mathrm{Q^{Jan}_d} \dots$	$\mathrm{H^{Jan}_{T,\,field}/Q^{Jan}_d} \dots$	$\mathrm{V_{ice}}$	-	-	-	-	-	-
M_2	$\mathrm{Q^{Jan}_d} \dots$	$\mathrm{H^{Jan}_{T,\,field}/Q^{Jan}_d} \dots$	$\mathrm{V_{ice}}$	$\mathrm{Q^{Jan}_{sh}/\ Q^{Jan}_{dhw}} \dots$	-	-	-	-	-
M_3	$\mathrm{Q^{Jan}_d} \dots$	$\mathrm{H^{Jan}_{T,\,field}/Q^{Jan}_d} \dots$	$\mathrm{V_{ice}}$	$\mathrm{Q^{Jan}_{sh}/\ Q^{Jan}_{dhw}} \dots$	$\mathrm{T^{Jan}_{amb}} \dots$	-	-	-	-
M_4	$\mathrm{Q^{Jan}_d} \dots$	$\mathrm{H^{Jan}_{T,\,field}/Q^{Jan}_d} \dots$	$\mathrm{V_{ice}}$	$\mathrm{Q^{Jan}_{sh}/\ Q^{Jan}_{dhw}} \dots$	$\mathrm{T^{Jan}_{amb}} \dots$	$\mathrm{(H^{Jan}_{T,\,field}/Q^{Jan}_d)^2} \dots$	$\mathrm{(V_{ice})^2}$	-	-
M_5	$\mathrm{Q^{Jan}_d} \dots$	$\mathrm{H^{Jan}_{T,\,field}/Q^{Jan}_d} \dots$	$\mathrm{V_{ice}}$	$\mathrm{Q^{Jan}_{sh}/\ Q^{Jan}_{dhw}} \dots$	$\mathrm{H^{winter}_{T,\,field}/Q_d}$	$\mathrm{T^{winter}_{amb}}$	$\mathrm{Q^{winter}_{sh}/Q_{sh}}$	-	-

Table 9: List of the different input sets used to test the performance of machine learning methods. Sets labelled with Y represent yearly values, while those denoted with M represent monthly values where applicable.

5.2 Machine learning methods

Fig. 28 shows the relative prediction error distribution for linear regression, the nearest neighbour method, the neural network and XGBoost. The distributions are shown for the two input sets Y_2 and M_2, as indicated by the different colors. These input sets were chosen because they can be compared directly, as M_2 simply features the monthly values for the yearly parameters that are included in Y_2. This does not apply to V_{ice}, since the volume of the ice storage stays constant throughout the year. All four methods show an error distribution with more weight around 0 and hence a better performance for M_2 as compared to Y_2. This is expected, since the number of input parameters is $n = 37$ for M_2 and $n = 4$ for Y_2.

For the yearly input set, the linear regression, nearest neighbour and the neural network method show very similar error distribution, with 50 % of the points between -10 and +13 %. When going to monthly values half of the distribution of each of the three show $|E_r| < 9\,\%$, while nearest neighbour even improves to $|E_r| < 5\,\%$ in this respect. For both input sets XGBoost exhibits the best performance with 50 % of the points with an absolute value below 3 % for yearly data and only a slight improvement when going from Y_2 to M_2.

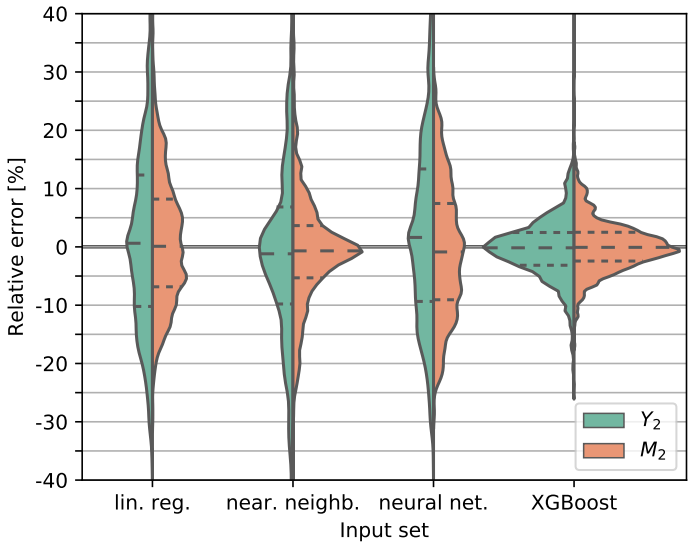

Figure 28: Prediction error distributions of different prediction methods for the yearly input set Y_2 and the monthly M_2 with a random 70:30 split between training and test data.

5.2.1 Linear regression methods

Only relative error distributions resulting from applying simple linear regression are presented graphically here, although methods featuring regularisation were applied during the exploration of different methods. The reason for this omission is that these showed a strong equivalency to the simple linear regression. In particular, Lasso, Ridge, and Elastic Net were employed with input sets Y_5 and M_3. For both input sets Ridge returned the same coefficients w_i (cf. Eq. 4) as the simple linear regression, while for the Elastic Net $\alpha = 1$, meaning that it is equal to the Lasso method. The equivalence of Ridge and the linear regression can be attributed to the fact that the linear regression employed is based on a least square method, i.e., the two methods have the same loss function, while Lasso uses the mean absolute error as the loss function. All three regularisation methods return constant terms $b \approx 0$, whereas the linear regression features finite values in this respect.

The feature selection capabilities of Lasso (and Elastic Net), i.e., setting coefficients of insignificant parameters to zero, do not play a role for the input set Y_5 based on yearly values. For the monthly M_3, however, there are coefficients for some non-winter monthly values of Q_d, Q_{sh}/ Q_{dhw}, and T_{amb} being set to zero. This is expected, since the relevant contributions to the SPF_{SHP} occur during the winter. For Y_5 the deviations of

the Lasso/Elastic Net coefficients from the linear regression/Ridge ones are within 30 %, while they are more substantial for M_3 beyond the ones set to zero, for a few exceeding 100 %.

All four methods based on linear regression needed around two minutes to be trained with $m_{\text{train}} = 2400$ points on the input set Y_5 and to be tested on $m_{\text{test}} = 1029$ points with the computational setup used. As described before, Ridge gave coefficients equivalent to the simple linear regression, and Elastic Net is equal to Lasso through $\alpha = 1$. For the two resulting coefficient sets, the performance with respect to the error distribution is almost identical, both for Y_5 and M_3. Since all four are so similar in the run time as well as the prediction error performance, only the simple linear regression will be further examined, because it is the most straightforward method of those at hand.

5.2.2 Linear interpolation, XGBoost, nearest neighbour, and neural networks

As described in section 2.3 predictions with linear interpolation can only be made for points within the convex hull of the training set. When increasing the number n of parameters of the input set, it becomes increasingly difficult to fulfill this condition and the fraction of the test set for which predictions can be made, i.e. its coverage, decreases. This applies to the current application, too, and is shown in Fig. 29. For Y_1 with $n = 3$ a prediction can be made for almost all points of the test set, whereas this coverage drops to around 50 % for Y_5 with $n = 7$. Since this makes it difficult to compare this method with others and also poses a serious problem for its application in an estimation tool, multi-dimensional linear interpolation was not further examined.

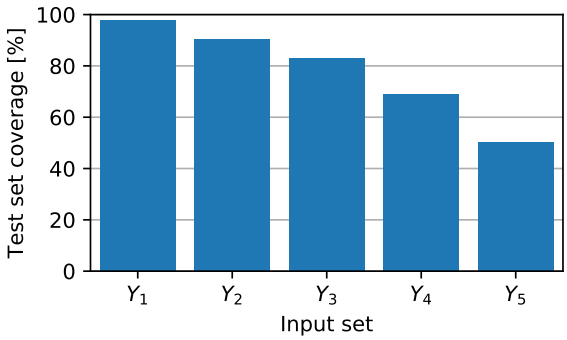

Figure 29: Coverage of the test set prediction for linear interpolation. Since staying inside the convex hull of the training set becomes increasingly difficult with higher n, the coverage decreases with the increase of the input set index. 100 % correspond to $m_{\text{test}} = 1029$.

Between the three remaining methods not directly based on linear regression, i.e., nearest neighbour, neural network, and XGBoost the latter clearly performs the best with respect to prediction error. The comparatively poor performance of the neural network originates in it being somewhat unsuited for the problem at hand. The strength of neural networks are incomplete data sets and situations in which the input-output relation is rather unclear. What it is employed for in the current project, however, is a problem quite disparate from this area of strength. Both input and output are well defined and their underlying relation is known from the simulations at least to some degree. A different picture emerges for the nearest neighbour method. Considering its simplicity in directly taking the value of the data point closest in parameter space to make a prediction, its performance is comparatively satisfying as shown in Fig. 28. It even outperforms the linear regression.

On the computational setup used with $m_{\text{train}} = 2400$, $m_{\text{test}} = 1029$, and input set Y_2, the run time to train and test the nearest neighbour method (for this method this means looking up the respective values for the test set in the train set) was around 2 minutes, for XGBoost around 5 minutes, and for the neural network roughly one hour. This means that the neural network requires substantially more computational effort than the other two methods, which are comparable to the linear regression methods in their run times. Also taking into account that XGBoost clearly shows the best performance with respect to the prediction error, it is the method that is examined with more detail in the following together with the linear regression.

5.3 Input variation

The prediction performance of a machine learning method naturally depends on the input it was trained on. This is true in a threefold manner: The performance depends on the number n of inputs given, what they represent (i.e. how relevant they are), and how many points m_{train} constitute the training set. All input sets $\mathbf{x}$ listed in Tab. 9 were tested on linear regression and XGBoost to gain insight towards the question which are the relevant input parameters and how many of them are needed to attain a satisfactory prediction performance.

The prediction error distributions for linear regression and XGBoost for the input sets from Y_1 to Y_6, which are based on yearly values, are shown in Fig. 30. The number of parameters increases with each index, where every higher index includes the set with the lower one. With the three input parameters Q_d, $H_{T,\,field}/Q_d$, and V_{ice} of Y_1, 50 % of the points for the linear regression are within ±12 %, while they are within ±3 % for XGBoost. Adding $Q_{sh}/\ Q_{dhw}$ with Y_2, $H^{winter}_{T,\,field}/Q_d$ with Y_3, and T^{winter}_{amb} with Y_4 all only slightly improve the performance of XGBoost, while they have basically no effect on the linear regression. A substantial improvement can be seen, however, when Q^{winter}_{sh}/Q_{sh} is added in Y_5. This collapses almost the entire distribution for XGBoost to an interval within ±5 %, while more than 50 % of the points for linear regression are within ±8 %. Finally, adding $(H_{T,\,field}/Q_d)^2$ and $(V_{ice})^2$ for Y_6 compared to Y_5 still slightly improves the performance of the linear regression, while it has little effect on XGBoost.

This behavior points towards the winter share of the space heating demand Q^{winter}_{sh}/Q_{sh}, introduced with Y_5, being the most relevant parameter besides those already present in Y_1. The improvement in the performance of the linear regression between Y_5 and Y_6, when the squared values for $H_{T,\,field}/Q_d$ and V_{ice} are added, shows that the dependence of SPF_{SHP} on these two parameters is not purely linear over the whole test set. This can be clearly seen in results from chapter 4 such as those presented in Fig. 15.

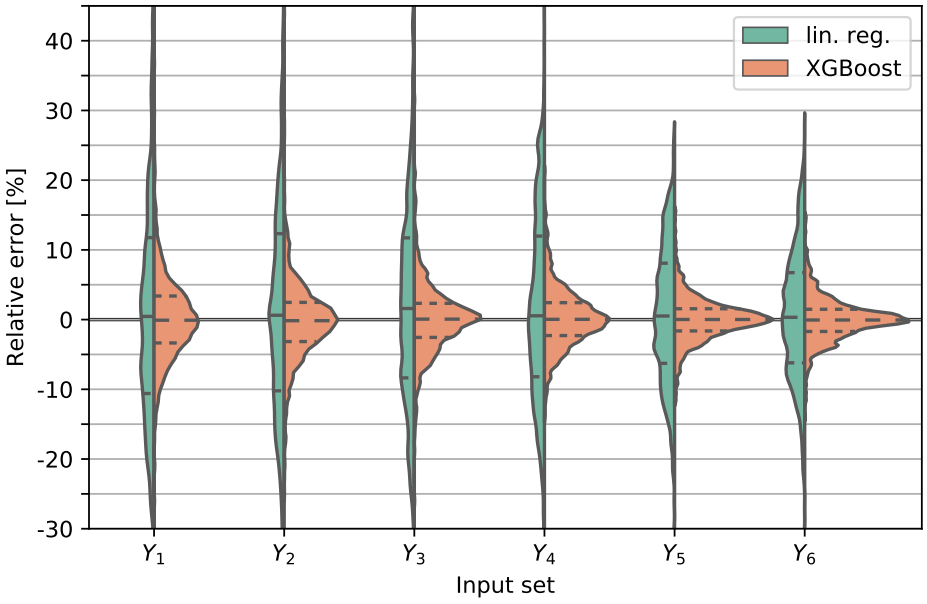

Figure 30: Prediction error distributions for different yearly input sets for linear regression and XGBoost with a random 70:30 split between training and test data.

Likewise, the error distributions for input sets based on monthly values are shown in Fig. 31. M_1 and M_2 are equivalent to Y_1 and Y_2, except that the former feature monthly values for Q_d and $H_{T,\,field}/Q_d$. While for M_1 50 % of the points are within ±10 % for the linear regression, for XGBoost they are within ±2 %. Adding monthly values for $Q_{sh}/\ Q_{dhw}$ improves the prediction capability of the linear regression to some degree, while it worsens the one of XGBoost. Adding monthly values for T_{amb} with M_3 and monthly values for $(H_{T,\,field}/Q_d)^2$ and $(V_{ice})^2$ with M_4 does not affect XGBoost, but enhances the linear regression, such that for M_4 50 % of

the points are within ±5 %. Finally, to test how adding winter values affects the performance $H^{winter}_{T,\,field}/Q_d$, T^{winter}_{amb} and Q^{winter}_{sh}/Q_{sh} were added to M_2, thus forming M_5. While this improves the performance of both methods with respect to M_2, compared to M_4 it is worse for the linear regression and roughly the same for XGBoost.

While the linear regression improves from M_1 to M_4, XGBoost remains largely unaffected. Hence, it appears that M_1 already saturates the performance improvement of XGBoost with its 25 input parameters. This shows that good predictions can be made by knowing only a few parameters on a monthly basis instead of more on a yearly basis. The winter values were included in M_5 to test whether this additional information leads to a better performance, since it proved to be relevant for the yearly input sets. This, however, leads to only some improvement for the linear regression and very little for XGBoost.

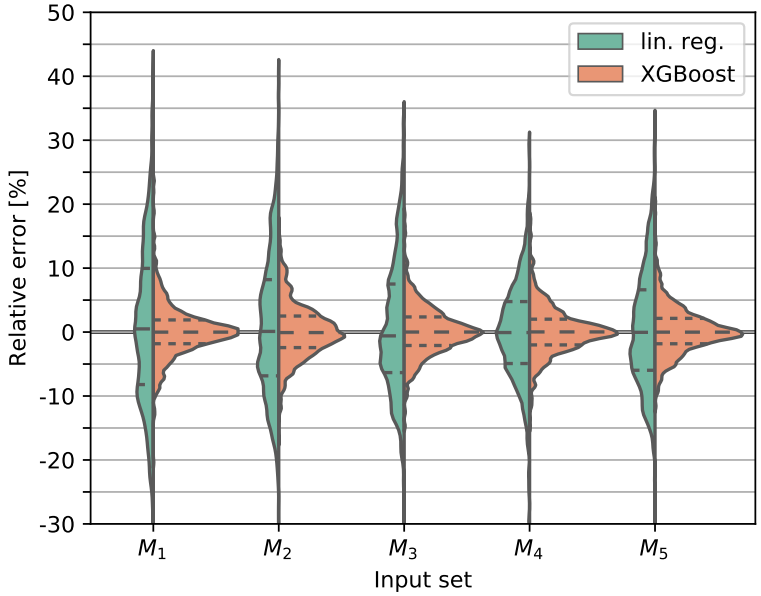

Figure 31: Prediction error distributions for different monthly input sets for linear regression and XGBoost with a random 70:30 split between training and test data.

To test whether the size of the training set is sufficient, the number of training points m_{train} was varied between 400 and 2400 in steps of 400. Here, the test set was fixed as before with a size of $m_{\text{test}} = 1029$. Each training set of increasing size contains the smaller ones in order to exclude effects from randomly selecting different subsets of the full training set. The respective results are presented in Fig. 32. While the error distribution for the linear regression basically stays the same while increasing m_{train} except for a few fringe cases, the performance of XGBoost does improve with each increase up to $m_{\text{train}} = 2000$, while it stays constant through the next step to 2400.

This shows that the default number of training points $m_{\text{train}} = 2400$ is sufficient to train XGBoost. The fact that the performance of the linear regression is already saturated with $m_{\text{train}} = 400$, the lowest value tested, can be rationalized when considering that with the input set Y_5 there are seven coefficients plus a constant to optimize. Compared to 400 data points this is a small number, such that the marginal benefit of adding additional training points tends to zero for this method.

5.4 Extrapolation

So far only a random split of the full data set into a training and test set was considered. This means that most test points are within the parameter space spanned by the training set, and only a few will be outside. For practical purposes, however, going beyond the known data set might be important, because a finite number of data points should be employed to train a method to predict the output for more or less arbitrary input.

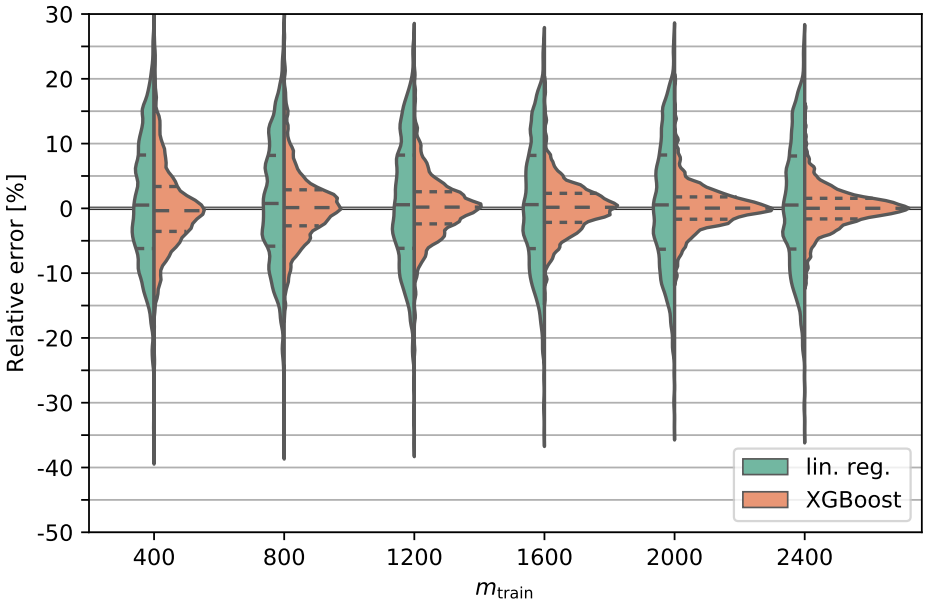

Figure 32: Prediction error distributions for different sizes of the training set of inputs Y_5 for linear regression and XGBoost. The test set is kept at a constant size, such that a ratio of 70:30 is achieved for 2400 training points.

In particular, the method should be capable of making predictions for arbitrary locations within Switzerland, since the location is the one boundary condition that will definitely change for each new system. To test how robust the examined methods are when changing location, training and test set were not simply generated by randomly splitting the full data set, but by splitting it according to the locations. The eight "standard" locations (cf. section 4.4.1) were allocated to the training set, while additional locations formed the test set. The test locations were selected to represent a wide range of climates existing in Switzerland: BUS (Buchs, Aarau) for the Central Plateau, CDF (La Chaux-de-Fonds) for a cold and elevated location, LUG (Lugano) for a location south of the Alps, and SIO (Sion) for a location in an Alpine valley.

As illustrated in Fig. 33a a location is added to the training set with each step. The data set for one location has a nominal size of 300 data points. The resulting prediction error distributions for the input set Y_5 are shown in Fig. 33b for linear regression and XGBoost. Both methods show a negative bias in their prediction error up until the fourth step, after which DAV is added. From then on the medians are centered around zero and the performance of the linear regression remains fairly constant. XGBoost still shows a slight improvement in the last step, when STG is added. From the fifth step on half of the points for the linear regression are within $\pm 9\,\%$, and half of the points for XGBoost within $\pm 5\,\%$. Here, the reduction of the biases in the error distributions is reflecting the improving match between locations in the training and the test set.

Beyond the geographical extrapolation described above, extrapolations in the variables that were used for parametric studies in the simulations, V_{ice} and A_{col}, were examined. For A_{col} this was done indirectly by using $H_{T,\,field}/Q_d$ for splitting up the data set in a lower and an upper half, as indicated with the blue and red colors in Figs. 27 and 34a. Then three cases were investigated:

1. The lower half of the data points was used as the training and the upper as the test set (train ↗ test)
2. The upper half of the data points was used as the training and the lower as the test set (test ↙ train)
3. The data set was split 50:50 randomly for comparison

Furthermore, a second version of this was tested, where each test set was reduced to the range between 3.5 and 4.5 in SPF_{SHP}, which is the most relevant for real systems. The results for the ensuing six configurations while

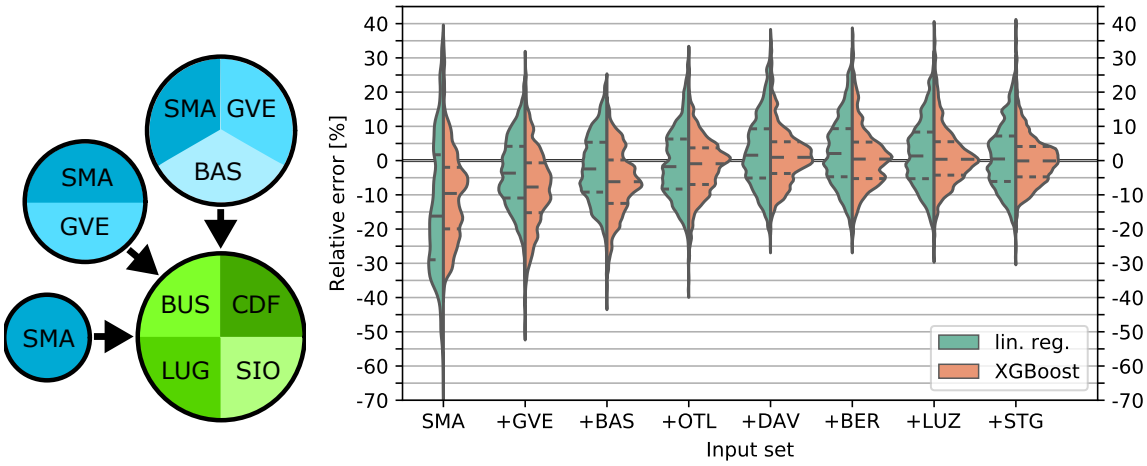

(a) Illustration

(b) Distributions

Figure 33: Geographical extrapolation: The training set is increased location by location, while a set of size 1151 with locations distinct from the training ones is used for testing. This is illustrated in (a) and the resulting prediction error distributions are shown in (b). Y_5 is used as the input set.

using Y_5 as the input set are shown in Fig. 34b. Looking at the extrapolations for the full ranges in SPF_{SHP} both the linear regression and the XGBoost exhibit very poor performances. For the first case described above (↗) the linear regression shows a bias around $+8\,\%$ and a spread of the central $50\,\%$ over almost $18\,\%$ in the relative error distribution, while for XGBoost the bias is $-3\,\%$ and the $50\,\%$ spread almost $14\,\%$. For the second case (↙), the bias is $+19\,\%$ for the linear regression and almost $+29\,\%$ for XGBoost.

Reducing the range of SPF_{SHP} to (3.5, 4.5) significantly improves the performances. This applies especially to the linear regression and the case (↙), where $50\,\%$ of the error distribution is within $\pm 5\,\%$, while the XGBoost still shows a bias which is larger than $+10\,\%$. For the first case (↗) reducing the test set range leads to similar performances of the linear regression and XGBoost with the $50\,\%$ spread below $14\,\%$ and slight biases for both methods. Lastly, it is noteworthy that reducing the range in SPF_{SHP} introduces a bias in the prediction error of the linear regression for the random 50:50 split.

Since the parametric study in V_{ice}/Q_d was done for the six discrete values of $0.2\,m^3/MWh$, $0.4\,m^3/MWh$, $0.6\,m^3/MWh$, $0.8\,m^3/MWh$ and $1.0\,m^3/MWh$, the data set was not split 50:50, but rather 60:40, as depicted in Fig. 35a. This leads to three cases as above:

1. The data points with $V_{ice} \in \{0.2, 0.4, 0.6\}$ were used as the training and those with $V_{ice} \in \{0.8, 1.0\}$ as the test set (train ↗ test)

2. The data points with $V_{ice} \in \{0.6, 0.8, 1.0\}$ were used as the training and those with $V_{ice} \in \{0.2, 0.4\}$ as the test set (test ↙ train)

3. The data set was split 60:40 randomly for comparison

Again a second version with $SPF_{SHP} \in (3.5, 4.5)$ was tested, and the error distributions for the resulting six configurations with Y_5 as the input set are shown in Fig. 35b. For all configurations with non-random splits XGBoost performs poorly, with biases between $-7\,\%$ for the reduced range and the first case (↗) and $+8\,\%$ for the reduced range and the second case (↙). The linear regression also exhibits a rather meager prediction capability for the full test set range and non-random splits. Reducing the test sets in their SPF_{SHP} range, however, leads to more reasonable error distributions. Here, the bias is around $-3\,\%$ with a $50\,\%$ spread below $9\,\%$ in the first case (↗), while the bias is almost zero with the same respective spread in the second case (↙).

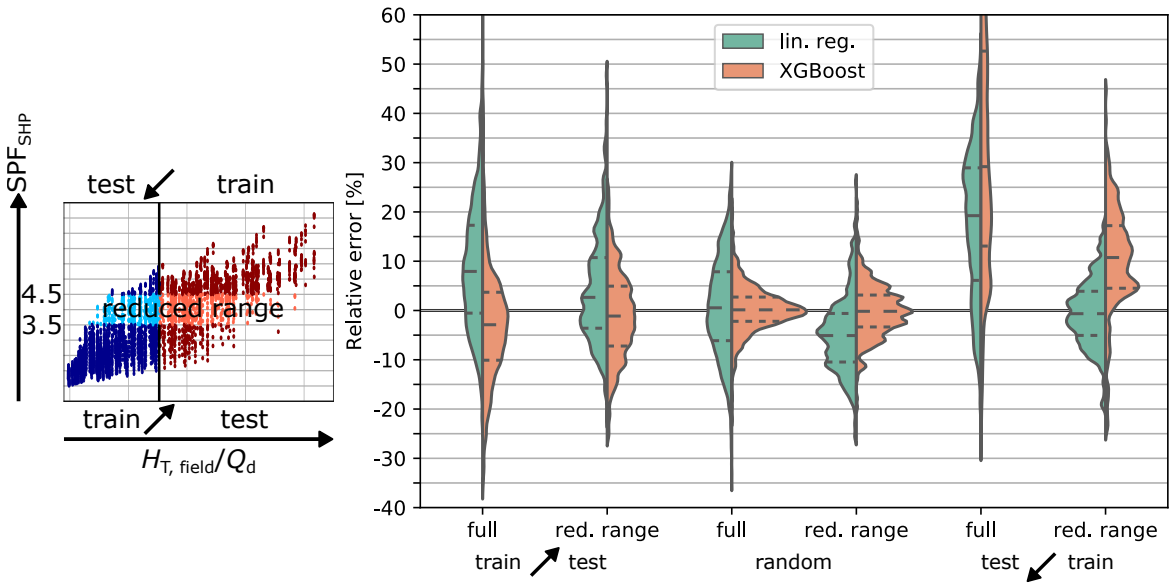

(a) Distribution of $H_{T,\,field}/Q_d$

(b) Prediction error distribution

Figure 34: Extrapolation in $H_{T,\,field}/Q_d$: The data set is split into a lower and an upper half according to the values of $H_{T,\,field}/Q_d$ (see also Fig. 27). As illustrated in (a) the lower is then used as a training and the upper as a test set and vice versa. A reduced range for second versions of the test set is also indicated. The resulting prediction error distributions are shown in (b) together with random 50:50 splits for comparison. Y_5 is used as the input set.

Extrapolating over the full range of SPF_{SHP} in $H_{T,\,field}/Q_d$ and V_{ice} leads to very poor performance of both linear regression and XGBoost. In general, for XGBoost this is rooted in the fact that the decision trees generated are optimized for the training set and are not well suited to operate out of the training range. For linear regression predicting out of range is not a problem in principle, but naturally will lead to incorrect results, when dependencies of the output on input parameters become nonlinear, which is apparently the case for the full SPF_{SHP} range. Reducing the test sets to points with $SPF_{SHP} \in (3.5, 4.5)$ consistently improves the performance of the linear regression and for a few cases also for XGBoost, though there are also cases without any real improvement, e.g., the second case (↙) in V_{ice}. Reducing the range of SPF_{SHP} brings the scaling of both $H_{T,\,field}/Q_d$ and V_{ice} to a more linear regime, since their behavior becomes nonlinear in particular for high values in SPF_{SHP}, which can be seen, e.g., in Fig. 15. Extrapolation in the scaling parameters constitutes the only realm within this study, where XGBoost was outperformed.

5.5 Proposed linear regression model

The XGBoost model has shown to be the most accurate method for predicting yearly energetic efficiencies. However, it can not be adopted easily by planners unless a user interface connected to the respective model file is developed. As discussed in section 8, an online tool will be our preferred approach to provide the methods developed within this project to planners. However, until this tool is available, we recommend to use a simple linear regression model to do the first assessments. Notice that this is not meant as a planning tool but as a rule-of-thumb approach.

The linear regression model has the following form:

$$\begin{aligned} SPF_{SHP} = b + w_1 \cdot Q_d + w_2 \cdot H_{T,\,field}/Q_d + w_3 \cdot V_{ice,lat} + w_4 \cdot Q_{sh}/\ Q_{dhw} + w_5 \cdot H^{winter}_{T,\,field}/Q_d + w_6 \cdot T^{winter}_{amb} \\ + w_7 \cdot Q^{winter}_{sh}/Q_{sh} + w_8 \cdot (H_{T,\,field}/Q_d)^2 + w_9 \cdot {V_{ice,lat}}^2 \end{aligned} \tag{22}$$

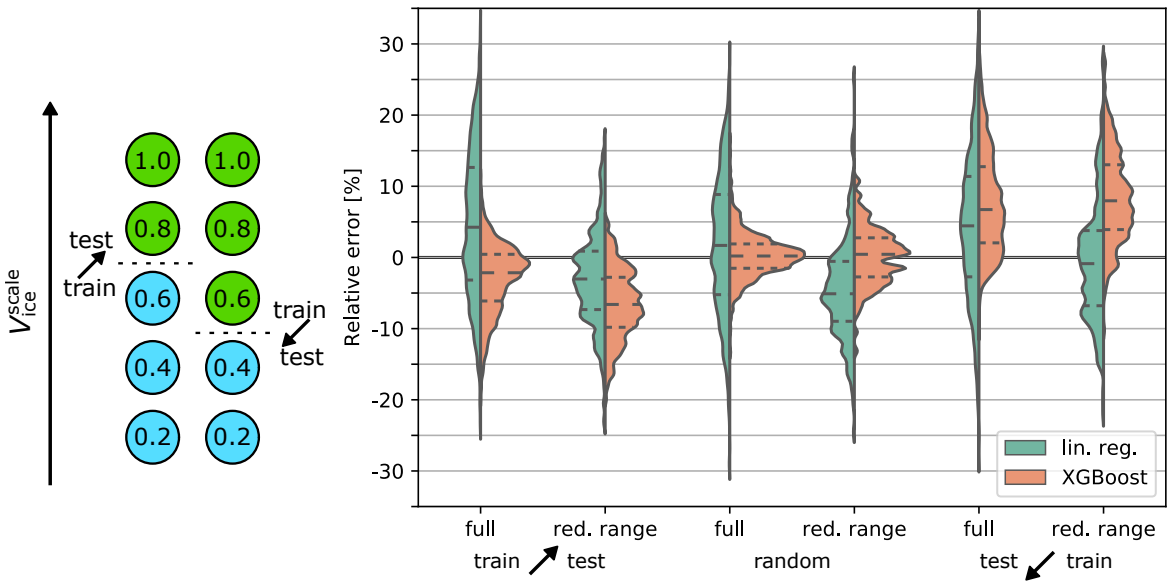

(a) Distribution of V_{ice} in m^3/MWh

(b) Prediction error distribution

Figure 35: Extrapolation in V_{ice}: Based on the five cases simulated either the lower three are used for training and the upper two for testing or the upper three for training and the lower two for testing as illustrated in (a). As outlined in Fig. 34a also test sets with a reduced range were explored. The resulting prediction error distributions are shown in (b) together with random 60:40 splits for comparison. Y_5 is used as the input set.

The values of the constant b and the coefficients w_i can be found in Tab. 10 for the yearly input sets Y_2, Y_5 and Y_6. In this table also the units, in which the quantities with which the coefficients are multiplied need to be in, are specified. The resulting error distributions for predictions on the test set with linear regression and these input sets are shown in Fig. 30. Furthermore, the 50 and 90 % quantile boundaries of these distributions can be found in Tab. 11.

	b	w_1	w_2	w_3	w_4	w_5	w_6	w_7	w_8	w_9
Y_2	0.929	-0.014	0.893	1.015	0.294	-	-	-	-	-
Y_5	3.131	0.041	0.419	1.004	-0.812	2.223	0.202	-4.085	-	-
Y_6	2.121	0.041	1.044	1.875	-0.800	2.414	0.203	-4.018	-0.118	-0.903
unit	-	MWh	-	m^3/MWh	-	-	°C	-	-	m^6/MWh^2

Table 10: Constants b and coefficients w_i for simple linear regression with yearly input sets Y_2, Y_5 and Y_6. Together with Eq. 22 these values can be used to calculate predictions for SPF_{SHP}. Also given are the units of the quantities that the coefficients need to be multiplied with.

input set	50 % of data between		90 % of data between	
Y_2	−10 %	+12 %	−23 %	+33 %
Y_5	−6 %	+8 %	−15 %	+17 %
Y_6	−6 %	+7 %	−15 %	+17 %

Table 11: 50 and 90 % quantile boundaries of the prediciton error distributions resulting from employing linear regression as described in equation 4 with the indicated input sets.

6 Cost analysis of solar-ice systems for multi-family buildings

Cost are based on the annuity method presented in section 3.10. Simulation results presented in chapter 4 are used to calculate the heat cost of solar-ice systems under many different boundary conditions. The main assumptions for the economic analysis are given in Table 12.

Table 12: Assumptions for calculation of heat generation costs.

Rate of interest	1.0 % p.a.
Analysis period	25 years
Yearly Maintenance	1 % of investment costs
Lifetime of all components	Analysis period
Electricity costs (incl. VAT)	Variable costs: 20 Rp./kWh
Increase of electricity costs	1.5 % p.a.

The first part of this chapter presented in section 6.1 provides the source cost data for all components. The second part in section 6.3 consists of the calculation of the solar-ice system cost.

6.1 Cost assessment of individual components

Most of the cost provided here are based on the report done by the authors presented in Alonso et al. (2020).

6.1.1 Cost assessment of heat pumps

The cost presented in the following are for state-of-the-art heat pumps in the power range from 5 kW to 55 kW. Cost are taken from Swiss price lists for heat pumps. Thus, only heat pump cost without installation is considered in this section. For the cost of brine-water heat pumps the following products are included:

- Oertli SIN (R410A)
- alterra SWC (R410A)
- alterra pro SWP (R407C)

All of these heat pumps feature a fixed compressor speed. Their cost are shown in Fig. 36. The unit cost vary between 10 000 CHF to 35 000 CHF for a power range of 5 kW to 55 kW. A linear regression is used to fit the data points. Assuming a 20 % uncertainty with respect to the regression, most to the data points fall within the range.

The linear regression cost of a brine water heat pump is:

$$\text{Cost of HP (CH)} = 6266 \text{ CHF} + 451.7 \text{ CHF/kW (validity range 5 kW to 55 kW)} \quad (23)$$

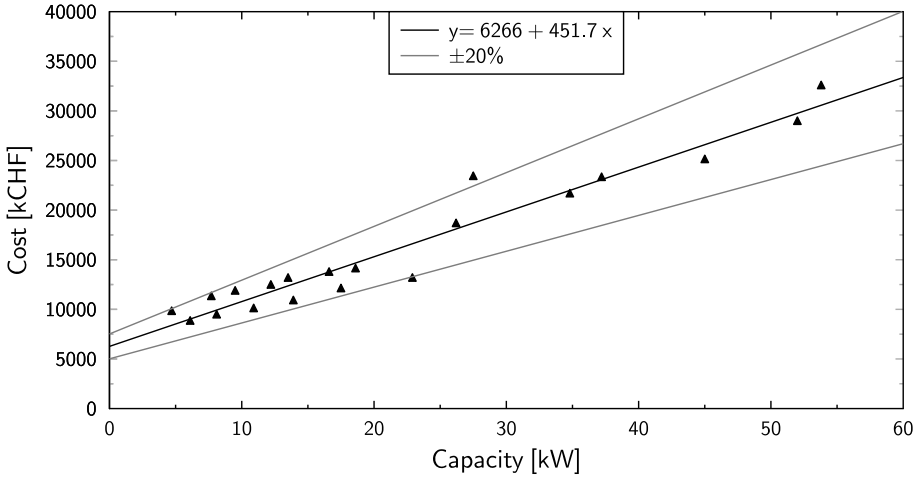

Figure 36: Cost of brine-water heat pumps with a linear regression and a ±20 % deviation range.

6.1.2 Cost of thermal hot water storage tanks

The cost of the hot water storage tanks has been derived separately for DHW and SH applications. For estimating the costs storage tanks for domestic hot water with a volume up to 2000 l and space heating buffer storage tanks with a volume up to 1000 l are considered. Tanks made of stainless steel are much more expensive than those made of steel. Stainless steel tanks can be used for domestic hot water for hygienic reasons and steel tanks for space heating. If a freshwater module is used for heating up the domestic hot water, it is possible to use a steel tank for domestic hot water as well. This is the approach followed in the simulations and thus the cost of black steel storages is used.

The following storage tanks are used to obtain the range of costs:

- Hoval (steel)
- CTA AG CHHS (steel)

The steel tanks for space heating prices range from 600 CHF to 2000 CHF for volumes in the range of 0.1 m^3 to 1 m^3. The cost for SH storages can be calculated as:

$$\text{Cost TES for SH} = 666\ \text{CHF} + 1214\ \text{CHF}/m^3\ \text{(validity range 0.1}\,m^3\ \text{to 1}\,m^3\ \text{black steel)} \quad (24)$$

where a 10 % uncertainty range is assumed to cover all data points within a linear model.

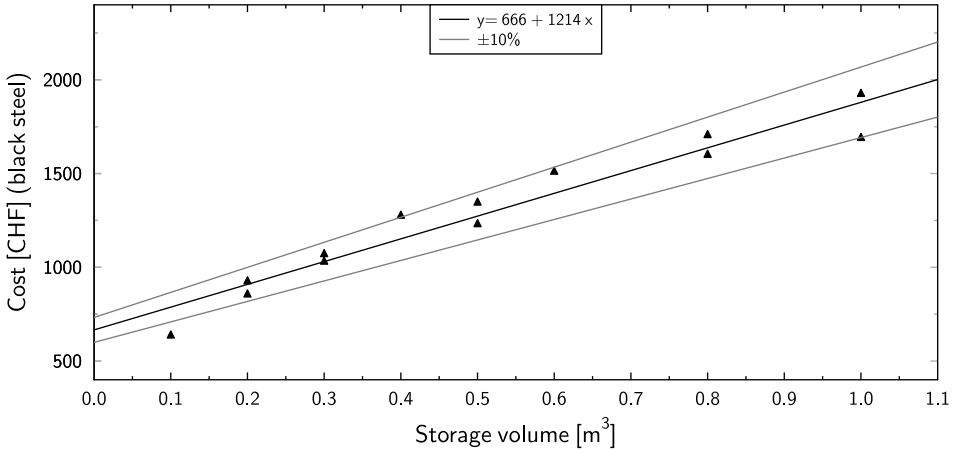

Figure 37: Cost of black steel storages with a linear regression and a ±10 % deviation for the relevant ranges.

6.1.3 Cost assessment of thermal installation

The thermal installation cost calculation considers everything in the machine room except for the heat pump and storage tanks, which are discussed above. The machinery room of a building includes the following items:

- Heat Pump (considered separately)
- SH water tanks (considered separately)
- DHW water tanks (considered separately)
- Circulation pumps, expansion vessels, heat exchangers, piping, valves, filters, sensors, etc.

To estimate the cost of the hydraulic system a set of data provided by different installers has been employed. The data were obtained for brine-water heat pumps with installed powers of 20 kW to 150 kW. The total cost is included in the equation, but the breakdown corresponds to the following items:

- Installation cost heat source
  - Hydraulic material (piping, valves, pumps, glycol filling, etc.)
  - Insulation
  - Labor
- Installation cost heat sink
  - Hydraulic material (piping, valves, pumps,water filling, etc.)
  - Insulation
  - Labor
- Electrical installation

The thermal installation cost is shown in Fig. 38. The base unit is the installed power in kW.

$$\text{Cost of hydraulic system} = 24596\ \text{CHF} + 193\ \text{CHF/kW (validity range 20 kW to 150 kW)} \quad (25)$$

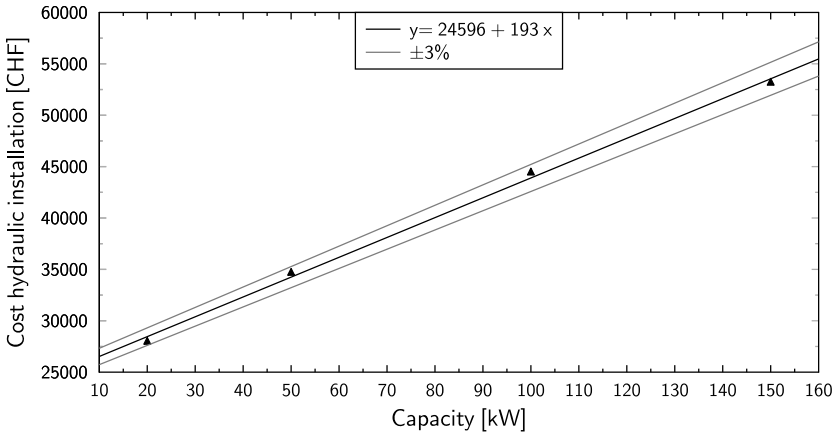

Figure 38: Cost of the hydraulic system including installation and everything in the machinery room except HP, hot water and ice storages.

6.1.4 Cost of collector field using uncovered selective absorbers

The specific cost for the solar thermal field using uncovered selective collectors is about 860 CHF/m^2 for collector fields of about 100 m^2 gross area, which is a common range of an ice storage system for a multi family building in Switzerland. The cost for the collectors themselves is about 515 CHF/m^2. The installation cost including the hydraulic facilities in the cellar is about 345 CHF/m^2.

$$\text{Cost for installed uncovered selective collectors (CH)} = 860\,\text{CHF/m}^2 \tag{26}$$

6.1.5 Cost ice storage

The cost of the ice storage is split into two parts, namely the casing and the heat exchangers. It is assumed that the casing is made of concrete and also that excavation is needed to accommodate the ice storage in the cellar of the building or for placing it underground. The cost of the ice storage casing and excavation is shown in Fig. 39.

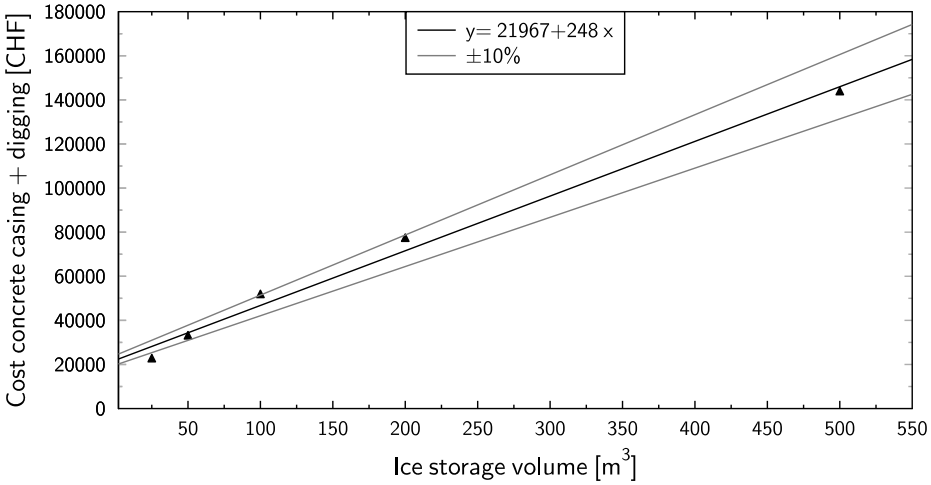

Figure 39: Costs of concrete casing on a new building including excavation.

For the heat exchangers inside the storage several offers have been collected with a price range that depends on the technology used. The cost is provided as a function of the ice storage volume:

$$\text{cost Hx ice storage} = 352^{+124}_{-152}\ \text{CHF/m}^3 \tag{27}$$

6.1.6 Cost of ground source heat exchangers

The GSHP system cost has been used as base line to compare solar-ice solutions. Several offers for vertical borehole heat exchangers with a total length up to 1800 m were used for the cost estimation. These cost had a large spread from 60 m to 100 m per borehole length, since they depend very much on the local conditions and supplier. To consider the large variety of cost per borehole length, the following assumption was used:

$$\text{Cost of borehole field} = 80 \pm 20\ \text{CHF/m} \tag{28}$$

6.2 Cost predictions of ground source systems as base line

In order to compare the costs of the solar-ice systems, a GSHP system without regeneration has been used as reference. Simulations and cost calculations of GSHP systems have been carried out using the same boundary conditions and methods as described for the solar-ice systems. In a GSHP system the SPF_{SHP} is depending on the ground temperature which decreases with time if no regeneration is implemented. Therefore the system has to be designed carefully to keep a good system efficiency after many years and to avoid freezing the ground. The dimensioning of the systems are based on the SIA-standard 384/6. System simulations in TRNSYS have been carried out to make sure that the ground temperature does not drop below 0.5 °C after a simulation time of 20 years.

Two cases for the city of Bern with normal weather conditions have been simulated. One for the new building MFB30 and the other for the refurbished building MFB90, both considering the real user behaviour. An example of the SPF_{SHP} development over the years is given in Fig. 40. The decrease of ground temperature and thus of the efficiency is higher in the first years and the slope of the decrease smooths after several years.

The heat costs for both cases are shown in Fig. 41 and the system performance, borehole length as well as heat cost are provided in Table 13. The twenty-years average SPF_{SHP} for both cases is around 3.9 to 4. The example for MFB30 uses four ground probes on a 2 x 2 field arrangement with a distance of 5 m each. The total probe length results in 280 m per probe. The example for MFB90 results in nine ground probes on a

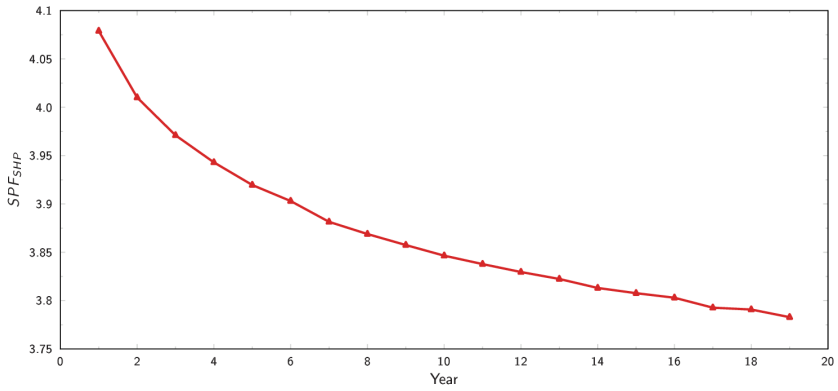

Figure 40: Development of the SPF_{SHP} over 19 years for MFB30 real in Bern with normal weather conditions.

3 x 3 field arrangement with a distance between boreholes of 5 m. The total borehole length results in 250 m per probe. Fig 41 shows the heat cost for these two cases using the cost data provided in section 6.1.6. The heat cost for the MFB90 is significantly lower.

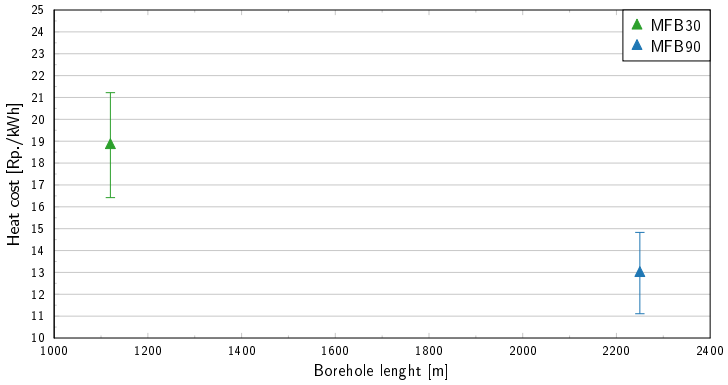

Figure 41: Heat cost for ground source heat pump systems for MFB30 and MFH90 buildings using real behaviour for Bern and normal weather conditions.

Table 13: Ground source heat pump reference case. Results for Bern and normal weather data.

building	Q_d	size Hp	Borehole length	Number of boreholes	Length per borehole	SPF_{SHP}	Heat cost
	MWh	kW	m		m		Rp./kWh
MFB30	64	28	1120	4	280	3.9	18.8±2.4
MFB90	156	50	2250	9	250	4.0	14.8±1.9

6.3 Cost predictions for solar-ice systems

The simulation data presented in section 4 have been used to calculate the heat cost for all the systems. The most important results of this section is the analysis of the heat cost with respect to different influencing factors such as weather data, building load profiles, as well as the sizes of key components like ice storage and collector area. In this regard, the absolute cost values are not too important since they depend on assumptions and boundary conditions. Solar-ice system are often seen as alternatives to ground source heat pumps, whose typical SPF_{SHP} is in the range of 4. Therefore, within this chapter, the focus is put on cases where the system performance is in this range. For presenting the cost in this section, the ice storage volume is given as the volume of the maximum ice fraction which was fixed to 80 % in all simulations. Thus, the ice storage volume is directly related to the latent capacity of the ice storage, which allows a better comparison between systems with different maximum ice fractions, which in turn depends on the heat exchanger and/or design concept used.

An overview of the heat cost for all simulations (all weather data sets, building types, and user behaviour) is given in Fig. 42 with a restriction to cases where the SPF_{SHP} ranges from 3.5 to 4.5. The median value for most of the cities is in the range of 22 Rp./kWh to 24 Rp./kWh. An exception is Davos with median cost in the range of 18 Rp./kWh. It is well known that the cold climate of Davos featuring intense irradiation due to clear skies in winter time Carbonell et al. (2017c) is well suited for solar-ice systems. One should keep in mind, however, that it has been assumed that collectors are not covered by snow, which could make a significant difference.

With the parameter values chosen for the simulations it can be seen in Fig. 42 that all cities have a non-symmetric heat cost distribution with respect to the median value. While the lower halves of the respective distributions show a density maximum at or slightly below the median, the situation is more complex for the upper half. There a local density minimum above the median with another somewhat stretched maximum above is visible for all locations. Although each location has a different irradiation profile the differences in heat cost are not significant in general, with the exceptions of Davos and Locarno.

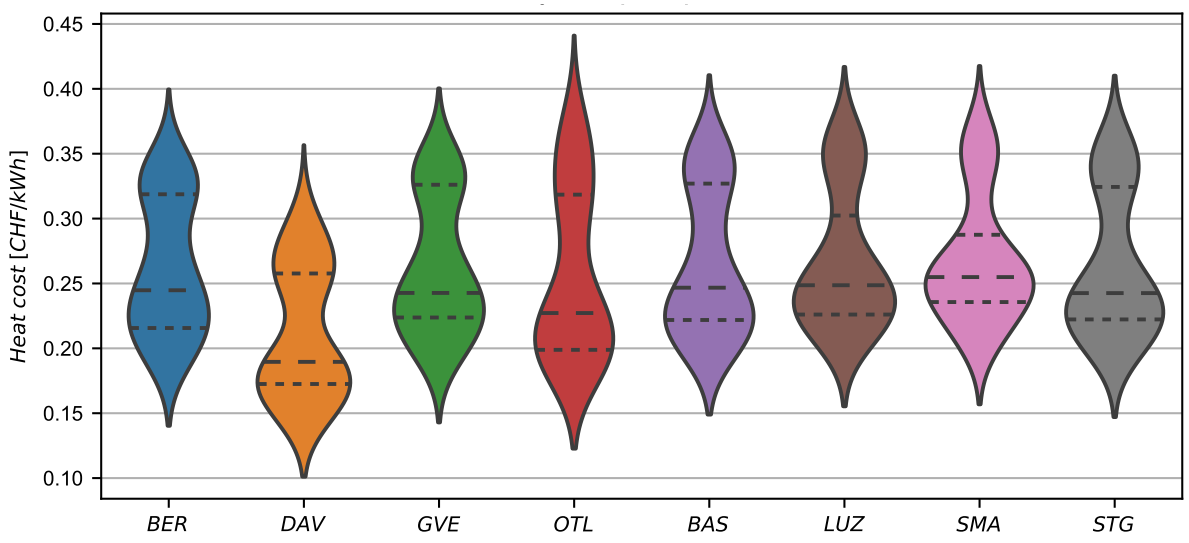

Figure 42: Heat cost for all cities, weather data, buildings and user behaviour for cases where the SPF_{SHP} ranges from 3.5 to 4.5.

In Fig. 42 the overall heat cost for all simulations with an SPF_{SHP} in the range of 3.5 to 4.5 has been presented without giving any information about uncertainties. The cost data presented in section 6.1, however, includes uncertainties and so does the cost calculation. As an example the SPF_{SHP} and heat cost with uncertainties for different cities, normal weather and an ice storage volume of $0.32\,m^3_{lat}/KWh$ is shown in Fig. 43. The average uncertainty for these results is in the range of 4 %. From these results it can be seen that large cost differences are obtained when changing the building profile, which is a result of the combination of

the building type and the user behaviour. This influence is way more significant than the location, at least for the cities considered here, i.e. Basel, Geneva, Bern and Zurich.

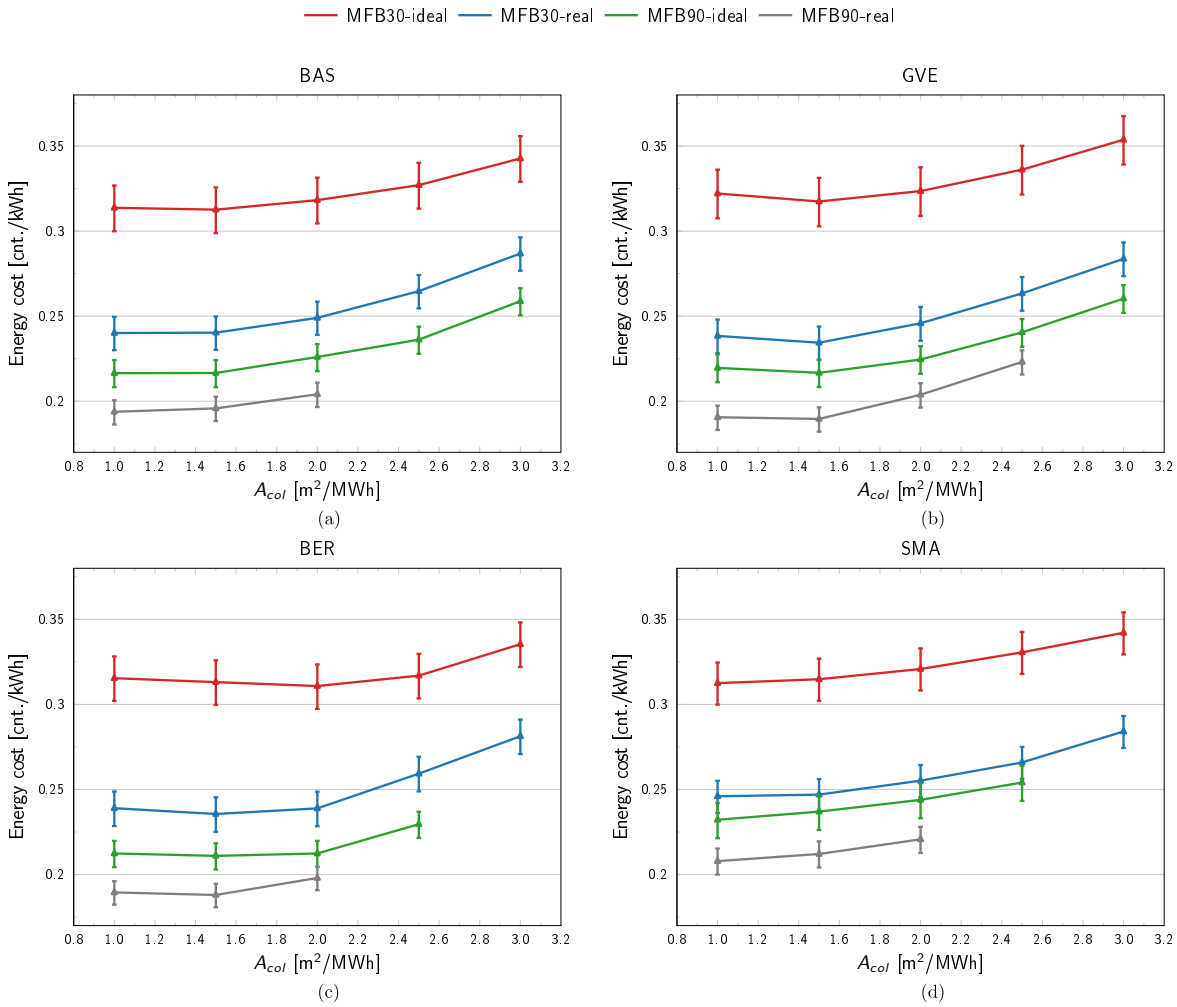

Figure 43: Heat cost with uncertainties for normal weather and an ice storage volume of 0.32 m^3_{lat}/KWh.

As discussed before, the highest interest is on systems that have a system efficiency equal to ground source heat pumps, i.e. an SPF_{SHP} of 4. The cost data including the cases where the SPF_{SHP} is equal to 4 are presented in Fig. 44 for normal weather data sets and location of Bern. Here, each plot features one of the two types of buildings (MFB30 and MFB90) with one of the two user behaviours (ideal and real).

The cost difference between the assumption of an ideal and a real user behaviour is very significant for MFB30. As can be seen in Fig. 44 for normal weather data, the heat cost for a system with an SPF_{SHP} of 4 is in the range of 30 Rp./kWh for an ideal behaviour and reduces to 23 Rp./kWh for a real behaviour, which represents a decrease of 24 %. As discussed in section 4.2 the lower winter demand share achieved when assuming real user behaviour improves the solar-ice system efficiency. For the case of Bern and normal weather data, the winter share is reduced by 32 % when a real user behaviour is used. Additionally, MFB30 with ideal user behaviour has a high share of domestic hot water demand of about 45 % of the total heat demand. This heat has to be provided at the higher temperature level for domestic hot water (as discussed in section 4.2 Fig. 14). This ratio decreases to about 30 % for MFB30 with real user behaviour and further decreases for MFB90. Therefore, in order to achieve an SPF_{SHP} of 4 the system sizes (collector area and ice storage volume) can be reduced and the system heat cost are improving. For the same reasons, the heat

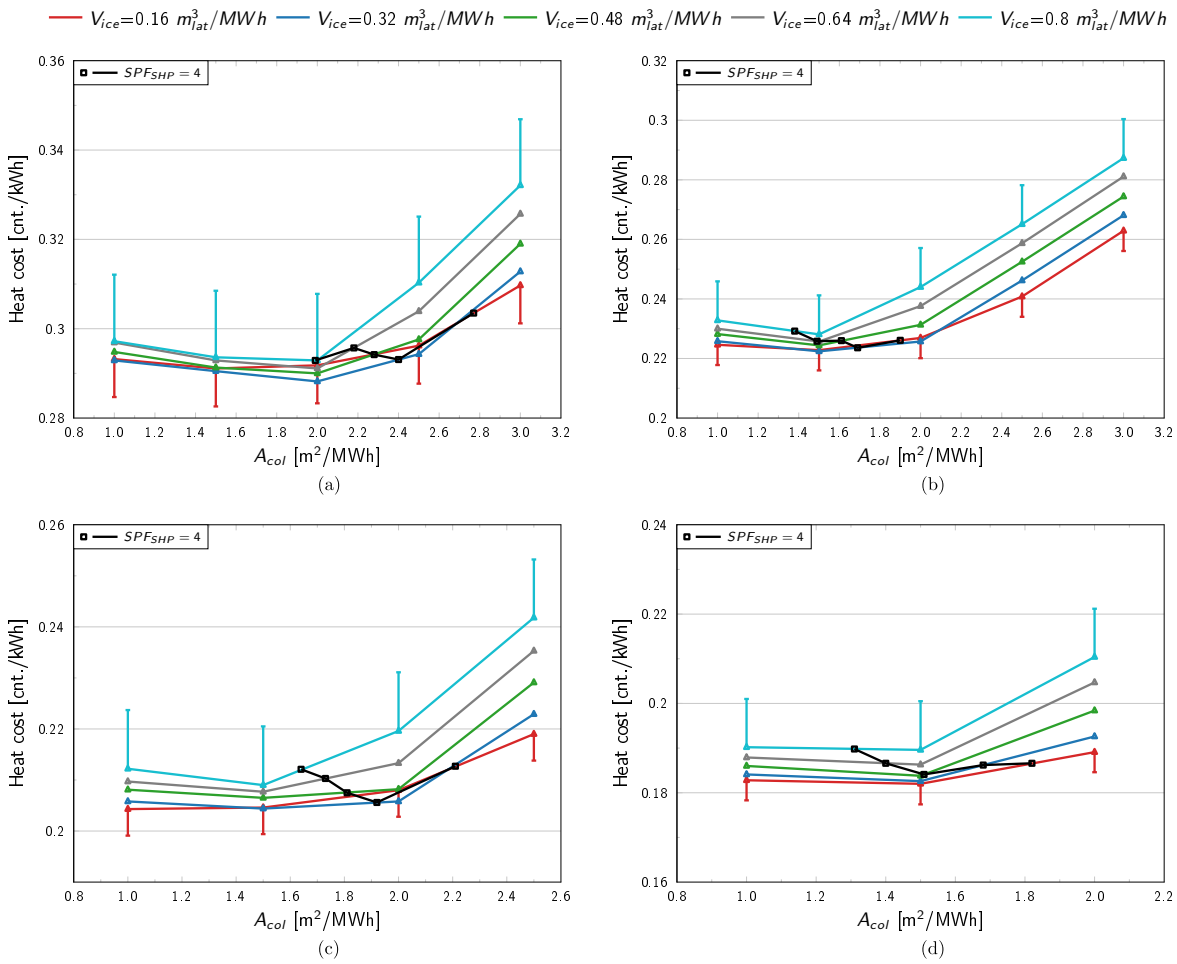

Figure 44: Heat cost and SPF_{SHP} for Bern and normal weather (a) MFB30-ideal (b) MFB30-real (c) MFB90-ideal (d) MFB90-real. Black lines represent the cost for cases where the SPF_{SHP} is 4. Heat cost are calculated with uncertainties, but are only shown in upper and bottom lines for visual clarity.

cost for MFB90 is lower in general. The fact that more demand needs to be covered in autumn and spring benefits solar-ice systems. Once a real behaviour is added this effect is even more prominent. The heat cost for MFB90 is in the range of 21 Rp./kWh for an ideal behaviour and goes down to 19 Rp./kWh for a real behaviour, which represents a 11 % reduction. In overall the cost is reduced by 18 % to 29 % when using the MFB90 instead of the MFB30 for real and ideal cases respectively. For all cases, the cost optimum for an SPF_{SHP} of 4 is reached by using an ice storage volume in the range of 0.32 m^3_{lat}/kWh to 0.48 m^3_{lat}/kWh. For three demand profiles in Bern, shown in Fig. 44, the cost minimum was reached for a latent capacity of the ice storage of 0.32 m^3_{lat}/MWh. Only for MFB90 with real user behaviour (Fig. 44 (d)) the cost minimum was achived for a latent capacity of 0.48 m^3_{lat}/MWh but the difference to 0.32 m^3_{lat}/MWh is not significant. The system targeting MFB30 with ideal user behaviour needs around 0.8 m^2/MWh larger collector area in comparison to MFB90 for reaching a SPF_{SHP} of 4.

An overview of heat cost for cases where the SPF_{SHP} is equal to 4 is shown in Fig. 45 for Bern, Locarno, Geneva, and Basel for warm (left column), normal (center) and cold (right) weather data sets. Missing data on the cold weather is due the limitation on the absolute collector area and thus the inability to reach an SPF_{SHP} of 4 for MFB90. In case of MFB30 with ideal user behaviour and cold weather conditions the target SPF_{SHP} could not be reached for some cities. Note that the components used are scaled by the total heat

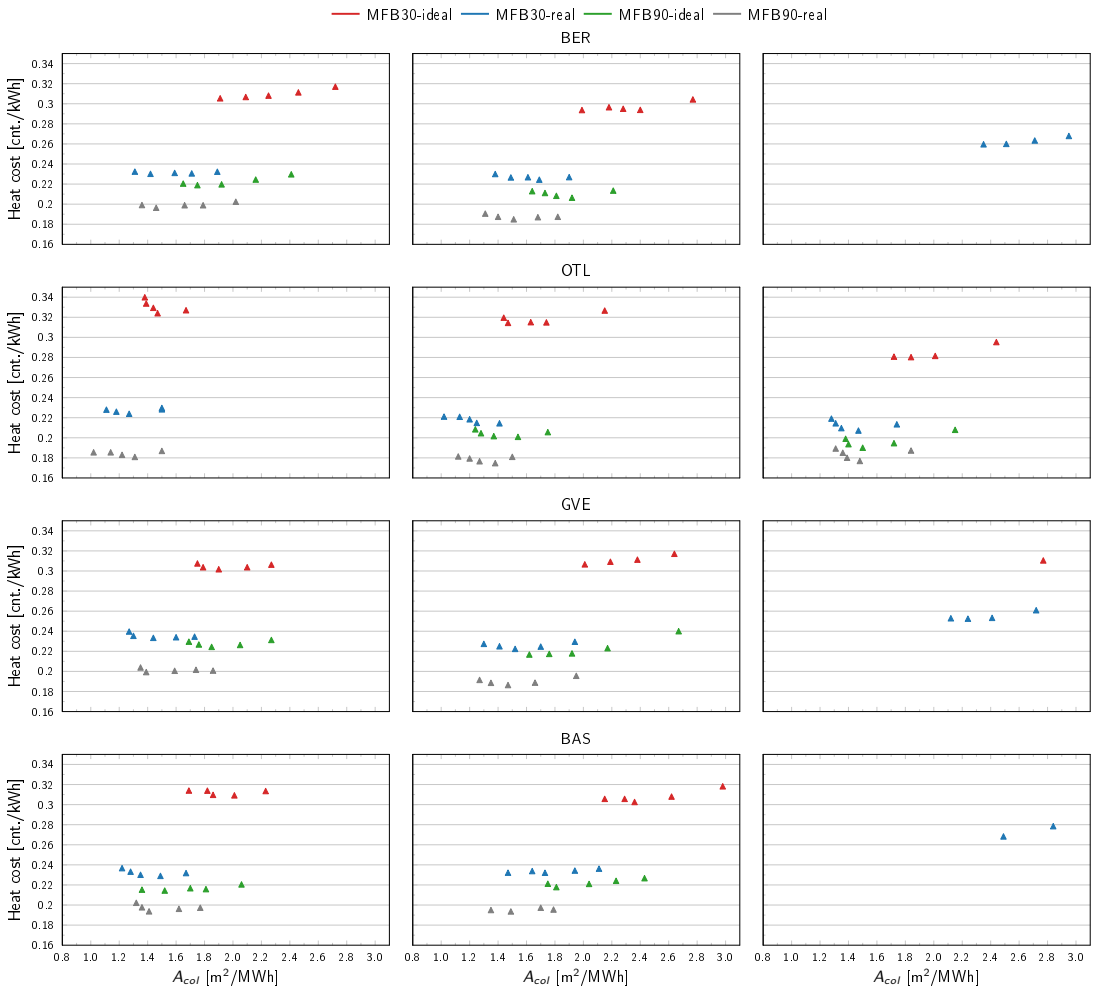

Figure 45: Heat cost as a function of collector area for Bern, Locarno, Geneva and Basel for simulations that reach an SPF_{SHP} of 4 for warm (left), normal (center), and cold (right) weather data. The different data points on each line represent the different ice storage volumes. Missing data on cold weather means that the SPF_{SHP} of 4 was not achieved.

demand, which depends on location, weather data used and building demand, i.e. the combination of building type and user behaviour. Thus, except for the data points of the same color in each plot, the absolute sizes are different, but all cases reach an SPF_{SHP} of 4, i.e. they can be compared to each other. For these cities the heat cost range from 17 Rp./kWh to 34 Rp./kWh, but as can be observed, the dominant cost factor is the building demand profile. The best case scenario for heat cost in cnt./kWh is an old building MFB90 with a real user behaviour. For this case the heat cost range 17 Rp./kWh to 20 Rp./kWh for all the four cities. Assuming an ideal behaviour for MFB90 the heat cost increases to a range of 19 Rp./kWh to 24 Rp./kWh. For a new building MFB30 and a real user behaviour the cost range from 19 Rp./kWh to 24 Rp./kWh for normal and warm weather. For cold weather the upper heat cost increases to 27 Rp./kWh. From all these cases, the worst case scenario for the competitiveness of solar-ice systems in spefici cost terms (cnt./kWh) is the assumption of a new building with an ideal user behaviour. This case leads to a cost range of 28 Rp./kWh to 34 Rp./kWh.

Results presented here show the very significant influence of the building demand profile on the heat cost of solar-ice systems. Depending on the boundary conditions systems achieving an SPF_{SHP}=4 can deliver heat cost of 18 Rp./kWh in the best case scenario and go up to 34 Rp./kWh in the worst case. Thus, attention must be paid to the building demand profile assumed for the sizing, since heat cost can almost double. Note that a solar-ice systems is stressed to the strongest level at peak winter times. All measures that relieve or smooth the winter peak heat demand will make a significant impact on efficiency and cost. It should be considered that the building reference type is a relatively small building with only six apartments. A solar-ice system is a system that has a high investment cost with a good energetic efficiency if well designed.

Cost per kWh is a standard measure for comparing different heating systems for the same building, hence, for the same demand profile. Well insulated buildings increase the costs per kWh but the total energy costs per year are still lower. The system efficiency and therefore the energy cost per kWh benefits from delivering high energy demands and can be more attractive for high energy demand buildings with lower winter share and lower share of domestic hot water, if there is enough roof space. This might, however, be an issue for large buildings with a relatively small roof area. All cases shown in Fig. 45 except Locarno (OTL) for warm weather conditions show that for the same scaling factors for the latent capacity of the ice storage the collector field has to be larger for reaching SPF_{SHP} of 4 with ideal user behaviour compared to real. For systems with an almost 50 % share of domestic hot water compared to the total demand, a heat pump should be used that is more optimized for the preparation of hot water demands.

Not only solar-ice systems but every heat pump system will be influenced by the domestic hot water share of the heat demand. In systems with a source temperature that is depending on the ambient temperature efficiency cost will always be related to the distribution of the heating demand over the year as well.

6.4 Cost comparison between solar-ice and ground source systems

In this section a one to one heat cost comparison between solar-ice and GSHP systems without regeneration is provided. Results for MFB30 and MFB90 using Bern with a normal weather data and real user behaviour are presented in Fig. 46. In both cases the average costs of GSHP systems are lower compared to solar-ice systems for the weather data of Bern. Notice, however, that the more accurate comparison of a solar-ice system would be the use of a GSHP system with full regeneration of the ground. In regions with dense populations the regeneration of the ground will probably become mandatory within the next years. In this scenario, GSHP systems will become more expensive than calculated in the present work. Nevertheless, the case without a regeneration is used here because this is the current state-of-the-art GSHP system. It is also important to remark that present cost calculations for solar-ice are based on a system using uncovered selective collectors which allow to produce DHW demands directly, but they are way more expensive compared to plastic absorbers used in other solar-ice concepts. Cost comparisons and system efficiencies of systems using plastic absorbers were not carried out in the present work due to missing data for system validation. This will be available in near future due to a collaboration with a German university partner.

In order to analyse the cost competitiveness of solar-ice systems in comparison to GSHP it is useful to compare the installation cost of the borehole field with the cost of the solar collector field and the ice storage. Let's take as an example the MFB30 case with a 68 MWh heat demand. The borehole length necessary is about 1120 m. Assuming a cost of 80 CHF/m one gets an installation cost of 89 600 CHF. For this particular

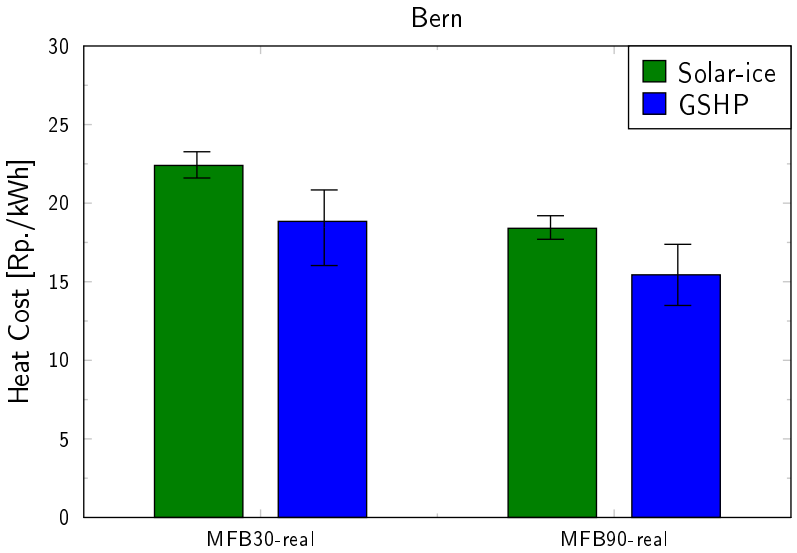

Figure 46: Heat cost for Bern and normal weather for MFB30 and MFB90 with real user demands for solar-ice and GSHP systems. Sizes were selected to reach an SPF_{SHP}=4.

case an ice storage of 25 m^3 and a collector field of 108 m^2 would be necessary. The installed cost target of 89 600 CHF from the borehole field can be achieved using different sets of costs:

- An ice storage cost of 560 CHF/m^3 and a collector field of 700 CHF/m^2
- An ice storage cost of 776 CHF/m^3 and a collector field of 650 CHF/m^2
- An ice storage cost of 992 CHF/m^3 and a collector field of 600 CHF/m^2

Notice that using the current cost for uncovered selective collectors of around 850 CHF/m^2 the cost of the collector field in this particular case is slightly above the cost of the borehole field. Thus, some kind of cost reduction of the collector field would be necessary to include the cost of an ice storage. Considering that the current cost of uncovered selective collectors is in the same range as covered collectors, we believe there is quite some room to improve here. Regarding the ice storage cost we believe that cost targets in the range of 500 CHF/m^3 are possible eliminating all heat exchangers in the ice storage and using an ice slurry technology which is currently under development at our institute. All together it is expected that future solar-ice systems would have a similar cost than GSHP with the benefit of not needing additional regeneration.

7 Conclusions

7.1 Conclusion on simulation study and costs

The simulation study, analysing a wide range of parameters for eight different cities, four different heat demand profiles (MFB30 and MFB90 with ideal and real user behaviour), three sets of weather data and different hydraulic implementations, gives important insight into the dependencies of the system and cost efficiency of solar-ice heating and cooling systems. For all locations simulated and all different buildings demand profiles it is possible to design a solar-ice system that has an SPF_{SHP} of 3.5 to 4.5 in normal and warm weather conditions with levelized cost of heat in the range of 18 Rp./kWh to 35 Rp./kWh. For reaching similar system efficiency, buildings with a high insulation standard have to be sized with larger relative collector fields (m^2/MWh) and/or ice storages (m^3/MWh) than those with a lower insulation standard despite of the lower absolute size requirements. For buildings with low insulation standard the limiting factors are the roof space for the solar thermal collectors and the space for the ice storage.

Besides the collector field area and the latent capacity of the ice storage the following main factors influencing the system efficiency and cost have been found:

a) **Demand profile**. The influence of the demand profile is decisive for the system efficiency. A high winter share of the space heating demand and/or a high domestic hot water share of the total demand lower the SPF_{SHP} for identical scaling factors for collector field area and ice storage volume. Therefore, buildings with a high insulation standard, which have a high winter share and a high domestic hot water share (MFB30 in this study), have a disadvantage in the direct comparison with same scaling factors. Ideally, the winter share of the heating demand would be considered during the planning phase for sizing the solar-ice system. The levelized cost of heat is also strongly dependent on the winter and the domestic hot water share of the total demand. The lower the heat winter and DHW demands are with respect to the total demand, the lower are the specific heat costs of the system.

b) **Winter irradiation**. Comparing the system efficiency of a solar-ice system for different cities with three sets of weather data each, the SPF_{SHP} strongly correlates with the winter solar irradiation. The high solar radiation in winter periods of Locarno and Davos is the main reason of the strong performance achieved at these locations. The results from Davos shown here are, however, overestimating this effect, since the impact of snow on the collectors is not considered. The real performance would depend on the frequency of snow removal. The system performance was observed to be much lower in regions with a foggy winter season. The SPF_{SHP} was up to 25 % lower for the cold weather data set compared to the normal one at locations, where the winter irradiation was much lower in the former set with respect to the latter. Large differences in SPF_{SHP} of up to 30 % between warm, normal and cold years have been observed.

c) **Hydraulic connection**. Different possibilities to integrate solar thermal heat into the solar ice system have been tested. The more options there are to use the solar heat, the higher is the efficiency of the solar-ice system. This is particularly important because the added cost for these hydraulic connections is very small compared to the total system cost. However, more options lead to an increased complexity of the heating system, hence, a carefully designed system control is essential for a system to work efficiently. Solar-ice systems benefit significantly when solar heat can be used in series on the heat pump. System efficiencies improve in the range of 20 % to 40 %. Fortunately, this hydraulic connection is often used in current multi-family buildings installations. The use of direct solar heat into the warm storage improves the SPF_{SHP} by 10 % to 20 % for cities with lower irradiation like Zurich and Bern and up to 50 % for cities with high irradiation like Locarno. Without this heat flow, the system efficiency will always be lower than the SPF of the heat pump alone, which is not the case for most of the systems simulated in this report. Notice that the use of solar heat directly in the warm storage is, at least, ten times more efficient compared to the heat pump operation.

d) **Cooling potential**. Results presented in section 4.5 demonstrate the general potential of the solar-ice system for cooling application. Using an economically feasible dimensioning of the system, almost sufficient cooling can be provided for locations with low cooling demand like Geneva for normal weather data by simply stopping the active melting of the ice during spring. A passive cooling approach is not sufficient, however, to cover the full cooling demand at locations such as Locarno with any weather data or Zurich and Geneva with warm weather data, but it allows to improve comfort for free by reducing the room temperature. Energetic performance considering the cooling demands increase by about 2 % to 5 %.

Using an insulated ice storage increases the cooling delivered to the building by up to 25 %. Due to the insulation, gains from the surrounding are reduced in winter months leading to a higher electricity demand for heating due to an extended use of the electric backup. Insulating the ice storage will add investment cost and reduce heating performance. It is not likely that the additional cooling demands provided can compensate these two negative impacts. By using the cold of the heat pump evaporator during the summer months the cooling potential of the system can be more than doubled. Since the heat pump replaces freely available heat from the solar collector, this approach leads to a decreased SPF_{SHP} (only heating) of the system by about 10 % to 20 %. Including the cooling provided, the overall system $SPF_{SHP,c}$ is reduced by only 5 % to 10 %. Whether such an approach is economically beneficial will largely depend on the case-to-case basis.

If the ice storage volume is defined according to the heating demand, a warmer climate will lead to a smaller ice capacity. Consequently, this is counterproductive when trying to cover a higher cooling demand during summer. Some optimization can be made by increasing the ice storage volume and reducing the collector field in a way that the same SPF_{SHP} is reached for heating, but more ice storage capacity is available for cooling. Optimization of cooling demands can also be achieved by stopping the melting of ice earlier in winter. We have used a very simple control strategy stopping the ice regeneration once the ice storage was below 50 % and February has passed on. Clearly, there is room to improve.

e) **Levelized cost of heat**. As a reference case to compare cost of solar-ice systems, the GSHP system without regeneration has been used. Simulations for the city of Bern with borehole lengths that reach an SPF_{SHP} in the range of 4 lead to heat costs of 19±2.4 Rp./kWh for MFB30 and 15±1.9 Rp./kWh for MFB90. For these two particular cases solar-ice systems are more expensive with heat cost in the approximate range of 22±0.8 Rp./kWh and 18±0.8 Rp./kWh respectively. If regeneration needs to be added in the GSHP systems, then the cost of solar-ice is expected to be lower compared to the GSHP with regeneration. However, this cost calculation has not been carried out. As an order of magnitude, the installation cost of ice storages in the range of 500 CHF/m^3 to 1000 CHF/m^3 together with collector field installation cost in the range of 600 CHF/m^3 to 700 CHF/m^3 will lead to same cost as GSHP systems calculated with 80 CHF/m for new buildings (MFB30 with around 1100 m borehole length). The current research at our institute on the ice slurry technology is expected to decrease installation cost of the complete system up to 10 % and increase the SPF_{SHP} significantly. With this technology, ice storage cost targets of 500 CHF/m^3 to 800 CHF/m^3 are well achievable. Besides the ice storage cost reduction, what will be necessary to reach same investment cost of GSHP, is a reduction of the collector field from the current cost of 850 CHF/m^2 to around 700 CHF/m^2. Considering that current uncovered selective collectors are in a similar cost range as covered flat plates, there is quite some room for cost reduction in this particular solar technology. It should also be noted that plastic absorbers are well below the solar cost target of 600 CHF/m^3 to 700 CHF/m^3 and therefore investment cost can certainly be reduced using plastic absorbers. This will, however, penalize the system efficiency demanding of higher collector field area and ice storage volume to reach same system efficiency. The cost comparison for using plastic absorbers without the possibility to provide solar direct heat to DHW and SH has not been carried out.

7.2 Conclusion on machine learning

The main result of the current study is that XGBoost clearly shows the best prediction performance of the methods tested with the exception of extrapolations in $H_{T,\,field}/Q_d$ and V_{ice}. Moreover, already for very little input information like in the case of Y_1, where only three parameters are provided, XGBoost delivers very satisfying results with more than half of the error distribution within ±3 % and 90 % of data points within ±10 %. The three parameters are Q_d, $H_{T,\,field}/Q_d$ and V_{ice}, which all will certainly be known for systems that are supposed to be examined.

An important question when applying machine learning methods is whether the training set provided is sufficient to generate reliable predictions. The improvement saturation that can be seen for XGBoost with $m_{\text{train}} \geq 2000$ validates the claim that the default $m_{\text{train}} = 2400$ is sufficient to train this method. Beyond that, to make predictions for input parameters that have not been simulated, which is the desired application, all 3437 data points available can be used to train the method, since there won't be a need for a test set. Furthermore, it was also shown that the number of training points is plentiful to optimize the linear regression. Another important question for the applicability of the explored methods for real cases is their robustness

towards new locations. There will always only be a finite number of locations represented in the training set, but the method should still be able to generate reliable predictions for all of Switzerland. As shown, having a training set including five diverse locations is adequate to generate solid predictions for another four diverse locations. Hence, using all twelve available locations to train a method should suffice the requirement to make meaningful claims for any inhabited location in Switzerland.

The poor performance of the linear regression and XGBoost for the extrapolations in $H_{T,\,\text{field}}/Q_d$ and V_{ice} indicates that the methods at hand are best used for interpolation along these parameters and less so for extrapolation. Hence, wide ranges in parameter space should be covered by the underlying simulations to ensure precise predictions can be provided for a ample range of boundary conditions. Reducing the test set to points with $SPF_{SHP} \in (3.5, 4.5)$, which is the range most real application cases will be tuned for, improves the performance of the linear regression.

For a reliable prediction of values that are not included in the training set, locations and scaling factors alike, the training set has to be chosen carefully. Locations should represent different climatic conditions that match with those that are supposed to be predicted. The data point distribution over scaling factors should be uniform to avoid introducing biases in the prediction, to which XGBoost is particularly susceptible.

As argued in section 5.2.1, there is no benefit from using regularisation methods as compared to simple linear regression with respect to run time and prediction performance. The feature selection capabilities of Lasso, though, could still be useful for exploring the relevance of different input parameters. As mentioned above, when operating with monthly values, several coefficients for non-winter values are set to zero. Lasso thus does not offer better prediction performance, but could be used for analyzing the impact of different parameters in the future. Furthermore, the nearest neighbour method provides a better prediction performance than the linear regression for both Y_2 and M_2, which shows that a table, that is sufficiently dense in parameter space, can be employed for directly looking up output values. Of course, this is strictly limited to the simulated parameter space.

8 Outlook and next steps

One goal of the current project was to identify the potential of solar-ice systems for typical multi-family buildings in Switzerland. The sizes of collector field and ice storage able to achieve energetic system efficiencies in the range of 3.5 to 4.5 are in a realistic range for new and refurbished MFB. However, the typical MFB has six apartments with only three levels and thus, it has a significant roof-area-to-demand ratio. A representative MFB building with 400 m^2 available roof area has been used, for which we limited the roof area available for collectors to 350 m^2. The absolute heat demand for Zurich ranges from 41 MWh to 153 MWh for MFB30 with ideal to MFB90 with real user behaviour respectively. For large buildings with many floors, where the roof-area-to-demand ratio is low, roof space might be a problem and façade collectors would need to be considered. It is also possible to increase the ice storage volume to partially compensate a lack of collector area, but this is of course only possible to a certain extent since solar energy is the only renewable heat source of the system. This is also an issue when thermal collectors compete with PV for roof space. In this regard, the use of PVT has been a solution for some real installations and further analysis towards this direction might be necessary, especially when considering a fast algorithm tool. Note that classical uncovered PVT collectors are not able to deliver a lot of solar heat at DHW levels and therefore results need to account for that. Alternatives such as covered PVT could also be investigated.

Well insulated buildings (MFB30) show lower system efficiencies due to a high winter share of the heating demand and a higher domestic hot water to space heating demand ratio when compared to refurbished buildings (MFB90). As domestic hot water has to be provided at much higher temperatures, an increase in said ration leads to a decrease in the system efficiency. This effect is even more prominent in MFBs due to the re-circulation losses of the DHW loop that need to be provided at high temperatures. In future projects, we might consider different kinds of heat pumps designed for providing higher temperatures with better efficiency (e.g. CO_2 heat pumps). This is, for example, the approach we are following in the H2020 TRI-HP project[5].

Results shown in this report are obtained with a simulation assuming an ice storage buried in the ground. This decision was taken for two main reasons: i) the coupling of a buried ice storage with the ground was validated with monitoring data in Carbonell et al. (2016b) and thus we have confidence in this situation provided that the ground around the ice storage has similar properties; ii) the complexity to find a "standard" case of an ice storage in a cellar of the building. The key factor here are the heat gains in winter, which depend very much on the cellar temperature. In this case, cellar temperature, heat gains of the ice storage as well as the heating demand of the building cannot be decoupled and need a detailed analysis. With this report we have highlighted the key aspect of winter conditions, both in irradiation availability as well as on the heat demand side. Heat gains to the ice storage in winter are directly reducing the electric back-up and thus the SPF has a linear dependence on these gains with a significant impact. In our simulations, for most cases, averaged winter heat gains in the ice storage are in the range of 30 kWh/m^3 to 50 kWh/m^3 with respect to the volume of the ice storage. The lower range is achieved for large ice storages in the range of 0.8 m^3_{lat}MWh. Heat gains are difficult to measure directly, but indirect calculations using monitoring data from a real installation (Carbonell et al., 2016b) lead to heat winter gains in the order of 30 kWh/m^3 with an storage volume of 1.3 m^3_{lat}/MWh. Thus, winter gains achieved are reasonable for ground buried ice storages. To arrive at a more accurate system analysis for cellar located ice storages, not only the coupling of the ice storage with the building needs to be considered, but also the effect of the gain/losses from the ice storage in the building demands. Thus, the question of how much can one expect to gain in winter from the cellar or basement of the building is still an open question that does not only need detailed simulations with building coupling, but also monitoring data to ensure reliability of simulation results.

Simulations reported in this report are based on using uncovered selective collectors that can provide direct solar heat for DHW. However, a system concept using cheap plastic collectors is also very common. Although its hydraulic integration has been analysed, it was done considering only one heat exchanger in the ice storage which underestimates the heat gains from the collector field since it can not charge the ice storage while the heat pump is discharging. Moreover, the cost analysis of these two system concepts is of importance. The main reason for not having presented these results yet is because we lack monitoring data to validate the second option and therefore results will not be reliable. However, we are in the process of acquiring this data

[5] www.tri-hp-eu

and we expect to have a validated simulation environment this year for this concept. Once this will be available a further analysis can be done to repeat all simulations carried out here using the second system concept and include this system setup in the fast algorithms.

The data bases and the algorithms to develop a fast and easy to use tool for feasibility analysis of solar-ice systems in Swiss climates were created. This can potentially increase the deployment for solar-ice systems since a feasibility study can be conducted with no effort, which reduces the need to conduct transient simulations for early assessments where also little information is available. Reducing engineering cost on this step has the potential to help the market deployment. The algorithms will serve a follow-up market oriented project to develop an appealing front-end graphical user interface. The development of a feasibility tool for a fast estimation of the optimal size of the different components for a certain location and building could be the basis for a broader use of solar-ice systems in new and in refurbished buildings. In order to build a feasibility tool that is broadly applicable the influence of different factors such as collector types or additional heat gains, e.g. from a heat recovery ventilation unit, could be included.

Cost analysis of solar-ice systems show that these systems, if well designed, can be cost competitive. However, a one to one comparison with a ground source heat pump system still leads to a higher cost for solar-ice systems. Thus, cost reductions are necessary to push these types of systems further. In this regard, eliminating the heat exchangers in the storage is a promising approach. For that, an ice slurry concept was proposed at our institute in the Slurry-HP project (Carbonell et al., 2017b) and followed up with a chain of consecutive projects to develop the supercooling method (Carbonell et al., 2023, 2020a) and the design of ice slurry storages (Carbonell et al., 2020b). With this technology, ice storage cost in the range of 500 CHF/m^3 to 800 CHF/m^3 are expected leading to a 10 % cost reduction in the overall system installation cost. Although this alone might not be enough to fully cover current cost differences with GSHP systems, it will bring solar-ice systems to a very cost competitive range.

Results of the projects together with advances in innovative concepts using ice slurries lead us to the concept of integrating ice storages into ultra-low temperature district heating networks. This concept will be analyzed in the upcoming project IceGrids also funded by SFOE. In this project we will study the potential of ice storages implemented into low temperature thermal “anergy” networks as seasonal storage as well as as short-term storage to cover peak winter demands.

9 National and International collaboration

A national collaboration has been carried out with planning companies that acted as an Advisory Board at the beginning of the project. The Advisory Board was composed by Bernard Thissen from Energie Solaire SA, Stefan Braendle and Romain Spaeth from Amstein & Walthert and Frank Doppenberg from BG Ingénieurs Conseils.

An international collaboration has been initiated with the Institute of Water and Energy Management at Hof University, Germany. Researchers from Hof are using the ice storage TRNSYS model and the system simulation framework pytrnsys with its GUI developed at our institute. The goal is to validate the ice storage model and the complete system for the Viessmann Vitrofriocal (Isocal) concept. These results are expected to provide a validation of our numerical tools in order to consider this system in future works. In particular, since the Viessmann system is largely deployed in Switzerland, we aim to include this one into the fast algorithm tool.

References

Alonso, L., Gerber, R., Schubert, M., Losada, R., Brand, J., Schmid, O., Nilsson, M., Pardiñas, A. A., Zendehboudi, A., and Carbonell, D. (2020). Economic assessment of TRI-HP solutions. *Deliverable 1.4 TRI-HP: Trigeneration systems based on heat pumps with natural refrigerants and multi renewable sources*, Horizon 2020 research and innovation programme under grant agreement N. 814888.

BFE (2020). Energieperspektiven 2050+. Zusammenfassung der wichtigsten Ergebnisse. Technical Report Bundesamt für Energie BFE.

Carbonell, D., Battaglia, M., Daniel, D. P., and Haller, M. Y. (2017a). *Ice-Ex - Heat Exchanger Analyses for Ice Storages in Solar and Heat Pump Applications*. Institut für Solartechnik SPF for Swiss Federal Office of Energy (SFOE), Research Programme Solar Heat and Heat Storage, CH-3003 Bern.

Carbonell, D., Battaglia, M., Philippen, D., and Haller, M. (2018a). Numerical and experimental evaluation of ice storages with ice on capillary mat heat exchangers for solar-ice systems. *International Journal of Refrigeration*, 88:383 – 401.

Carbonell, D., Battaglia, M., Philippen, D., and Haller, M. Y. (2018b). Numerical and experimental evaluation of ice storages with ice on capillary mat heat exchangers for solar-ice systems. *International Journal of Refrigeration*, 88:383–401.

Carbonell, D., Daniel, D. P., and Haller, M. Y. (2017b). *Slurry-Hp - A feasibility study on the use of a super-cooling ice slurry heat pump for solar heating applications*. Institut für Solartechnik SPF for Swiss Federal Office of Energy (SFOE), Research Programme Heat Pumps and Refrigeration, CH-3003 Bern.

Carbonell, D., Kauffeld, M., Nilson, M., Salom, J., de Mendibil, A. D., Raisch, S., Bischoff, C., Stiess, I., Ángel Álvarez Pardiñas, Gerber, R., Derjanecz, A., and Cruz, G. (2019-2023). *TRI-HP - Trigeneration systems based on heat pumps with natural refrigerants and several renewable sources.* European Union's Horizon 2020 research and innovation programme under grant agreement No. 814888.

Carbonell, D., Philippen, D., Battaglia, M., and Haller, M. Y. (2017c). Cost energetic analyses of ice storage heat exchangers in solar-ice systems. In *ISES Conference Proceedings. International Conference on Solar Heating and Cooling for Buildings and Industry (SHC 2017)*, Abu Dhabi, United Arab Emirates.

Carbonell, D., Philippen, D., Dudita, M., Schmidli, J., Schubert, M., and Erb, K. (2020a). *Slurry-Hp II - Development of a supercooling ice slurry heat pump concept for solar heating applications*. Institut für Solartechnik SPF for Swiss Federal Office of Energy (SFOE), Research Programme Heat Pumps and Refrigeration, CH-3003 Bern.

Carbonell, D., Philippen, D., Granzotto, M., and Haller, M. Y. (2016a). Simulation of a solar-ice system for heating applications. System validation with one-year of monitoring data. *Energy and Buildings*, 127(0):846 – 858.

Carbonell, D., Philippen, D., and Haller, M. Y. (2016b). Modeling of an ice storage buried in the ground for solar heating applications. Validations with one year of monitored data from a pilot plant. *Solar Energy*, 125:398–414.

Carbonell, D., Philippen, D., Haller, M. Y., and Frank, E. (2015). Modeling of an ice storage based on a de-icing concept for solar heating applications. *Solar Energy*, 121:2–16.

Carbonell, D., Theiler, D., Daniel, D. P., and Erb, K. (2020b). *Slurry-Store - Experimental and numerical investigations of ice slurry storages.* Institut für Solartechnik SPF for Swiss Federal Office of Energy (SFOE), Research Programme Solar Heat and Heat Storage, CH-3003 Bern.

Chen, T. and Guestrin, C. (2016). XGBoost: A scalable tree boosting system. In *Proceedings of the 22nd ACM SIGKDD International Conference on Knowledge Discovery and Data Mining*, pages 785–794. ACM.

Huber, A. and Pahud, D. (1999). *Erweiterung des Programms EWS für Erdwärmesondenfelder*. Huber Energietechnik Bundesamtes für Energie (BFE), Forschungsprogramm Umgebungs- und Abwärme, Wärme-Kraft-Kopplung, CH-3003 Bern.

ISO 13790:2008 (D) (2008). Energy performance of buildings – calculations of energy use for space heating. Standard, European Committee for Standardization, Brüssel, BE.

Iturralde, J., Alonso, L., Carrera, A., Salom, J., Battaglia, M., and Carbonell, D. (2019). Energy demands for multi-family buildings in different climatic zones d1.1. *Deliverable 1.1 TRI-HP: Trigeneration systems based on heat pumps with natural refrigerants and multi renewable sources*, Horizon 2020 research and innovation programme under grant agreement N. 814888.

Jakubcionis, M. and Carlsson, J. (2017). Estimation of European Union residential sector space cooling potential. *Energy Policy*, 101:225–235.

Kalogirou, S. A. (2001). Artificial neural networks in renewable energy systems applications: a review. *Renewable and Sustainable Energy Reviews*, 5(4):373–401.

Klein et al. (2010). Trnsys 17: A transient system simulation program, solar energy laboratory. Technical report, University of Wisconsin, Madison, USA, http://sel.me.wisc.edu/trnsys.

Klyachin, V. A. and Shirokii, A. A. (2012). The delaunay triangulation for multidimensional surfaces and its approximative properties. *Russian Mathematics*, 56(1):27–34.

Lamarche, L. and Beauchamp, B. (2007). A new contribution to the finite line-source model for geothermal boreholes. *Energy and Buildings*, 39(2):188–198.

Leconte, A., Chèze, D., and Jobard, X. (2014). TYPE 5897 - ISO building model, model description. unpublished.

Malenkovic, I., Eicher, S., and Bony, J. (2012). *Definition of main system boundaries and performance figures for reporting on SHP systems*. IEA-SHC Task44 Subtask B.

Marcucci, A., Guidati, G., and Giardini, D. (2021). Probabilistic assessment of the swiss energy strategy - scenario analysis with the SES-ETH model. Technical Report JASM final report.

Mojic, I., Luzzatto, M., Haller, M., Lehmann, M., Benz, M., and van Velsen, S. (2018). *Einfluss der Kombination aus Nutzerverhalten und Gebäudetechnik auf den Performance Gap bei Mehrfamilienhäuser*. Institut für Solartechnik SPF for Swiss Federal Office of Energy (SFOE), Gebäude und Städte.

Philippen, D., Carbonell, D., Granzotto, M., Zenhäusern, D., Haller, M. Y., and Brunold, S. (2015). *High-Ice - System development for high solar thermal gains with ice storage and heat pump*. Institut für Solartechnik SPF for Swiss Federal Office of Energy (SFOE), Research Programme Solar Heat and Heat Storage, CH-3003 Bern.

Philippen, D., Carbonell, D., Haller, M. Y., Frank, E., and Brunold, S. (2014). Auslegung und Betrieb einer hocheffizienten Solarthermie-Wärmepumpen-Heizung mit Eisspeicher. In *24. OTTI Symposium Thermische Solarenergie*, Kloster Banz, Germany.

Philippen, D., Haller, M. Y., Logie, W., Thalmann, M., Brunold, S., and Frank, E. (2012). Development of a heat exchanger that can be de-iced for the use in ice stores in solar thermal heat pump systems. In *Proceedings of EuroSun*, Rijeka and Opatija, Croatia. International Solar Energy Society (ISES).

Plugradt, N. (2010). Load profile generator. Technical report, Version 1.3.5. TU Chemnitz, Prof. Technische thermodynamik, Germany.

Russell, S. and Norvig, P. (2016). *Artificial Intelligence: A Modern Approach, Global Edition*. Pearson Education Limited.

Schmidli, J., Carbonell, D., Haller, M., and Biba, C. (2020). Weather data influence on a photovoltaic driven heat pump system for net-zero energy multi-family buildings. In *Proceedings of 37th european Photovoltaic Solarenrgy Conference and Exhibition*, online.

Schmidli, J., Carbonell, D., Philippen, D., and Haller, M. (2019). Vergleich des Einflusses unterschiedlicher Wetterdatensätze auf die Systemeffizienz von Solar-Eis-Systemen. In *OTTI Symposium Solarthermie Symposium*, Bad Staffelstein, Germany.

Schneider, C. (2015). Standard-Nutzungsbedingungen für die Energie- und Gebäudetechnik. Technical Report Schweizerischer Ingenieur- und Architektenverein, Merkblatt 2024.

scipy community (2021a). least_squares documentation: `https://docs.scipy.org/doc/scipy/reference/generated/scipy.optimize.least_squares.html`, accessed on 14.04.2021 at 10:36.

scipy community (2021b). Linearndinterpolator documentation: `https://docs.scipy.org/doc/scipy/reference/generated/scipy.interpolate.LinearNDInterpolator.html`, accessed on 23.03.2021 at 10:35.

Swiss Federal Council (2013). Botschaft zum ersten massnahmenpaket der energiestrategie 2050. Technical Report 2013-0462.

Waskom, M. (2021). seaborn.violinplot documentation: `https://seaborn.pydata.org/generated/seaborn.violinplot.html`, accessed on 30.03.2021 at 19:22.

Wetter, M. and Huber, A. (1997). *Vertical Borehole HEat Exchanger EWS Model*. Zentralschweizerisches Technikum Luzern Ingenieurschule HTL and Huber Energietechnik for Swiss Federal Office Of Energy (SFOE), CH-3003 Bern.

xgboost developers (2021). Xgboost documentation: `https://xgboost.readthedocs.io/en/latest/index.html`, accessed on 23.03.2021 at 10:32.

Yu, L., Wang, S., and Lai, K. K. (2006). An integrated data preparation scheme for neural network data analysis. *Knowledge and Data Engineering, IEEE Transactions on*, 18:217–230.

Zou, H. and Hastie, T. (2005). Regularization and variable selection via the elastic net. *Journal of the Royal Statistical Society: Series B (Statistical Methodology)*, 67(2):301–320. _eprint: https://rss.onlinelibrary.wiley.com/doi/pdf/10.1111/j.1467-9868.2005.00503.x.

Zweifel, G. (2010). Klimadaten für Bauphysik, Energie- und Gebäudetechnik. Technical Report Schweizerischer Ingenieur- und Architektenverein, Merkblatt 2028.